

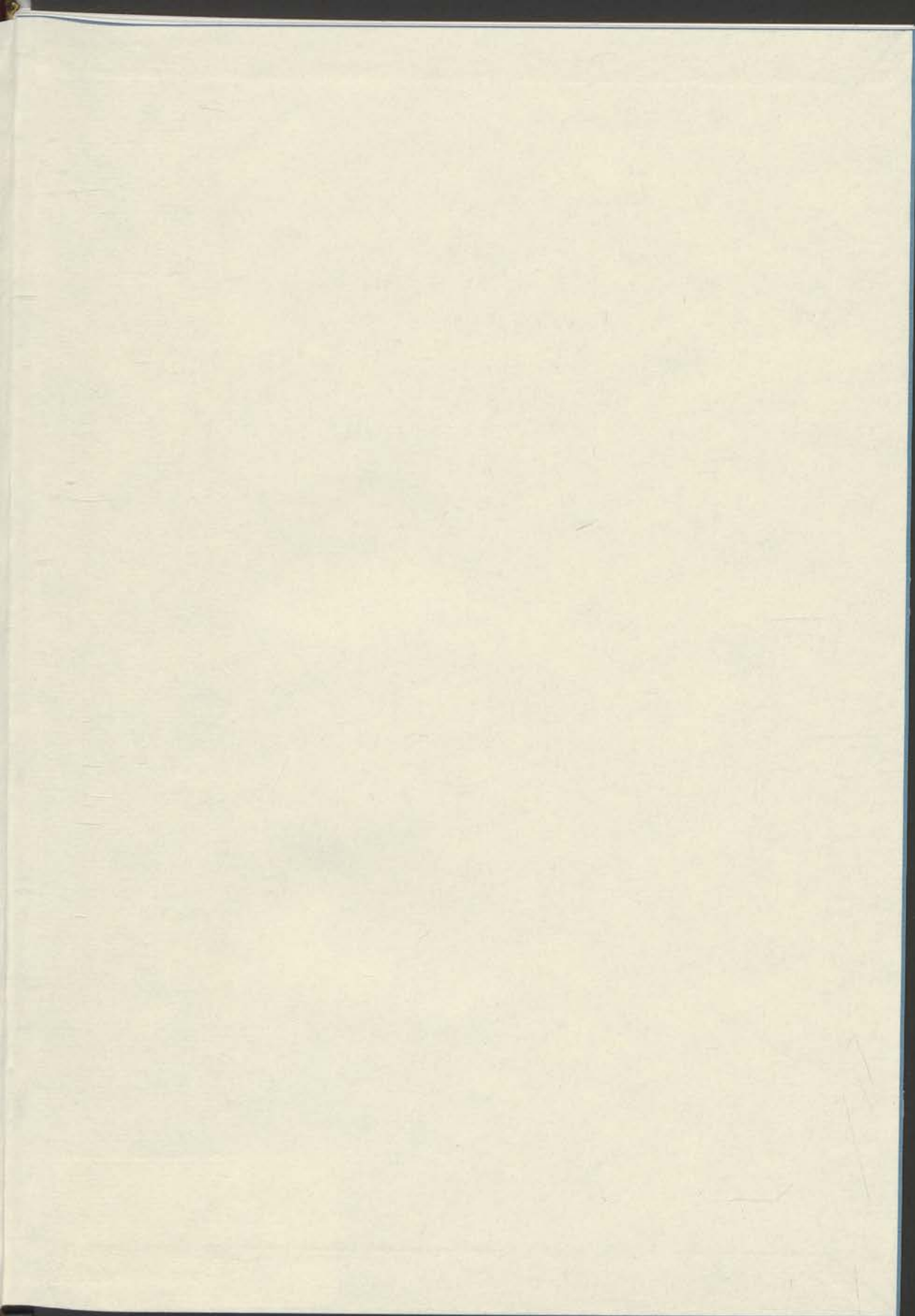


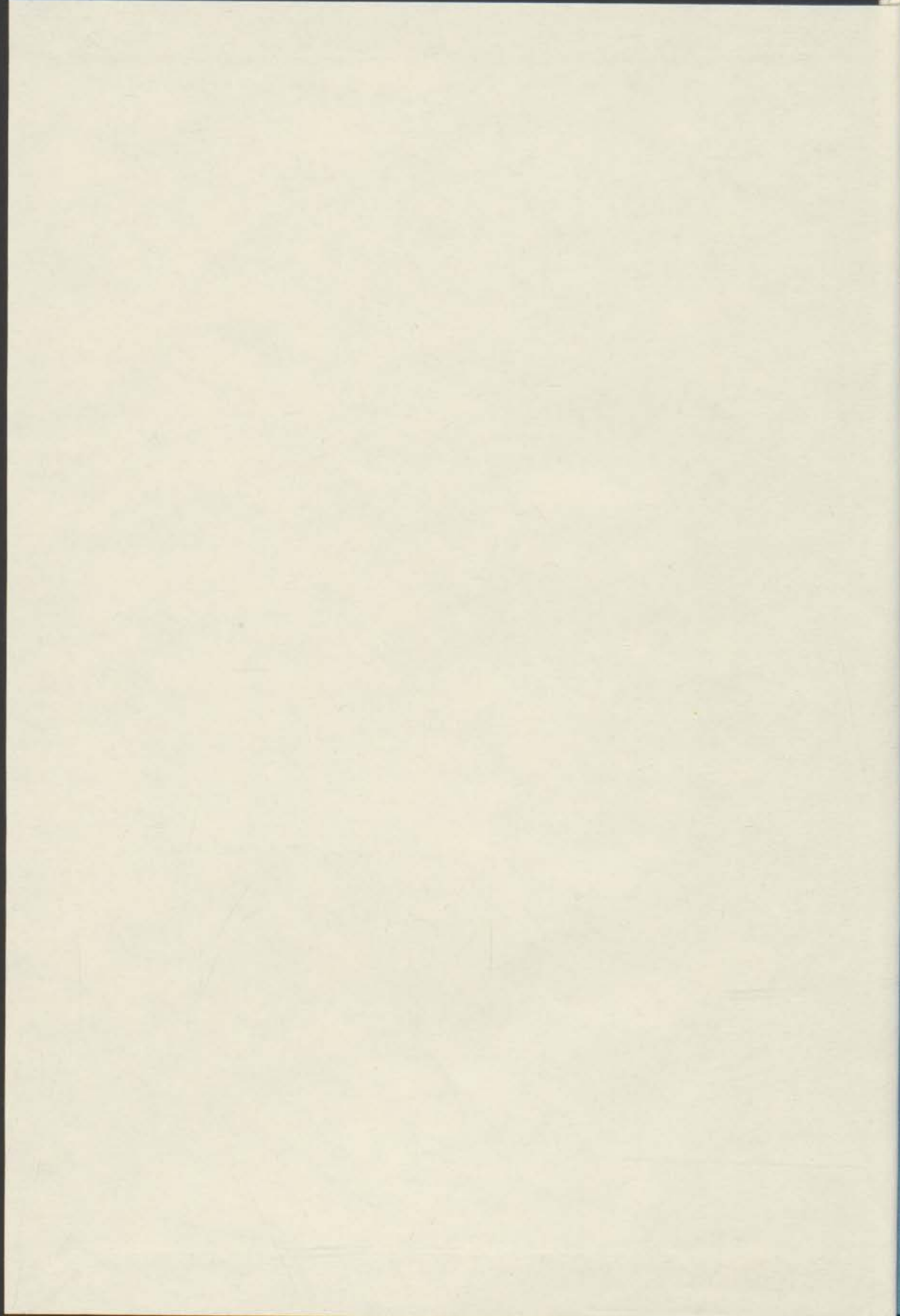
DISL 1970:109

Universiteit Leiden



2 406 469 8



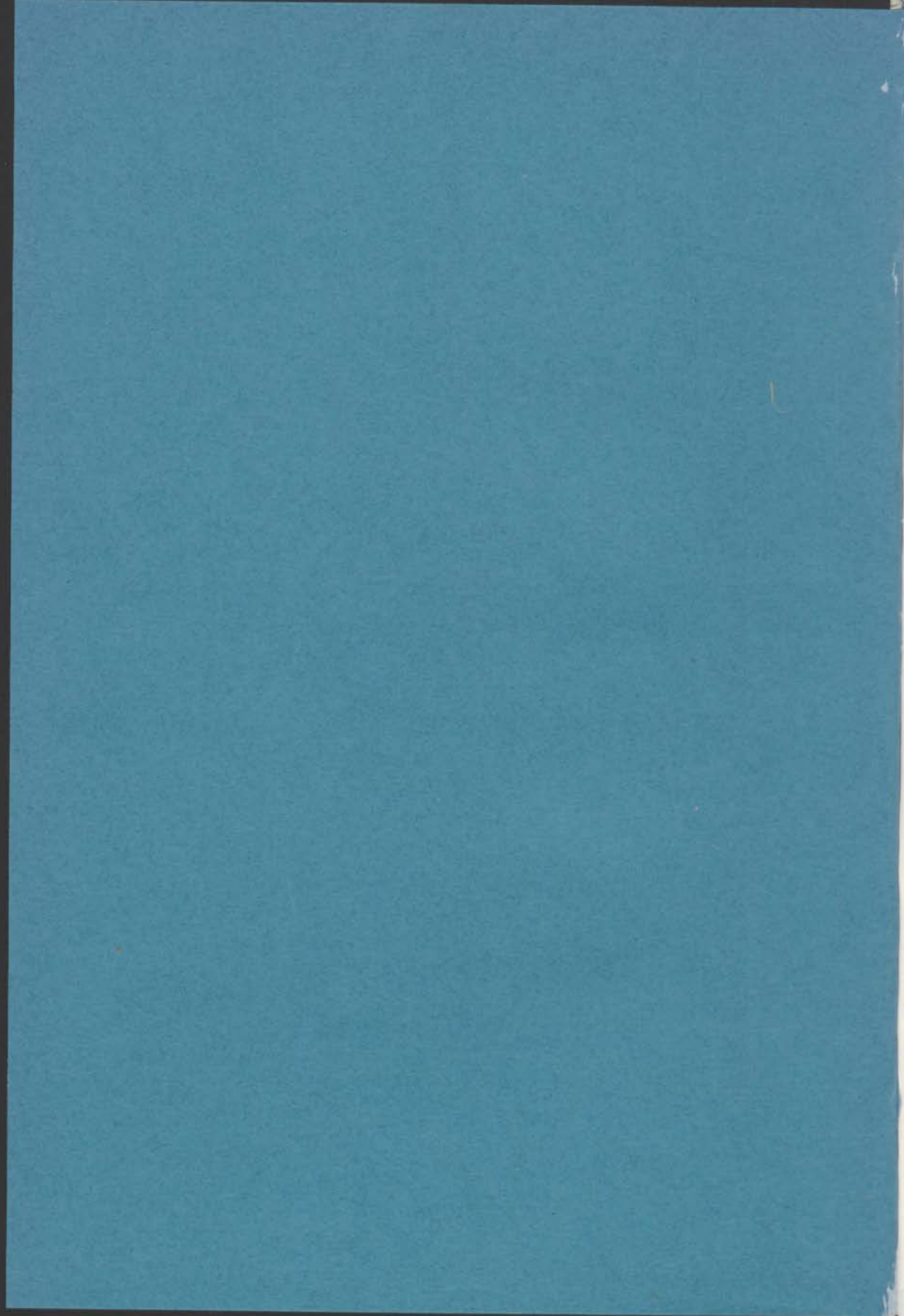


CALORIMETRIC INVESTIGATIONS  
ON A NUMBER OF FERROMAGNETIC  
PALLADIUM AND PLATINUM ALLOYS

B.M. BOERSTOEL

Diss. Leiden

1970 nr 109



**CALORIMETRIC INVESTIGATIONS  
ON A NUMBER OF FERROMAGNETIC  
PALLADIUM AND PLATINUM ALLOYS**

PROEFSCHRIFT

TER VERKRIJGING VAN DE GRAAD VAN DOCTOR  
IN DE WISKUNDE EN NATUURWETENSCHAPPEN  
AAN DE RIJKSUNIVERSITEIT TE LEIDEN, OP GEZAG  
VAN DE RECTOR MAGNIFICUS DR. C. SOETEMAN,  
HOGLERAAR IN DE FACULTEIT DER LETTEREN,  
TEN OVERSTAAN VAN EEN COMMISSIE UIT DE  
SENAAT TE VERDEDIGEN OP VRIJDAG 18 DECEMBER  
1970 TE KLOKKE 16.15 UUR

door

**BERNARD MARIUS BOERSTOEL**

geboren te Haarlemmermeer in 1939

1970

Beugelsdijk - Leiden

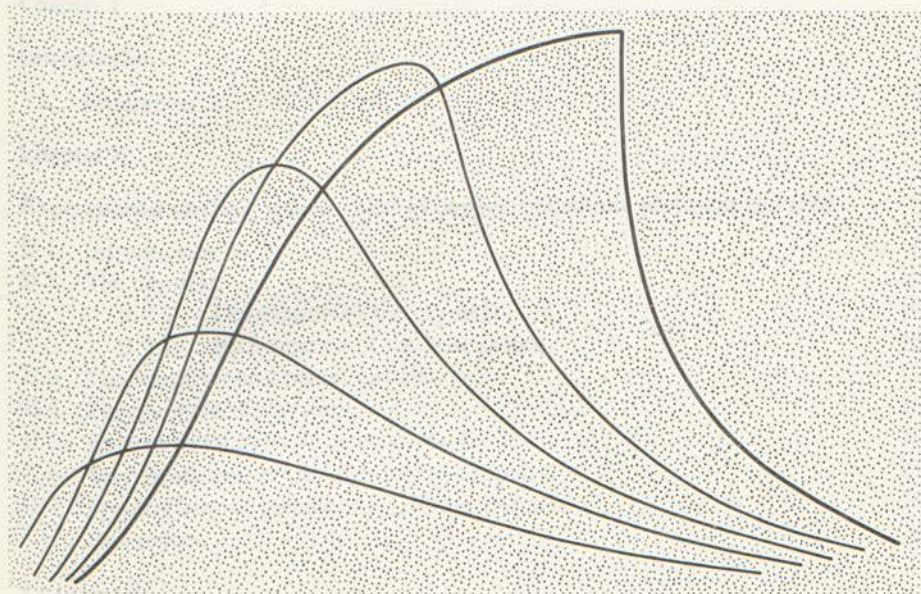
Promotor: Prof. dr. C.J. Gorter

Dit proefschrift is bewerkt onder toezicht van dr. C. van Baarle



This investigation is part of the research program of the 'Stichting voor Fundamenteel Onderzoek der Materie (F.O.M.)', financially supported by the 'Organisatie voor Zuiver Wetenschappelijk Onderzoek (Z.W.O.)' and by the 'Organisatie voor Toegepast Natuurwetenschappelijk Onderzoek (T.N.O.)'.

Contents



Review of the literature

II.1 Introduction

II.2 Review of experimental data

II.2.1. Measurement of susceptibility

II.2.2. Molecular effect

II.2.3. Molecular structure

II.2.4. Fractional conversion

II.2.5. Kinetic laws

II.2.6. Measurement properties

II.3 Some theoretical concepts

II.3.1. Propagation of the reaction

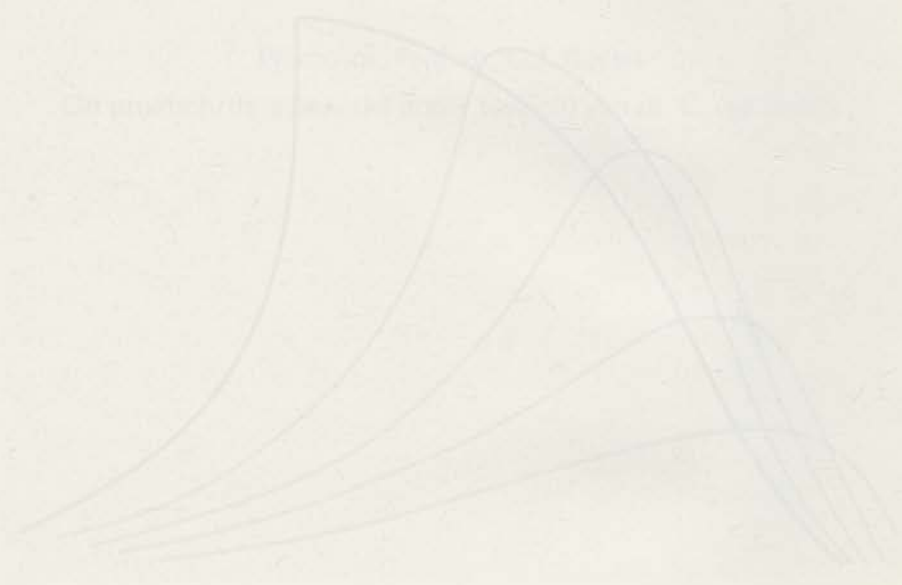
II.3.2. Propagation of the reaction in a polymer

Chapter IV

The kinetic law of the reaction in a polymer

IV.1. Introduction

*Aan mijn ouders  
Aan Elly,  
Erik en Lisette*



This investigation is part of the research program of the *U.S. Army Medical Research and Development Command* (DURMTC), generously supported by the *Department of the Army* (DPA) and by the *Department of the Army* (DPA) *Medical Research and Development Command* (DURMTC).

## Contents

### Chapter I

Introduction	7
Reference.	8

### Chapter II

Experimental method; specific heat of copper, palladium, platinum and gold	9
II.1 Introduction.	9
II.2 The cryostat.	10
II.2.1 Description of the cryostat.	10
II.2.2 Performance of the heat switch.	13
II.3 Thermometer and heater circuits.	14
II.4 Thermometer calibration.	16
II.5 Experimental procedure; magnetic field.	19
II.6 Test measurements on high-purity copper.	21
II.7 Specific heat of palladium, platinum and gold.	25
References.	26

### Chapter III

Review of the literature	27
III.1 Introduction	27
III.2 Review of experimental data.	30
III.2.1 Magnetization and susceptibility.	30
III.2.2 Mössbauer effect.	35
III.2.3 Neutron scattering.	38
III.2.4 Electrical resistivity.	40
III.2.5 Specific heat.	42
III.2.6 Miscellaneous properties.	42
III.3 Some theoretical concepts.	43
III.3.1 Ferromagnetism in metals.	43
III.3.2 Ferromagnetism in dilute Pd and Pt alloys.	45

### Chapter IV

The specific heat of dilute ferromagnetic alloys	50
IV.1 Introductory remarks.	50

IV.2	Presentation of specific-heat results on Pd,Pt and Au alloys containing Co or Fe.	51
IV.2.1	Pd-Co, Pd-Fe, Au-Fe.	51
IV.2.2	Pt-Co.	54
IV.3	Qualitative aspects of the specific-heat curves.	55
IV.3.1	Pd-Co results in zero magnetic field.	57
IV.3.2	Pd-Co results in applied magnetic fields.	59
IV.3.3	Intercomparison of Pd-Co, Pd-Fe and Au-Fe alloys.	60
IV.4	Presentation and discussion of the specific heat of Pd-Mn alloys.	61
IV.5	Entropy and spin.	65
IV.6	Some other details of the specific heat.	69
	References.	76
 <b>Chapter V</b>		
<b>Molecular-field calculation of the specific heat in external magnetic field; critical behaviour of Pd-Mn alloys</b>		80
V.1	Introduction.	80
V.2.1	Derivation of the specific heat.	80
V.2.2	Application to Pd-Mn alloys.	83
V.2.3	Calculation of the specific heat for a Gaussian distribution of molecular fields.	89
V.2.4	Application to Pd-Fe, Pd-Co and Pt-Co alloys.	91
V.2.5	Concluding remarks.	94
V.3	Analysis of the specific-heat cusp of Pd-Mn alloys.	95
V.3.1	Introduction.	95
V.3.2	Analysis of a rounded specific-heat peak.	97
V.3.3	Results.	98
V.3.4	Discussion.	101
	References.	105
 <b>Appendix I</b>		106
AI.1	Preparation of specimens.	106
AI.2	The tables.	108
	References.	109
 <b>Appendix II</b>		112
 <b>Summary</b>		115
 <b>Samenvatting</b>		119

## Chapter I

### INTRODUCTION

During the last decade and particularly since 1965, interest in the properties of palladium and platinum containing small amounts of nickel, cobalt, iron, manganese, chromium and some rare-earth metals has grown rapidly. Considerable information has been obtained on a wide variety of both macroscopic and microscopic properties. At present, the main features of the magnetic behaviour of these systems are reasonably well understood, though many details remain, as yet, unexplained while also several conflicting results have been reported.

Particular attention was paid to the ferromagnetic behaviour observed in alloys of e.g. Pd with Ni, Co, Fe, Mn and Gd. Whereas pure Pd and Pt essentially exhibit paramagnetism due to the conduction electrons (Pauli paramagnetism), ferromagnetism has been found to persist down to very low concentrations in e.g. dilute Pd-Fe and Pd-Co alloys \*) (< 0.05 at.%). Presumably this also occurs in Pd-Mn alloys, but in the case of Pd-Ni alloys ferromagnetism is only observed above a critical concentration, 2 at.% Ni. Among these Pd- and Pt-based alloys Pd-Mn was recently observed to exhibit an exceptional phenomenon. While all other alloys, which exhibit long-range ferromagnetic ordering at low concentrations, remain ferromagnetic at higher concentrations, a tendency towards antiferromagnetic ordering is found in Pd-Mn alloys at higher Mn concentrations. The transition from ferromagnetism to antiferromagnetism occurs at approximately 8 at.% Mn (see sections III.1 and IV.4).

The most remarkable property which in fact originally excited the interest into these alloys, is the magnetic moment per solute atom. For instance in dilute Pd-Fe and Pd-Co alloys, the saturation values of these moments are exceptionally high, namely up to 10-12  $\mu_B$  per Fe or Co atom (so-called giant moments). On the other hand, rather normal saturation moments were found in, for example, Pd-Mn and Pd-Gd alloys.

In this thesis specific-heat measurements on a number of dilute ferromagnetic Pd- and Pt-based alloys will be described. Thanks to a high experimental accuracy detailed information about the magnetic contribution to the specific heat could be derived for temperatures between 1 and 30 K, with as well as without

\*) Dilute alloys will be indicated by mentioning the solvent (base metal) first and secondly the solute element.

external magnetic fields. Originally, the measurements were set up in order to decide (by entropy determinations) whether the giant moments are associated with 'giant spins'. However, new data becoming available from the present work as well as from other investigations led to the conclusion that it was worthwhile to extend the scope of the investigations. For instance, it was considered to be interesting to search for a possible lower bound for the occurrence of ferromagnetism in Pd-Co alloys and to carry out measurements on the striking magnetic-field dependence of the specific heat of Pd-based alloys.

In a later stage of this investigation it was decided to carry out measurements on the Pd-Mn system. Presumably for historical reasons little attention has been paid to this system \*). The measurements on dilute Pd-Mn alloys have undoubtedly yielded the most remarkable and unexpected results of this investigation. While any other known dilute alloy, irrespective as to whether it exhibits ferromagnetism or any other type of 'magnetic behaviour' at low temperatures, shows a broad wedge-shaped specific-heat versus temperature curve, the specific heat of Pd-Mn alloys exhibits a sharp peak ('cusp') near the transition temperature (section IV.4, figures IV. 12-14). Besides, as will be shown in chapter V, the magnetic-field dependence of the specific heat of dilute Pd-Mn alloys is different from that of the other Pd-based ferromagnetic alloys. While for Pd-Mn alloys a calculation based on the Weiss molecular-field model yields a good description of the specific heat in the presence of 'high' external magnetic fields, such a fair agreement has not been found for the other alloys. These calculations were carried out as a simple approach to the problem, since no satisfactory analysis has so far been proposed for the specific heat of dilute ferromagnetic alloys.

Finally since up till now no review on the experimental and theoretical state of affairs has been reported for Pd- and Pt-based alloys, a review of the literature is given in chapter III which may also serve as a more comprehensive introduction to the subject of this thesis.

## Reference

1. R.M. Bozorth, D.D. Davis and J.H. Wernick, J.Phys.Soc.Jap. 17, Suppl. B1(1962) 112.

\*) In one of the first comprehensive reports, presented by Bozorth et al. [1], on the properties of dilute Pd-based alloys a 1 at. % Pd-Mn alloy had been reported to be non-magnetic.

## Chapter II

### EXPERIMENTAL METHOD; SPECIFIC HEAT OF COPPER, PALLADIUM, PLATINUM AND GOLD

#### II.1. Introduction

In this chapter a description of the experimental arrangement and the method for specific-heat measurements is given. The principle of the measurements follows directly from the definition of the specific heat

$$C_{x,y,\dots} = \lim_{\Delta T \rightarrow 0} (\Delta Q/\Delta T)_{x,y,\dots}, \quad (\text{II.1.})$$

where  $x, y, \dots$  are quantities which are kept constant during a measurement. Therefore, the specific heat of a specimen can be obtained by observing the temperature rise  $\Delta T$ , which occurs when a known amount of heat  $\Delta Q$ , is supplied to the specimen. Throughout this investigation the quantities which were held constant were the pressure  $p$  and the applied magnetic field  $H$ . In the range of temperatures below 30 K the difference between the specific heat at constant pressure  $C_p$  and the specific heat at constant volume  $C_V$  is negligible for metals, so that effectively  $C_{V,H}$  is measured. These subscripts will be dropped everywhere, but in all cases  $C$  will have the meaning of  $C_{V,H}$ . Unless otherwise stated the specific heat will always be given per gram-atom (g at).

In view of the sometimes quite small magnetic contributions to the specific heat it was decided soon after the beginning of this investigation that the existing equipment and method of temperature determination, as described by du Chatenier [1], had to be improved considerably. The main source of random errors was the so-called 'exchange-gas' method (see section II.2.). Temperatures derived from De Vroomen's table [2, 1] proved to be unreliable for high accuracy specific-heat measurements as systematic errors of the order of a few percents were introduced into the specific-heat results. Much attention has been paid to remove these error sources.

A cryostat has been constructed in which a mechanical heat switch is used to establish heat contact between the specimen and the cooling reservoir (liquid He or  $H_2$ ). De Vroomen's method has been replaced by a calibration method in which the resistance-temperature relation of a carbon thermometer is analysed with the aid of a computer, using an empirical formula expressing  $\log T$  in terms of powers of  $\log R$  where  $R$  is the resistance of the carbon thermometer at temperature  $T$ .

A substantial reduction of the error level has been achieved, as is illustrated in section II.6, where a number of test measurements has been described.

No attempts have been made to automatize the equipment because the main concern was improvement of the measurements rather than increment of the speed of data processing. However, it should be mentioned that the equipment, as it exists at present can, in principle, be easily automatized using a data logging system. Furthermore, it is well-known that the calculation of the specific heat involves a great deal of tedious computation per data point. Therefore much effort has been given to carry out as much computational work as possible on a computer.

In the following sections the cryostat, the thermometer and heater circuits, and the calibration method will be described. The error sources will be discussed and the reliability of the experimental procedure will be checked by comparison of specific-heat results on pure Cu with those obtained by other investigations. In the last section results obtained on Pd, Pt and Au will be presented.

## II.2. The cryostat

### II.2.1. Description of the cryostat

A specific-heat determination based on eq. (II.1) requires a calorimeter which can be thermally isolated from its environment. Formerly, gaseous helium was commonly used for precooling of the calorimeter in specific-heat investigations at liquid helium temperatures. In spite of its simplicity this method had a number of serious drawbacks. The main disadvantage was the impossibility to dislodge, even with fast pumps, all the helium gas from the calorimeter and the walls of the vacuum-container because of strong adsorption of helium gas on metallic surfaces at low temperatures. Consequently, during heat-capacity measurements heating curves were sometimes quite irregular which seriously hampered their interpretation, unknown errors being made due to the heat of evaporation of the adsorbate. In the last decade the use of mechanical heat switches has become the vogue. Such a switch avoids all problems inherent in the 'exchange-gas' method without introducing any serious new problem, provided the switch has been properly designed and constructed.

All specimens used in this investigation could be readily machined. The addenda (thermometer, heater and clamping post) were mounted on two small bolts, M4, which could be screwed into the specimen. In this way the use of a calorimeter could be avoided.

A sketch of the lower end of the cryostat is shown in fig. II.1. The vacuum-container has been suspended from the top of the cryostat by a pumping tube, into which a number of radiation traps has been inserted. The lid and the bottom of the vacuum-container are connected by four brass rods. The specimen is suspended from these rods by thin silk threads (0.5 mm in diameter). In order to facilitate specimen

exchanging the bottom can be detached. The vacuum-container is sealed by a brass jacket attached to bottom and top by Wood's-metal joints.

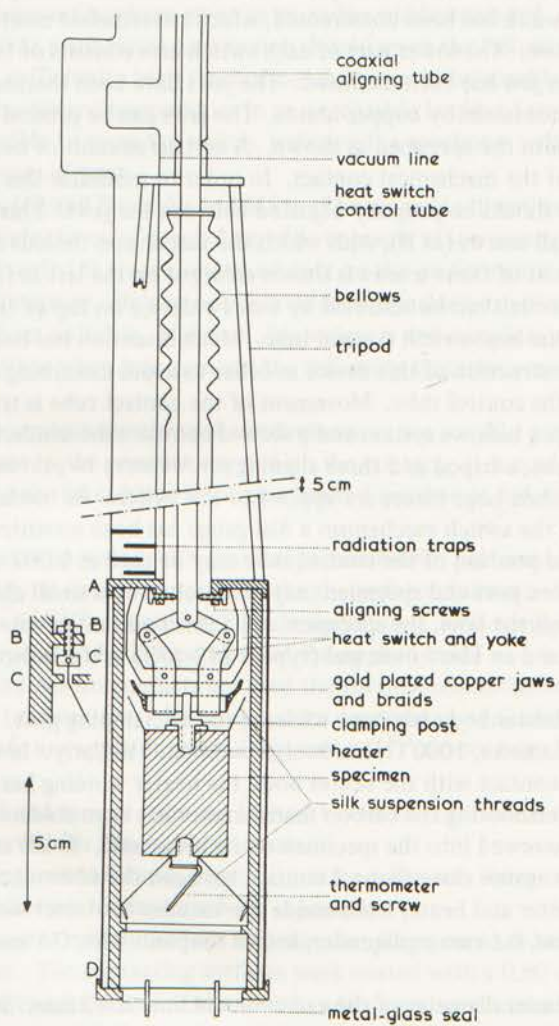


fig. II.1. The cryostat.

The heat switch has been mounted on a yoke attached to the lid of the vacuum-container. As discussed in section II.2.2 quite large forces have to be exerted on the surfaces which establish heat contact. Therefore, quite rugged

constructions are commonly used [3,4] in order to withstand these forces. In the present mechanism the yoke and all moving parts, except the jaws, have been made of 1 mm stainless-steel sheet. The pivots are small stainless-steel pins. In this way a less robust switch has been constructed, which nevertheless meets the requirement mentioned above. The lower part of each switch arm consists of two sheets between which a copper jaw has been mounted. The jaws have been thermally anchored to the lid of the container by copper braids. The jaws can be pressed on a clamping post screwed into the specimen as shown. A certain amount of heat will be generated upon release of the mechanical contact. In order to minimize this amount the clamping post should be properly adjusted between the jaws. This may be achieved by turning small screws (at B), with which the suspension threads are tightened. The arrangement of these screws is shown enlarged on the left in fig. II.1.

The switch can be actuated by a screw device on top of the cryostat which pushes down the heat-switch control tube. Much attention has been paid to the design and construction of this device in order to avoid disturbing vibrations and distortion of the control tube. Movement of the control tube is transmitted to the switch through a bellows system and a second control tube inside the vacuum-container. An aligning tube, a tripod and three aligning screws serve to prevent bending the control tube when large forces are applied to the switch. As too large a force could easily damage the switch mechanism a dial gauge has been mounted on the cryostat with which the position of the control tube may be read at 0.002 mm intervals. Contact between jaws and specimen may be checked by a small electrical current running through the jaws, the specimen and a fine constantan wire connected to the specimen and an Electrovac seal (type S 112 A/B) in the bottom of the vacuum-container.

The heater body has been soldered to the clamping post. A constantan wire of 0.03 mm diameter, 1000  $\Omega$ , has been wound on it bifilarly. In order to ensure good thermal contact with the heater body the heater winding has been varnished. To prevent overshooting the carbon thermometer has been soldered to a second bolt which is screwed into the specimen on its lower side. Small amounts of silicone oil are used to ensure close thermal contact between the addenda and the specimen. The thermometer and heater leads inside the vacuum-container were made of constantan wire, 0.1 mm in diameter, and of niobium wire, 0.1 mm in diameter, respectively.

The inner diameter of the vacuum-container is 40 mm. Specimens with diameters up to 27 mm can be mounted in it. In the later stages of this investigation a second cryostat has been put into use, which can accommodate specimens with diameters up to 45 mm. Apart from a number of small improvements, facilitating specimen mounting, it operates in the same way as the one described above.

## II.2.2. Performance of the heat switch

A few remarks will be made concerning the performance of the heat switch. A more detailed account has been given in an earlier publication [5].

An efficient mechanical heat switch should meet the following requirements:

- a. It must have a sufficiently high thermal conductance to be capable of cooling a specimen to the desired temperature in an acceptable length of time.
- b. It must be possible to open the switch, isolating the specimen, without generating excessive amounts of heat.

Berman [6] and Berman and Mate [7] have made direct measurements of the thermal conductance of pressed metallic contacts at low temperatures. In a recent article Colwell [3] gives a review of data on the performance of heat switches described in the literature. He was not able to draw conclusions as to which metals are preferable in heat switches. However, his review is not complete and if more information [5,8,9] is taken into account the following tentative conclusions may be drawn.

1. At a fixed temperature the thermal conductance varies roughly proportionally to the load, but not to the pressure exerted on the contact. It is commonly believed that heat flow only takes place through a limited number of deformed surface asperities.
2. When the junction is coated with a soft superconductor, preferred because of their malleability at room temperature, the thermal conductance varies proportionally to  $T^{2-3}$  at liquid-helium temperatures. This temperature dependence appears to be independent of the applied load.
3. When Cu-Cu and Au-Au contacts are used the thermal conductance decreases less rapidly at low temperatures. Its temperature dependence varies between  $\propto T^{1.7}$  when small loads are applied (about 1 kg), and  $\propto T^{1.3}$  at very large loads (tens of kilograms).
4. At a given load and temperature the highest values of the thermal conductance have been observed for Au-coated contacts.

Some of these conclusions should, however, not be taken too stringent, since also a number of contradictory results have been reported.

In the present switch the jaws and the clamping post have been made of high-purity copper. The contacting surfaces were coated with a 0.02 mm layer of gold. The thermal conductance of the switch, when measured under the load actually used during specific-heat measurements, proved to be considerably larger than those observed by the majority of other investigators [3,5,8]. In this state the thermal conductance varies proportionally to  $T^{1.3}$  at liquid-helium temperatures. When measured just after initial contact, i.e. under a very small load, its temperature dependence changes to  $T^{1.7}$  and its magnitude drops by more than a factor of ten. It will be clear that it is not easy to measure the load exerted on the junction in the

present design of the heat switch. However the above mentioned loads could be estimated to be of the order of tens of kilograms and of one kilogram, respectively.

Development of heat resulting in a rise of the temperature of the specimen cannot be avoided when a heat switch is opened. Amounts of heat ranging from 1 to 100  $\mu\text{J}$  have been quoted in the literature. The development of heat is primarily determined by the degree of misalignment of the contacting surfaces. Some authors observed it to depend on the load exerted on their switches, e.g. Colwell [3] states 2 to 3  $\mu\text{J}/\text{kg}$ . In the present switch amounts ranging from 4 to 15  $\mu\text{J}$  have been observed hardly depending, however, on the applied load. Sometimes much larger amounts of heat have been observed when the switch is opened the first time after the cryostat has been cooled down from room temperature. This may be due to re-setting of the specimen. When the switch is closed and opened again the amount of developed heat drops to a value commonly observed.

It may be concluded that the heat switch described here does meet the requirements set out initially. The specimen is cooled down in a time competitive with the one observed when exchange gas is used. Besides, its temperature rise due to development of heat on release never exceeds a few hundredths of a degree.

### II.3. Thermometer and heater circuits

The thermometer circuit is shown in fig. II.2. The resistance of the carbon thermometer  $R_T$  is measured by means of a 6-dial dc Wheatstone bridge, Pye model 7361, calibrated to an accuracy of 0.01%. Applying a three-probe technique, as shown, the resistance of the thermometer leads and, consequently, its changes during an experiment cancels, provided the leads have been made of the same material.

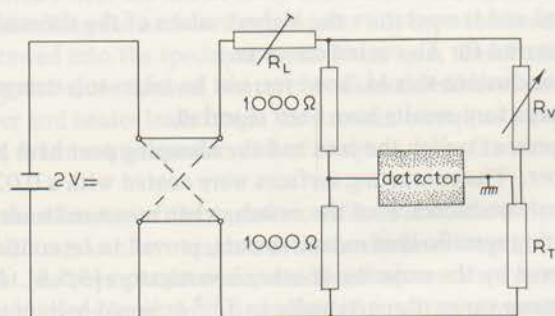


fig. II.2. The thermometer circuit.

During the calibration of the thermometer a Leeds-Northrup dc microvolt amplifier, Cat. 9835-B, is used as a null-detector. During specific-heat measurements the heating curves are displayed on a Philips PR 2210 A/21 chart recorder, receiving the out-of-balance signal of the Wheatstone bridge from the dc amplifier. In a later stage of the investigations a Kipp en Zonen Micrograph BD 5 - recorder replaced both the Philips-recorder and the microvolt amplifier. The majority of the specific-heat measurements have been carried out with this instrument.

The bridge current is adjusted by the resistance  $R_L$ . The thermometer current is commonly adjusted to  $0.2 \mu\text{A}$  at 1.2 K and increases to  $1 \mu\text{A}$  at 30 K as a result of the temperature dependence of the thermometer resistance. The amount of heat dissipated varies between 1 and 4 nW. Star et al. [10] derived a relation for the temperature rise due to dissipation of heat by the measuring current in the type of thermometers used in the present investigation. This rise as calculated from their expression does not exceed  $2 \cdot 10^{-5}$  K.

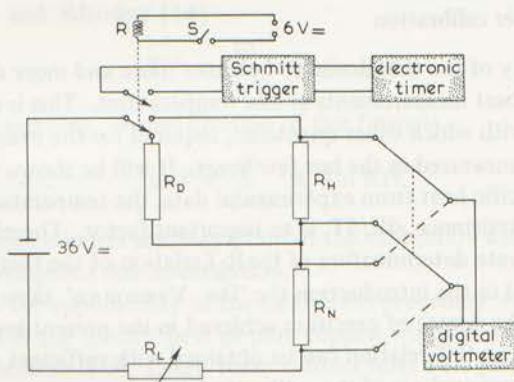


fig. II.3. The heater circuit.

The heater circuit is presented in fig. II.3. When switch S is closed relay R is actuated. In its hold position the heater current runs through the heater  $R_H$  and a Bleeker precision resistance  $R_N$  ( $1000 \Omega$ ). When R is released the heater is disconnected from the circuit and the current is passed through a dummy resistance  $R_D$ . The potential drop across  $R_H$ ,  $V_H$ , as well as across  $R_N$ ,  $V_N$ , is measured by standard four-probe technique. A Solartron LM 1402.2 digital voltmeter has been used to measure  $V_H$  and  $V_N$  with an accuracy better than 0.1%. The duration of the heating time,  $t$ , is obtained by means of an electronic timer, Philips PW 4062, switched by a Schmitt trigger. It is put into operation simultaneously with the

heater circuit by means of R, as shown. The accuracy of the time measurement is 0.01% or 1 ms whichever is higher. The two relay contacts switch simultaneously to within 0.3 ms as was verified in a separate experiment. Heating times are chosen between 4 and 20 s by adjustment of the heater current by means of  $R_L$ . The amount of heat  $\Delta Q$  developed in the heater is thus  $V_H V_{NT}/R_N$ ; it is estimated to be accurate to 0.1%.

When the current leads of the heater inside the vacuum-container (Nb wires) are in the normal state, heat is developed in these leads by the heater current. It is easy to show that approximately half of this amount of heat flows to the specimen. An asymmetrical method has been applied for the potential leads of the heater to account for the resulting extra rise of the temperature of the specimen. One potential junction has been made on one of the terminals of the heater winding, the other one on the metal-glass feed-through in the bottom of the vacuum-container. In this way one accounts for just half of the amount of heat developed in the current leads, which actually never exceeds 0.2% of  $\Delta Q$ .

#### II.4. Thermometer calibration

The accuracy of the thermometry becomes more and more decisive for the accuracy of specific-heat measurements at low temperatures. This is due to the improved precision with which other quantities, required for the evaluation of the specific heat, can be measured in the last few years. It will be shown that, in the derivation of the specific heat from experimental data, the temperature derivative of the thermometer resistance,  $dR/dT$ , is an important factor. Therefore, it is obvious that an accurate determination of the R-T relation of the thermometer is required. As stated in the introduction the 'De Vroomen' table did not meet this requirement at the degree of precision achieved in the present investigation. It will be shown that an R-T relation can be obtained with sufficient accuracy by means of a least-squares analysis of the calibration data.

The film-type carbon resistance thermometers have been developed by the F.O.M. Metals group of the Kamerlingh Onnes Laboratorium. The manufacture and a detailed study of their characteristics have been reported by Star et al. [10]. The main drawback of the thermometers is their irreproducibility with respect to thermal cycling. However, there is a number of important advantages, when compared to germanium thermometers and Allan-Bradley and Speer resistors, which makes them suitable for measurements of small temperature differences over a wide range of temperatures, e.g. 1 – 30 K or more, by means of a simple Wheatstone bridge. These advantages have been discussed in ref. 10 to which one is referred for detailed information.

After each thermal cycling to room temperature the thermometer was calibrated against the vapour pressure of liquid  $^4\text{He}$ , normal  $\text{H}_2$  and liquid  $\text{N}_2$ .

Temperatures were obtained from the 1958-<sup>4</sup>He scale [11] and from the L-60 H<sub>2</sub> scale [12]. The vapour pressure was read on a mercury manometer by means of a cathetometer. An oil manometer has been used for temperatures below 2.17 K. The vapour pressure of the bath was controlled by means of an oil differential manometer and a photo-transistor circuit in order to restrict thermal fluctuations to 10<sup>-4</sup> K at liquid-<sup>4</sup>He temperatures and to a few millidegrees at liquid-H<sub>2</sub> temperatures. Standard temperature and, when relevant, hydrostatic pressure corrections were applied. A small correction was applied in order to take into account the ortho-para conversion of normal H<sub>2</sub>. Hydrostatic pressure corrections proved to be unreliable in the temperature range between 2.17 and 2.7 K due to thermal instabilities. This has been shown previously by Durieux [13] and therefore no calibrations were carried out in this range of temperatures.

At the start of this investigation a calibration procedure was sought for which would give an accurate representation of the R-T relation for the whole range of temperatures between 1 and 30 K using only a restricted number of calibration points made at liquid-<sup>4</sup>He-, H<sub>2</sub>- and N<sub>2</sub>-temperatures. An empirical formula given by Moody and Rhodes [14]

$$T^{-1} = \sum_{i=0}^m A_i (\ln R)^i \quad (\text{II.2})$$

was used at the beginning. A modification of this formula,

$$\ln T = \sum_{i=0}^m A_i (\ln R)^i, \quad (\text{II.3})$$

proved to give a much better representation of the calibration data. This formula has been used throughout this investigation.

Initially the applicability of the calibration procedure was verified by means of measurements of the specific heat of pure copper, which is well known between 1 and 30 K (see section II.6). Later, these indirect tests were justified by a gas-thermometer experiment carried out by Star et al. [10]. They made calibrations at a large number of temperatures between 1 and 80 K and fitted the calibration points to formula (II.2) as well as formula (II.3). Furthermore, they made a fit using a restricted number of these calibration points distributed in temperature as in the present experiments. Using formula (II.3) with  $m = 6$ , they found that differences in  $T$  were well within 0.1% when the fit to all calibration data was compared with the fit to the limited set of calibration data. Below 60 K, differences in  $dR/dT$  were found to be smaller than 0.3%. Their analysis also demonstrated that formula (II.3) should be preferred over formula (II.2). These results were in excellent agreement with the conclusions, drawn previously from specific-heat measurements on pure copper [5].

A sixth-degree ( $m=6$ ) polynomial proved to be necessary and sufficient to represent the calibration data [5,10]. About 13 points were chosen at He temperatures,

7 at  $H_2$  temperatures and one at  $N_2$  temperatures so that the calibration points outnumbered the coefficients of the polynomial by a factor of three. The calibration points were fitted to formula (II.3) with the aid of a computer, using the least-squares method. All points were given equal weight, so that the sum over all points of  $(\Delta \ln T)^2 = (\Delta T/T)^2$  was minimized. The r.m.s. of  $\Delta T/T$  was commonly found between  $8 \times 10^{-5}$  and  $2.5 \times 10^{-4}$ . When a value larger than  $4 \times 10^{-4}$  was obtained the fit was considered to be poor. In most cases such a high value could be traced back to some trivial error. Therefore, the r.m.s. proved to be a sensitive indication on the accuracy of the fit.

Differences between measured and calculated temperatures were generally smaller than 0.5 mK and 5 mK at liquid He and  $H_2$  temperatures, respectively. Calibration points deviating more than 3 mK at He temperatures and more than 10 mK at  $H_2$  temperatures, which after all occurred rarely, were excluded from the minimization procedure by means of an (adjustable) rejection criterion. It is rather surprising that a single calibration point made at the  $N_2$  boiling point is sufficient to obtain a satisfactory fit between 20 and 30 K. Omission of this point leads to erroneous results at these temperatures, extrapolations of course being extremely unreliable.

Originally, temperatures were obtained from p-T tables by hand calculation. In the later stages of the investigation this calculation was incorporated in the computer program. The input consisted of the measured pressure, the room temperature and the height of the pressure head only. Temperatures were derived from an expression relating pressure to temperature by means of the Newton-Raphson iterative procedure [15].  $H_2$  temperatures were obtained from expressions given by Durieux et al. [12]. Liquid- $^4\text{He}$  temperatures were calculated from two empirical expressions\*):

$$\text{He I: } \ln p = A_1/T + B_1 + C_1 T + D_1 T^2 + E_1 T^3 - \ln(10^4 \times p_0) \quad (\text{II.4})$$

$$\text{He II: } \ln p = A_2/T + B_2 + C_2 T + D_2 T^2 + E_2 T^3 + \left(\frac{5}{2}\right) \ln T - \ln(10^4 \times p_0) \quad (\text{II.5})$$

where

$$A_1 = -8.846548; B_1 = 13.20872; C_1 = 0.7318486; D_1 = -0.04143823; E_1 = 0.001101094;$$

$$A_2 = -7.927456; B_2 = 14.03655; C_2 = -2.163890; D_2 = 1.018420; E_2 = 0.1844473,$$

and  $p_0$  is the measured pressure in cm Hg. Initiating the computation with  $T_0 = 3.3$  K for He I and  $T_0 = 1.5$  K for He II it never takes more than four iterations to obtain the temperature from these expressions to within  $10^{-5}$  K.

In fig. II.4 the differences between the temperature  $T_F$  derived from the expressions and the temperature calculated from the 1958- $^4\text{He}$  scale,  $T_{58}$ , have

\*) We are indebted to Ir. A. Herwyer of the Technische Hogeschool, Eindhoven, for providing these expressions.

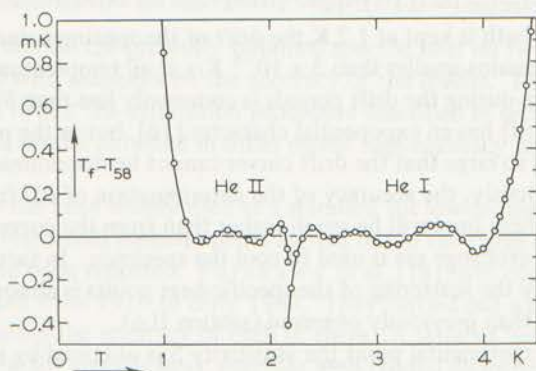


fig. II.4. Deviation plot of the temperature  $T_f$  according to formulae (II.4) and (II.5) from the 1958- $^4\text{He}$  table  $T_{58}$

been plotted as a function of temperature. In the temperature range of interest (1.2 – 4.2 K) these differences are smaller than 0.1 mK, except in a narrow range around  $T_\lambda$ , where differences up to 0.4 mK occur. Below 1.2 K and above 4.3 K agreement rapidly becomes less.

## II.5. Experimental procedure; Magnetic field

Prior to the measurements the cryostat is evacuated to a pressure of  $10^{-5}$ – $10^{-6}$  torr by means of an oil diffusion pump backed by a rotary pump. Next, the specimen is precooled by liquid  $\text{H}_2$  and subsequently cooled down by liquid  $^4\text{He}$ . The switch is opened after the specimen has attained its lowest temperature, usually about 1.2 K. Specific-heat measurements can be started immediately; the complete run up to 30 K is made without changing the temperature of the  $^4\text{He}$  bath.

The temperature of the specimen is displayed on the recorder as a function of time, as was mentioned in section II.3. The specific heat is measured essentially according to the Keesom-Kok method [16], taking fore-, heating- and afterperiods. The analysis of the drift- and heating-periods has been described extensively by Ferreira da Silva [17] and will not be repeated here except for a few details.

The temperature interval of any given point,  $\Delta T$ , is always smaller than 5% of the mean temperature of the heating period. In this way errors due to curvature of the specific heat-temperature relation are smaller than 0.1%. During the heating period the thermometer resistance changes by  $\Delta R = (dR/dT)\Delta T$ . The resulting scale deflection  $\Delta U$  is related to  $\Delta R$  by the sensitivity  $S$  of the bridge at the given amplification factor of the detecting system;  $S = \Delta U/\Delta R$ .  $\Delta R$  has been chosen in such a way as to keep the alinearity of the bridge, due to unbalance, smaller than the

alinenity of the detector ( $\approx 0.1\%$ ).

When the bath is kept at 1.2 K the drift of the specimen due to heat leak to the environment remains smaller than  $5 \times 10^{-5}$  K/s at all temperatures. The temperature change during the drift periods is commonly less than 5% of  $\Delta T$ . The temperature drift has an exponential character [16], but in the present set-up its time constant is so large that the drift curves cannot be discriminated from straight lines. Obviously, the accuracy of the determination of  $\Delta U$  from extrapolations of these lines will be much higher than from the curved drift periods which occur when exchange gas is used to cool the specimen. In fact, this is the primary reason why the scattering of the specific-heat points is almost an order of magnitude smaller than previously observed (section II.6).

At each experimental point the sensitivity  $S$  is obtained by observing the scale deflection when the variable bridge resistance is changed by  $\Delta R$ . All data needed for the evaluation of  $\Delta T$  are obtained graphically from the heating curves and the rest of the computations are performed by the computer. Within the limit of experimental accuracy the inverse of the sensitivity can be represented by  $S^{-1} = A_0 + A_1 R + A_2 R^2$ , the last term contributing but a few percent to  $S^{-1}$ . The constants  $A_0$ ,  $A_1$  and  $A_2$  are calculated by a least-squares analysis from the observed  $S^{-1}$  values.

The heat capacity is computed from  $C_t = \Delta Q/\Delta T = (V_S V_N t / R_N) (dR/dT) / (\Delta U.S^{-1})$ . The heat capacity of the addenda,  $C_A$ , measured in a separate run, is subtracted from the observed heat capacity. The specific heat is subsequently computed from  $C = (C_t - C_A)/m$ , where  $m$  is the mass of the specimen.

The thermometer is calibrated **after** the actual specific-heat measurements. Helium exchange gas is used to establish heat contact with the bath. Sometimes the calibration at  $H_2$  temperatures was carried out prior to the specific-heat measurements, but this did not involve difficulties because the cryostat could be readily evacuated at 20 K. In a few experiments separate calibrations made with the heat switch and with exchange gas have been compared. The observed differences were insignificant. However, to be certain that the specimen attains the temperature of the bath in all circumstances, exchange gas is preferred.

Magnetic fields are obtained by means of an Oerlikon C3 magnet capable of producing 27 kOe at the distance of the pole pieces used in the experiments (90 mm). Fields have been calibrated to an accuracy of a few percent by means of an induction coil. Thermometer calibrations can be carried out in exactly the same way as in zero field; a small negative resistance change is observed at high temperatures and a positive one at low temperatures.

The preparation of the specimens is described in Appendix I and, if necessary, in the text.

## II.6. Test measurements on high-purity copper

In this section the presently obtained specific heat on two copper specimens will be discussed with emphasis on the accuracy of the results. These measurements were carried out to test the calibration procedure described in section II.4. Comparison with results obtained in other recent high-accuracy measurements will be made.

Copper has been widely used as a standard for low-temperature specific-heat measurements. Numerous measurements carried out in the range of temperatures below 300 K have been reported. Furukawa et al. [18] have compiled all data in this range reported from 1914 to early 1967. They carried out a critical analysis of these data evaluating the accuracy of each of them. A table of 'selected values' has been compiled for the specific heat, together with related quantities such as entropy etc. Approximately at the same time Osborne et al. [19] proposed a 'reference equation' for the specific heat in the range of temperatures between 1 and 30 K on the basis of measurements carried out in the preceding ten years. The 'reference equation' expresses the specific heat in terms of a polynomial of odd powers of  $T$  up to  $T^{11}$ . Preference will be given to the analysis in terms of the 'reference equation', which is easy to handle with a computer. The 'selected values', however, could just as well be used because mutual differences hardly exceed 0.1%.

It is well-known that minute quantities of transition elements, dissolved in copper, may affect the specific heat considerably (see e.g. Martin [20]). For this reason a program was started at the 19<sup>th</sup> Annual Calorimetry Conference, 1965, which offers the possibility to compare the specific heat of samples taken from a single 20 kg batch cast from high-purity ASARCO-copper, 99.999 + % Cu [19]. These samples are available from the Argonne National Laboratory, Ill. \*). The purity of the samples is such that the specific heat due to impurities is expected to be smaller than 0.1% at 1 K. The sample used in this investigation has been labelled T 3.4 and will be further denoted as Cu II. Another sample (Cu I) has been prepared in this laboratory (Appendix I).

Barron and Morrison [21] have derived theoretically that the specific heat at low temperatures of a metal can be represented by

$$C = \gamma T + \beta T^3 + \delta T^5 + \dots \quad (\text{II.6})$$

where the first term is the electronic specific heat and the remaining terms are a low-temperature expansion for the lattice specific heat. Osborne et al. [19] have fitted the specific heat of copper below 30 K to this equation; the 'reference equation'

$$C_{\text{r.e.}} = \sum_{i=1}^6 A_i T^{2i-1} \quad (\text{II.7})$$

\*) We are indebted to Dr. D.W. Osborne for making one of these samples available to us.

The six coefficients  $A_j$  are given in table II.1. It was shown that six terms were sufficient to represent the specific heat of copper; no significant improvement of the standard deviation was obtained when more terms were included.

The difference of the specific-heat data of Cu I and Cu II with  $C_{r.e.}$  is shown in fig. II.5 (circles). As can be seen the present data are, on an average, slightly higher than  $C_{r.e.}$ . The results of Cu I and Cu II have also been fitted directly to an expression having the form of eq. (II.7), giving each experimental point  $j$  a weight  $C_j^{-2}$ . This means that relative deviations of the measured specific heat were minimized. The computed coefficients are given in table II.1, together with those obtained by other workers. The standard fractional deviations are 0.22% and 0.24%

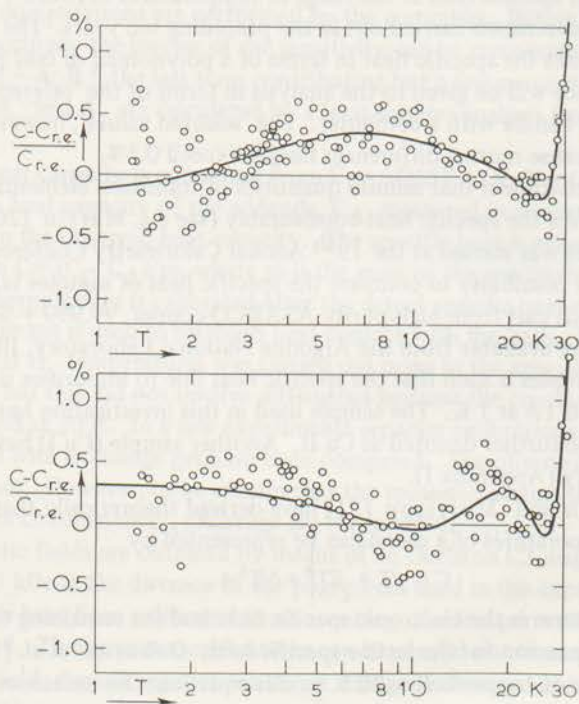


fig. II.5. Relative deviations of the measured specific-heat points from  $C_{r.e.}$ . The curves represent the deviations of the mean specific heat calculated from eq. II.8, using the coefficients listed in table II.1.

for Cu I and Cu II, respectively. Computed specific-heat values are given in Appendix II at one degree intervals, together with percentage deviations from  $C_{r.e.}$ . The differences of the computed C-T relations with  $C_{r.e.}$  are shown as drawn curves in fig. II.5. It may be noted that these differences never exceed 0.35% for Cu I and 0.30% for Cu II in the range of temperatures between 1 and 28 K.

Table II.1

C in mJ/(g at) K					
	$C_{r.e.}$ [19]	Cu I	Cu II	Ahlers [22]	Gmelin [23]
$A_1$	$6.9434 \times 10^{-1}$	$6.9327 \times 10^{-1}$	$6.9677 \times 10^{-1}$	$6.9597 \times 10^{-1}$	$6.9691 \times 10^{-2}$
$A_2$	$4.7548 \times 10^{-2}$	$4.7878 \times 10^{-2}$	$4.7586 \times 10^{-2}$	$4.7828 \times 10^{-2}$	$4.7524 \times 10^{-2}$
$A_3$	$1.6314 \times 10^{-6}$	$-7.2188 \times 10^{-7}$	$-5.1337 \times 10^{-7}$	$-1.2613 \times 10^{-5}$	$1.775 \times 10^{-6}$
$A_4$	$9.4786 \times 10^{-8}$	$1.0407 \times 10^{-7}$	$1.1159 \times 10^{-7}$	$2.1747 \times 10^{-7}$	$9.6185 \times 10^{-8}$
$A_5$	$-1.3639 \times 10^{-10}$	$-1.5516 \times 10^{-10}$	$-1.7230 \times 10^{-10}$	$-4.9552 \times 10^{-10}$	$-1.4372 \times 10^{-10}$
$A_6$	$5.3898 \times 10^{-14}$	$6.6967 \times 10^{-14}$	$7.6796 \times 10^{-14}$	$3.9236 \times 10^{-13}$	$6.1357 \times 10^{-14}$

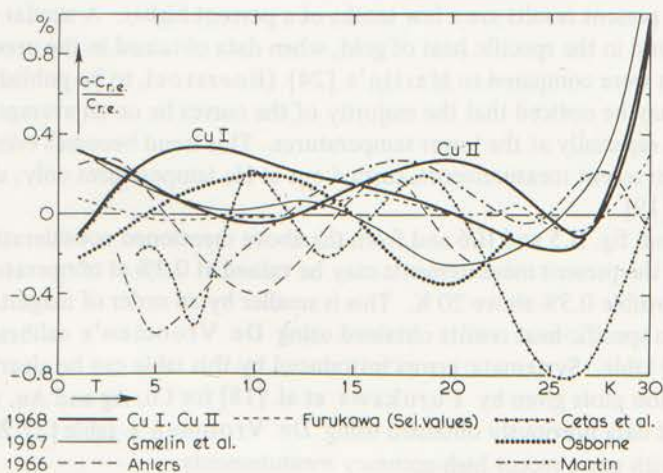


fig. II.6. Relative deviations from  $C_{r.e.}$  for Cu I and Cu II, for a number of recently reported specific-heat results on pure copper and for Furukawa's 'selected values'.

In fig. II.6 the same differences have been plotted on a linear temperature scale for all copper measurements in the temperature range between 1 and 30 K reported since 1966 [5,19,22-25], together with Furukawa's 'selected values' [19]. In all cases the inaccuracy was claimed to be 0.5% or less. All curves show oscillating deviations from  $C_{r.e.}$ . It is impossible, of course, to decide which result most accurately represents the specific heat of copper. However, a few tentative remarks can be made.

In general, differences between results obtained by different workers do not exceed 0.6%. The 'internal precision' of the measurements is often better than the accuracies stated. However, it is well-known that uncertainties may arise from the use of different temperature scales. Therefore, part of the observed oscillations may be due to temperature-scale errors. The specific heat above 20 K, as reported by Cetas et al. [25] deviates from all other measurements in this range of temperatures by almost 1%. In this investigation a new Pt-resistance temperature scale,  $T_{618}$  [26], has been used. However, it is hard to see whether this deviation is just accidental or due to this temperature scale.

In fig. II.6 all curves extending to temperatures above 25 K, except Martin's [24], rapidly curve upwards above 27 K. Furthermore, the 'reference equation' has been based solely on Martin's data at temperatures above 25 K. Therefore, it may be quite possible that Martin's results are in error by almost 1% at 30 K. At about 5 K Martin's results are about 0.6% lower than  $C_{r.e.}$ , whereas the present results are a few tenths of a percent higher. A similar deviation has been found in the specific heat of gold, when data obtained in the present investigation were compared to Martin's [24] (Boerstael, to be published [29]). Finally, it may be noticed that the majority of the curves lie on an average slightly above  $C_{r.e.}$ , especially at the lower temperatures. This trend becomes even more evident when recent measurements, carried out at He temperatures only, also are considered [19].

From fig. II.5 and II.6 and from the above mentioned considerations the accuracy of the present measurements may be valued at 0.3% at temperatures below 20 K and possible 0.5% above 20 K. This is smaller by an order of magnitude when compared to specific-heat results obtained using De Vroomen's calibration method and table. Systematic errors introduced by this table can be clearly seen from deviation plots given by Furukawa et al. [18] for Cu, Ag and Au, where specific-heat data previously obtained using De Vroomen's table [27,28] are compared with more recent high-accuracy measurements.

## II.7. Specific heat of Palladium, Platinum and Gold

In order to evaluate the excess specific heat of dilute Pd, Pt and Au alloys presented in the next chapters, accurate values of the specific heat of their base metals are required in the range of temperatures between 1 and 30 K. As no sufficiently accurate measurements have been reported for this range it was necessary to carry out specific-heat measurements on these metals. A full account of this work will be given elsewhere [29].

The specific heats of Pd and Pt have been analysed in terms of the expression

$$C = \sum_{i=1}^6 A_i T^{2i-1} \quad (\text{II.8})$$

Just as in the case of Cu 6 coefficients were found to be sufficient to represent the specific heat between 1 and 30 K. These coefficients and the specific heat computed from eq. (II.8), using the appropriate coefficients have been tabulated in Appendix II.

Due to the rapid increase of the specific heat of Au many more coefficients would be required to represent the specific heat between 1 and 30 K. Therefore, the Au results have been analysed graphically for temperatures above 4.3 K and, according to a three-terms expression, analogous to eq. (II.8), for temperatures below 4.3 K. The specific heat of Au has also been tabulated in Appendix II.

## References

1. F.J. du Chatenier, Thesis, Leiden, 1964.
2. A.R. de Vroomen, Thesis, Leiden, 1959. Bull. Inst. int. Froid, Leuven, Annexe 1958-1, 137.
3. J.H. Colwell, Rev. sci. Instr. 40(1969) 1182.
4. R.W. Hill and G.R. Picket, Ann. Acad. sci. Fennicae AVI, No. 210 (1966) 40.
5. B.M. Boerstoel, W.J.J. van Dissel and M.B.M. Jacobs, Physica 38 (1968) 287, Comm. Kam. Onnes Lab., Leiden, No. 363a.
6. R. Berman, J. appl. Phys. 27 (1956) 318.
7. R. Berman and C.F. Mate, Nature 182 (1958) 1662.
8. E. Gmelin, Cryogenics 7 (1967) 225.
9. R.G. Scurlock and E.M. Wray, J. sci. Instr. 42 (1965) 421.
10. W.M. Star, J.E. van Dam and C. van Baarle, J. Phys. E 2 (1969) 257.
11. F.G. Brickwedde, H. van Dijk, M. Durieux, J.R. Clement and J.K. Logan, J. Res. natl. Bur. Std. 64A (1960) 1.
12. M. Durieux, H. van Dijk, H. ter Harmsel and C. van Rijn, Temperature, its Measurement and Control in Science and Industry (Reinhold, New York, 1963), vol. 3, p. 383.
13. M. Durieux, Thesis, Leiden, 1960.
14. D.E. Moody and P. Rhodes, Cryogenics 3 (1963) 77.
15. D.R. Hartree, Numerical Analysis, Oxford University Press, London, 1955, p. 194.
16. W.H. Keesom and J.A. Kok, Proc. kon. Akad. Wet., Amsterdam 35 (1932) 294 and 35 (1932) 301, Comm. Leiden, No. 219c and 219d, resp.
17. J. Ferreira da Silva, Thesis, Leiden, 1967.
18. G.T. Furukawa, W.G. Saba and M.L. Reilly, National Standards Reference Data Series - Nat. Bur. Std. 18, 1968.
19. D.W. Osborne, H.E. Flotow and F. Schreiner, Rev. sci. Instr. 38 (1967) 159.
20. D.L. Martin, Rev. sci. Instr. 38 (1967) 1738.
21. T.H.K. Barron and J.A. Morrison, Can. J. Phys. 35 (1957) 799.
22. G. Ahlers, Rev. sci. Instr. 37 (1966) 477.
23. E. Gmelin and K.H. Gobrecht, Z. ang. Phys. 24 (1967) 21.
24. D.L. Martin, Phys. Rev. 141 (1966) 576.
25. T.C. Cetas, C.R. Tilford and C.A. Swenson, Phys. Rev. 174 (1968) 835.
26. J.S. Rogers, R.J. Tainsh, M.S. Anderson and C.A. Swenson, Metrologia 4 (1968) 47.
27. F.J. du Chatenier and J. de Nobel, Physica 32 (1966) 1097, Comm. Leiden, No. 347c.
28. F.J. du Chatenier, J. de Nobel and B.M. Boerstoel, Physica 32 (1966) 561, Comm. Leiden, No. 347a.
29. B.M. Boerstoel, to be published.

## Chapter III

### REVIEW OF THE LITERATURE

#### III.1. Introduction

Palladium and a number of palladium alloys exhibit a series of remarkable and interesting magnetic properties at low temperatures. Although to a lesser extent, the same is true for the corresponding alloys of platinum. Pure palladium may be characterized as a nearly ferromagnetic metal [1,2], sometimes called an incipient ferromagnet (it has once been said that Pd might be regarded as a ferromagnet with a transition temperature of about - 10 K). It has a very high paramagnetic susceptibility and is, accordingly, easily polarized (i.e. magnetized). A strong magnetic polarization of the Pd-matrix is effected by a number of elements of the first row of transition metals in the periodic system (3d-elements), particularly by the elements Fe, Co and Ni. At the same time, this polarization of the matrix induces magnetic coupling between the 3d-moments carried by the solute atoms, leading to ferromagnetism of the alloys at low temperatures, even when the concentration of solute atoms is extremely low, e.g. as low as 0.05 at. %.

Following up earlier work of Gerstenberg [3] and of Crangle [4], Bozorth and coworkers [5] demonstrated in 1961 by means of magnetization and susceptibility measurements that ferromagnetism persists in Pd-Co alloys at Co contents as low as 0.1 at. %. Since then a large number of investigations have been carried out on many properties of dilute \*) Pd-Co, -Fe and -Ni alloys, showing that these alloys are ferromagnetic at concentrations even below 0.1 at. %, except for the Ni alloys which exhibit ferromagnetic behaviour at concentrations above 2 at. % only. Ferromagnetism has also been reported by Crangle [6,7] in alloys of Pd with a rare earth metal (4f-element), viz. Gd. In this case their ferromagnetic transition was not corroborated by resistivity measurements carried out by Sarachik and Shaltiel [8]. On the other hand, more recent resistivity experiments by Chen et al. [9] did show a ferromagnetic transition in dilute Pd-Gd alloys and also in Pd-Nd alloys.

---

\*) *The meaning of the word dilute is not always (properly) defined in the literature. In the present context it will mean that there is no appreciable direct interaction between the solute atoms.*

Alloys with Cr and with Ni at concentrations below 2 at. % show properties which are different from those found for the Co and Fe alloys. The behaviour of Pd-Cr is reminiscent of that of Cu-Fe and Au-V alloys which exhibit the so-called Kondo effect, recently reviewed by Kondo [10], Heeger [11], Abrikosov [12] and van Dam and van den Berg [13]. Pd-Ni alloys with concentrations below 2 at. % exhibit properties which in their turn resemble those observed for Pd-Cr alloys and which are usually described in terms of recently developed critical spin-fluctuation or paramagnon theories [14]. Speculations about a possible similarity between the Kondo effect and spin-fluctuation theory lie, however, outside the scope of the present investigation.

In view of the large number of investigations reported on the properties of Pd-Fe, -Co and -Ni alloys it is quite remarkable that the system Pd-Mn has so far attracted little attention and has not been explored until recently. Resistivity measurements carried out by Sarachik and Shaltiel [8] and by Williams and Loram [15] were indicative of ferromagnetic behaviour at low Mn concentrations. Recently this has been confirmed by magnetization and susceptibility measurements of Rault and Burger [16]. They found ferromagnetism at low concentrations, but at higher concentrations a gradual change towards antiferromagnetism was observed (i.e. the transition temperature, initially increasing with concentration, reaches a maximum at 2.5 at. % Mn and then decreases as the concentration is increased further; at concentrations above 8 at. % the alloys were found to be antiferromagnetic). From these observations it is tempting to conclude that, apart from the gradual change to antiferromagnetism at higher Mn content, which is most probably due to direct Mn-Mn interactions, the magnetic behaviour of Pd-Mn alloys is quite similar to that found in Pd-Fe or Pd-Co alloys. However, the present specific-heat measurements prove irrefutably that Pd-Mn alloys exhibit a magnetic behaviour quite different from that of the Co or Fe alloys (section IV.4).

Another remarkable property of Pd-Co, -Fe and -Ni alloys, i.e. those alloys from the series of Pd alloys mentioned so far which present the strongest tendency to ferromagnetism, is the large magnetic moment which has been found to be associated with each of the dissolved Co, Fe or Ni atoms, as was shown by the early measurements of Gerstenberg [3], Crangle [4] and Bozorth et al. [5]. These observations and those reported by a great many other investigators can be summarized as follows. For example, in the Co alloys, the saturation moment per Co atom first rises slowly from  $1.7 \mu_B$  in pure Co to about  $5 \mu_B$  in Pd<sub>90</sub>Co<sub>10</sub>, where  $\mu_B$  is the Bohr-magneton. Below 10 at. % Co, the saturation moment rises rapidly to values of about  $10 \mu_B$  at 0.1 at. % Co (see fig. III.1). A similar behaviour has been found in Pd-Fe and Pd-Ni alloys, although the moments are smaller in the latter case. These 'giant moments' have also been observed in Pt-Co and Pt-Fe alloys, the moments per solute atom being, however, appreciably smaller than those in the corresponding Pd-based alloys [7]. Obviously, such large moments cannot reside

entirely on the Co atoms \*), since the maximum moment arising from 3d-electrons cannot exceed  $5 \mu_B$  due to the Pauli exclusion principle. Therefore, part of the observed moment must be due to the polarization of the matrix. Models proposed to explain the giant moments will be discussed in due course. The possibility that the giant moment is associated with some kind of 'giant spin' has been a point of considerable discussion in the literature, because some experiments could while others could not be interpreted in terms of a giant spin. This point will also be discussed later (section III.2.2 and IV.5).

Contrary to the Co, Fe and Ni moments in Pd there are experimental indications that Mn dissolved in Pd has a moment roughly equal to the one usually associated with the free  $Mn^{2+}$  ion ( $5 \mu_B$ ). In the case of Pd-Gd alloys the moment per solute atom has been found to be smaller than the 'free'  $Gd^{3+}$  moment ( $7 \mu_B$ ), which might indicate a negative polarization of the Pd matrix [17]. At the same time the transition temperatures of the Mn and Gd alloys increase much less rapidly as a function of concentration than do those of the Co, Fe and Ni alloys. These points will be a basis for some speculations concerning the different behaviour of the specific heat of these alloys (section IV.4 and V.3).

In the next section results of experiments on various properties of Pd alloys are reviewed. One can use the following simple model in order to understand many of the properties of dilute ferromagnetic alloys. When an Fe atom is dissolved into Pd it carries a magnetic moment, which polarizes its Pd environment by exchange interaction. In a local picture one might attribute this to a polarization of the moments on the Pd atoms in the vicinity of the Fe atom, but in terms of the more appropriate band model it means that the Pd 4d-band is locally polarized. The giant moment consists of such a 'sphere' or 'complex' of polarized d-electrons rigidly coupled to the Fe moment, the latter thought to be fairly localized at the Fe site. From certain experiments it follows that the induced d-band polarization extends over large distances in the matrix; e.g. in Pd-Fe alloys it is still appreciable at  $10 \text{ \AA}$  from the Fe site. (i.e. at the thirteenth nearest-neighbour shell).

When the number of Fe atoms is increased the polarized d-electron spheres begin to overlap, effecting a decrease of the total moment per Fe atom. Moreover, when overlap occurs it offers the possibility of an effective interaction between the Fe moments leading to ferromagnetism at low temperatures. However, it should be noted at this stage that this model, bearing some resemblance to the localized picture of ferromagnetism in metals, is not the only way in which the magnetic state of the dilute alloys may be described. It has also been proposed that magnetic atoms enhance exchange effects in the narrow Pd 4d-band, already large in pure Pd, leading to

---

\*) In many respects Pd-Co and Pd-Fe alloys exhibit a similar behaviour. Therefore the words Co-atom or -ion and Fe-atom or -ion may be interchanged freely, unless the contrary is apparent from the context.

splitting of this band as is assumed in the itinerant picture of ferromagnetism. This means that bandferromagnetism appears below a certain critical temperature and at a concentration of dissolved magnetic atoms above a critical value, the latter case being relevant to e.g. Pd-Ni alloys. To date no explicit critical concentration, i.e. lower bound, has been observed in Pd-Fe and Pd-Co alloys.

### III.2. Review of experimental data

After the discussion of the two most striking phenomena of dilute Pd (and Pt) alloys, i.e. the occurrence of different types of magnetism at low concentrations of solute atoms and the large moments which in some cases appear to be associated with each of the solute atoms, a brief review will be given of experiments carried out on the properties of these alloys. The number of investigations has grown so rapidly, however, that it is not feasible to discuss all reports in detail; instead, some general comments will be made. Some cases which are important for the interpretation of the data will be considered at some length.

#### III.2.1. Magnetization and susceptibility

Magnetization ( $\sigma$ ) and susceptibility ( $\chi$ ) measurements on dilute ferromagnetic Pd-Fe, Pd-Co, Pt-Fe and Pt-Co alloys have been reported by a many-investigators [3-5, 7, 17-30]. In fact, as discussed in the introduction, the ferromagnetic behaviour of these alloys has been revealed by magnetization and susceptibility measurements. In general, the magnetization turns out to be a rather complicated function of magnetic field and temperature, especially at temperatures close to the transition temperature of the alloys. At low concentrations of solute atoms the magnetization associated with the local moments is of the same order of magnitude as the magnetization due to the large Pauli susceptibility of the alloys\*). A more serious problem is that the interpretation is hampered by effects arising from the statistical distribution of solute atoms in the matrix which may lead to local variations of the transition temperature. Several extrapolation schemes have been used to evaluate the saturation magnetization at  $T = 0$  and the (mean) transition temperature  $T_c$  (ferromagnetic Curie temperature) of the alloys.

The moment associated with each solute atom is calculated from the saturation magnetization at  $T = 0$  ( $\sigma(0,0)$ ). In order to obtain  $\sigma(0,0)$  from the measured magnetization versus magnetic-field isothermals some authors assume, for example, that  $\sigma(H,T)$  can be written as  $\sigma(H,T) = \sigma_L + \chi_m H$ , where  $\sigma_L$  is the local-moment magnetization and  $\chi_m$  is the matrix susceptibility, which is equal to  $\chi_{Pd}$  at low concentrations. At a given temperature the saturation magnetization

---

\*) It should be remembered that, although the moment associated with each solute atom is large, the magnetization per gram-atom of alloy is small.

$\sigma(0,T)$  is then obtained by extrapolation from the high-field data to  $H = 0$ , assuming the local moments to be completely saturated at high fields.  $\sigma(0,0)$  is subsequently obtained by extrapolation of a  $\sigma(0,T)$  versus  $T$  curve to  $T = 0$ .

The moments,  $n_B$ , associated with each solute atom, derived from magnetization measurements, are shown in fig. III.1 for Pd-Fe, Pd-Co, Pt-Fe and Pt-Co alloys at concentrations below 10 at. %, together with some data obtained from Mössbauer-effect (M) experiments.

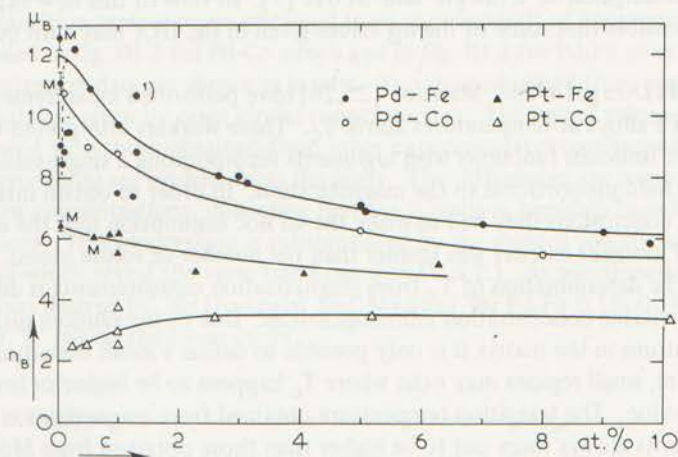


fig. III.1. Moment per solute atom  $n_B$ , expressed in Bohr-magnetons, versus concentration. All data have been obtained from magnetization and susceptibility measurements, excepts those indicated by M, which have been derived from Mössbauer experiments. Data sources: Pd-Fe,  $\sigma$  or  $\chi$ : ref. 4,7,18-22,26; M: ref. 43,51. Pd-Co,  $\sigma$  or  $\chi$ : ref. 5. Pt-Fe,  $\sigma$  or  $\chi$ : ref. 7,18,23; M: ref. 46,51. Pt-Co,  $\sigma$  or  $\chi$ : ref. 7,18,29. 1) Moment obtained by Phillips [22] when  $s$ -band polarization has been subtracted (see section III.2.3.).

The apparent decrease of  $n_B$  at very low concentrations observed for Pd-Fe (dashed curve, fig. III.1) and Pt-Co alloys by e.g. Crangle and Scott [7] has been explained by these authors as being due to the finite range of the induced matrix polarization. When the concentration is decreased some of the complexes cease to

be coupled to the magnetization of the whole specimen and do not contribute to the calculated  $n_B$  value. However, when measurements could be made in sufficiently strong fields the decrease would not occur. Indeed, these workers did not observe complete saturation at the lowest temperatures in fields up to 20 kOe. Recently, Foner and coworkers [31,29] (see also [28]) have shown experimentally that fields of 60 kOe for Pd-Fe and even over 100 kOe for Pt-Co are required to suppress nonlinear variations in the magnetization, even at temperatures low compared with  $T_C$ . This means that complete saturation (of  $\sigma_I$ ) has not been achieved in earlier measurements performed at fields up to only 20 or 30 kOe, in accordance with the assumption of Crangle and Scott [7]. In view of this new experimental fact it is possible that some of the  $n_B$  values given in fig. III.1 may turn out to be too small.

McDougald and Manuel [25,26] have performed measurements on very dilute Pd-Fe alloys at temperatures above  $T_C$ . These workers interpreted their results in terms of Brillouin functions with arguments incorporating a single-valued molecular field proportional to the magnetization. In order to obtain internally consistent conclusions they had to make the ad hoc assumption that the effective number of moment carriers was smaller than the number of solute atoms.

The determination of  $T_C$  from magnetization measurements is difficult in view of inevitable concentration inhomogeneities. Due to the random distribution of solute atoms in the matrix it is only possible to define a mean transition temperature, small regions may exist where  $T_C$  happens to be higher or lower than the mean value. The transition temperature obtained from magnetization measurements always turns out to be higher than those obtained from Mössbauer and resistivity measurements and it seems to correspond to that temperature at which spontaneous magnetization first appears. Therefore it may depend on the detection limit of the experiment concerned. Further evidence for this interpretation comes from specific-heat measurements, because the transition temperature derived from magnetization experiments roughly corresponds to a temperature at which the high-temperature specific-heat tail falls beyond the limit of experimental accuracy. Craig et al. [21] first demonstrated experimentally the difference between the  $T_C$  values derived from magnetization and from Mössbauer experiments carried out on a Pd-Fe 2.65 at. % alloy. They found  $T_C = 106.6$  K from their magnetization and  $T_C = 90$  K from their hyperfine-field measurements using the Mössbauer effect.

The  $T_C$  values obtained from magnetization experiments also seem to depend upon the method of data analysis as shown by Craig et al. [21]. Using the classical Weiss-Forrer method [32] they obtained 106.6 K for Pd-Fe 2.65 at. %. Applying a more recent method [33-35], based on the molecular field model and making use of a series expansion of Brillouin functions, they arrived at  $T_C = 100$  K. In this method, which is now commonly used,  $H/\sigma$  is plotted as a function of  $\sigma^2$  at fixed temperatures near  $T_C$  (Arrott-plot). Straight lines can in general be drawn

through the high-field points. Subsequently, the intercepts of these lines on the  $\sigma^2$ -axis are plotted as a function of  $T$ . The temperature at which a curve drawn through these points intersects the  $T$ -axis is taken as the transition temperature. However, as mentioned above,  $T_C$  values obtained by this technique are still higher than those derived from other experiments. This has also been pointed out by McDougald and Manuel [26] who examined very low-field data; although a  $T_C$  value could have been obtained satisfactorily from their high-field data by the Arrott plot technique, this  $T_C$  was found to be considerably higher than the one they derived from their low-field measurements, the latter being in good agreement with the one obtained from other kinds of experiments.

Transition temperatures obtained from various kinds of experiments have been compiled in fig. III.2 for Pd-Co alloys and in fig. III.3 for Pd-Fe alloys. Low-concentration data are shown in inserts.  $T_C$  values obtained from magnetization measurements are given by open circles (upper curves). The higher values of these data compared with those obtained from other experiments (except from ferromagnetic resonance) are evident from the plots. The differences are comparatively largest at low concentrations, indicating that the transition becomes broader at lower concentrations. This observation is substantiated by the present specific-heat experiments which reveal the same trend (section IV.3.2.). As mentioned above the four  $T_C$  values derived by McDougald and Manuel for Pd-Fe 0.15, 0.10, 0.07 and 0.05 at. % fall on the lower curve.

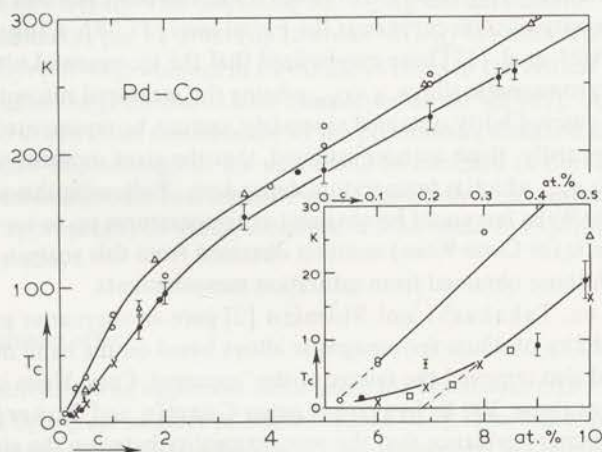


fig. III.2. Transition temperatures of Pd-Co alloys as a function of Co concentration  
Data sources:  $\sigma, \chi$  (O) ref. 3,5,18,20,85; ME (●) ref. 49,52;  $\rho$  (X) ref. 70;  
Ferrom. res. ( $\Delta$ ) ref. 81; Spec. Heat Max. ( $\square$ ) present work.

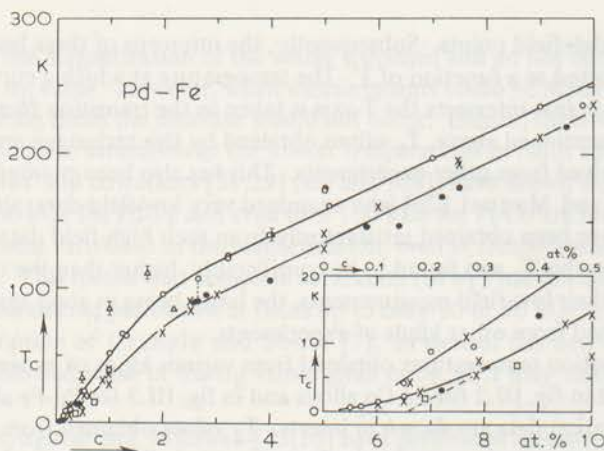


fig. III.3. Transition temperatures of Pd-Fe alloys as a function of Fe concentration  
 Data sources:  $\sigma, \chi$  (○) ref. 3,4,7,18-20,26; ME (●) ref. 21,50,55;  $\rho$  (X)  
 ref. 63,65-67,69; Ferrom. res. ( $\Delta$ ) ref. 81; Spec. Heat Max. ( $\square$ ) ref. 63,77.

The paramagnetic susceptibility of the alloys is also a complicated function of temperature and applied magnetic field [3,5,17-20,23]. Moreover, the susceptibility of pure Pd is temperature dependent and extremely sensitive to traces of magnetic impurities (e.g. Fe) at low temperatures, as verified by Foner et al. [36]. The peculiar maximum of  $\chi_{Pd}$ , observed at about 85 K, has been ascribed to a particular shape of the density-of-state curve near the Fermi level [37,38]. Clogston et al. [19] and Shaltiel et al. [17] have emphasized that the incremental susceptibility of the dilute ferromagnetic alloys,  $\chi - \chi_m$ ,  $\chi$  being the measured susceptibility and  $\chi_m$  the matrix susceptibility obtained separately, cannot be represented by a Curie-Weiss law. Essentially, these authors assumed, that the giant moment would be proportional to  $\chi_m$ , which is temperature dependent. Following this procedure an 'apparent' Curie-Weiss law could be obtained at temperatures up to room temperature. The paramagnetic (or Curie-Weiss) moment obtained from this analysis was in fair agreement with those obtained from saturation measurements.

Later on, Takahashi and Shimizu [2] gave an alternative explanation of the susceptibility of dilute ferromagnetic alloys based on the band model of ferromagnetism, and also removed the failure of the 'apparent' Curie-Weiss law analysis for temperatures above 300 K. In a recent paper Guertin and Foner [30] presented preliminary evidence that the proportionality between the giant moment and  $\chi_m$  would not be entirely justified. Yet, the data seem to provide enough evidence to conclude that the giant moment still exists at temperatures above the ferromagnetic Curie temperature, indicating that the induced polarization of the Pd matrix is rigidly coupled to the moment of the solute atom. This conclusion

forms a crucial point in the interpretation of the entropy removed in the transition from the disordered to the ordered state (section IV.5).

As was referred to in the introduction, some magnetization and susceptibility measurements on Pd-Mn alloys have been reported by Rault and Burger [16]. Earlier data on one alloy (3 at. %) were given by Shaltiel et al. [17]. From the latter measurements it was concluded that the moment per Mn atom was only slightly larger than the  $Mn^{++}$  moment. No experiments on Pt-Mn alloys have been reported to date. Measurements on ferromagnetic Pd-Ni alloys have been reported by Gerstenberg [3], Bozorth et al. [18], Burger [20], Shaltiel et al. [17] and Crangle and Scott [7]. The general behaviour of these alloys is quite similar to that of Pd-Fe or Pd-Co alloys. The moments per Ni atom are larger than the moment in pure Ni ( $0.61 \mu_B$ ) but, on the other hand, appreciably smaller than those in Pd-Fe or Pd-Co alloys.

The phenomenon of ferromagnetism in dilute alloys is not restricted to Pd or Pt-based alloys. By means of magnetization and susceptibility measurements ferromagnetism has been detected e.g. in Pd-Ag, Pd-Cu and Pd-Rh alloys containing 1 at. % Co by Bozorth et al. [18], in Pd-Rh alloys containing 1 at. % Fe by Clogston et al. [19] and in Pt-Ir alloys with 1 at. % Fe by Geballe et al. [23], at concentrations up to roughly 40 at. % Ag or Cu and 50 at. % Rh or Ir (see also ref. 30). In all these cases giant moments are observed. In Pd-Rh and Pt-Ir alloys at Rh and Ir concentrations up to 7 at. % moments larger than those in Pd and Pt, respectively, have been found. Beyond this limit and in all Ag and Cu alloys the moment decreases rapidly with increasing Rh, Ir, Ag and Cu content. The occurrence of very large moments per Fe atom (up to about  $40 \mu_B$ ) has been reported in  $Ni_3Ga$  and  $Ni_3Al$  alloys [39-41], whereas in Cu-Ni alloys close to the critical concentration for ferromagnetism large moments have been reported on Mn [42]. Although these results bear no doubt close resemblance to the phenomena observed in Pd and Pt alloys, the review and subsequent discussion will be confined to the latter cases, because the present specific-heat measurements have only been performed on these alloys. When appropriate, however, reference will be made to experiments carried out on ternary alloys.

### III.2.2. Mössbauer effect

Measurements of hyperfine fields using the Mössbauer effect (ME) have been reported by a great number of workers [21,43-55]. The ME is an effective tool to study dilute magnetic systems because (1) measurements are possible at concentrations low enough to eliminate interactions among the solute atoms (paramagnetic systems) and (2) the Curie temperature of ferromagnetic alloys can be obtained directly from measurements in zero magnetic field, and is accordingly not subject to uncertainties arising from extrapolation methods to zero field. The most

commonly used Mössbauer isotope is  $^{57}\text{Fe}$ , while the  $^{119}\text{Sn}$  isotope has also been used [52,53]. The splitting of the  $^{57}\text{Fe}$  nuclear levels arises from the hyperfine field  $H_i$  acting on the  $^{57}\text{Fe}$  nucleus. The major contribution to this field arises from the Fermi-contact term and can be expressed by  $H_c = (8\pi/3) g \mu_B [\rho_+(0) - \rho_-(0)]$ , where  $[\rho_+(0) - \rho_-(0)]$  is the difference in density at the nucleus of s-like electrons with spin up and spin down with respect to some reference direction (e.g. the applied field) [47].  $H_i$  is thus a magnetic field characteristic of  $^{57}\text{Fe}$  in its environment because the polarization of s-like electrons is assumed to emanate principally from overlap with the d-electrons about the Fe in the host;  $H_i$  is assumed to be proportional to the average moment  $\mu$  associated with the  $^{57}\text{Fe}$  atom [47], as discussed in detail by Watson and Freeman [57]. When an external magnetic field  $H$  is applied the total field acting on the nucleus is  $H_{\text{eff}} = H + H_i$ ; contributions to  $H_i$  other than  $H_c$  can be neglected [47].

In order to analyse the data one must rely upon some model describing the dependence of  $H_i$  upon  $H/T$ . For very dilute alloys ( $T_c$  much lower than the actual temperature) the localized moments are considered to be associated with completely free spins (paramagnetic system). The magnetic-field and temperature dependence of the time average of  $\mu$  is given by  $\langle \mu \rangle = \mu B_J (\mu H/kT)$ , where  $B_J (\mu H/kT)$  is the Brillouin function and  $J$  the spin associated with  $\mu$ . For such a system  $\langle H_i \rangle / H_{\text{sat}} = \langle \mu \rangle / \mu = B_J (\mu H/kT)$ , where  $H_{\text{sat}}$  is the hyperfine field at complete polarization [47]. Measurements on ferromagnetic alloys at temperatures below and above  $T_c$  are commonly analysed in terms of the molecular field model. In this case the hyperfine field is assumed to be proportional to the bulk specimen magnetization

$\langle H_i \rangle / H_{\text{sat}} = \langle \sigma \rangle / \sigma_{\text{sat}} = B_J \left( \frac{\mu H}{kT} \frac{3J}{J+1} \frac{T_c}{T} \frac{\langle \sigma \rangle}{\sigma_{\text{sat}}} \right)$ , where  $\langle \sigma \rangle$  and  $\sigma_{\text{sat}}$  refer to the specimen magnetization at temperature  $T$  and at  $T = 0$ , respectively. This expression has been verified to hold satisfactorily by Craig et al. [21].

The ME of very dilute Pd-Fe and Pt-Fe specimens has been measured by Craig et al. [43], Kitchens et al. [46], Maley et al. [51] and Blum and Frankel [54]. Provided the measurements are sufficiently accurate and carried out over a wide range of  $H/T$  values, the analysis in terms of Brillouin curves yields values of  $H_{\text{sat}}$ ,  $J$  and  $\mu$ . Craig et al. [43] obtained  $J = 13/2 \pm 3/2$  and  $\mu = 12.6 \pm 0.4 \mu_B$  for Pd-Fe, while Kitchens et al. [46] obtained  $1 \leq J \leq 4$  (and  $\mu = 6 \mu_B$  if  $J$  is chosen to be 2) for Pt-Fe 0.6 at. %. The large uncertainties in  $J$  are due to the fact that the Brillouin curves are not very sensitive to variations of  $J$ . Moreover, it follows from magnetization measurements [7] that the Pt-Fe alloy used by Kitchens et al. would be ferromagnetic at the temperatures at which the ME was measured; the condition that Fe-Fe interaction should be negligible may not have been satisfied in this sample.

Recently, Maley et al. [51] have reinvestigated the ME of  $^{57}\text{Fe}$  dissolved in Pd and Pt (<0.1 at. % Fe) with improved precision in order to examine the

disagreement between spin values obtained from ME studies on paramagnetic specimens on the one hand, and from specific-heat and ME studies on specimens in the ferromagnetic state ( $J \approx 1-2$ ; see below and section IV.5) on the other hand. The parameters deduced from their data by a computer fit to Brillouin curves were:  $J = 3.76 \pm 0.4$ ,  $\mu = 11.1 \pm 0.3 \mu_B$  for Pd-Fe and  $J = 2.98 \pm 0.18$ ,  $\mu = 6.46 \pm 0.13 \mu_B$  for Pt-Fe. At temperatures below 4 K, however, marked deviations from 'free-spin behaviour' have been observed. The substantial reduction of  $J$  compared with the previously reported value for Pd-Fe [43] is, however, still insufficient to account for the disagreement with  $J$ -values deduced from other properties. In a recent short note Blum and Frankel [54] state that their low  $H/T$  data 'do not uniquely fit to any proposed model'. A further discussion of this problem will be given in section IV.5. Moments per Fe atom deduced from ME studies have been indicated by an M in fig. III.1.

A number of experiments have been performed to investigate the order-disorder transition of Pd-Fe [21,47,48,50,55] and Pd-Co alloys [49,52]. The results can be summarized as follows. (1) The  $H_i/H_{\text{sat}}$  versus  $T$  curve of a Pd-Fe 2.65 at. % alloy obtained by Craig et al. [21] can be represented satisfactorily, but perhaps fortuitously, by a molecular-field curve for  $J = 1$  (Woodhams et al. [48] obtained  $J = 2 \pm 1$  from similar experiments). In applied magnetic fields the measured curves deviate from any curve calculated on the basis of the molecular-field theory, except at  $T \gg T_c$  where agreement is found with curves for  $J = 4$  in reasonable accordance with the ME studies in the paramagnetic state discussed above. (2) The transition is remarkably sharp for the sample used by Craig and coworkers ( $T_c = 90 \pm 1$  K). The transition temperature is chosen to be that temperature at which the single Mössbauer line observed in the paramagnetic state begins to broaden. Other workers have studied less-concentrated alloys and observed a broader transition. Dunlap and Dash [49] and Trousdale et al. [50] could explain their results reasonably well on the basis of a molecular-field-model calculation, taking into account the statistical concentration variations by means of a Gaussian distribution function. As already mentioned in section III.2.1, in all cases the (mean) Curie temperatures are appreciably lower than those deduced from magnetization data. Curie temperatures (dots) obtained from ME studies on Pd-Fe and Pd-Co alloys obviously scatter around the lower curves in fig. III.2 and fig. III.3, respectively. (3) Line broadening has been observed by Woodhams et al. [48], Trousdale et al. [50] and Carlow and Meads [55]. This broadening increases progressively at increasing velocity. This effect has been interpreted as resulting from the distribution of hyperfine fields due to the statistical distribution of Fe atoms in the Pd-host. On the other hand, unique hyperfine-field values have been reported by Nagle et al. [44] and Craig et al. [45] for more concentrated Pd-Co and Pd-Fe alloys and by Skalski et al. [56] from nuclear magnetic resonance (NMR) experiments. This apparent contradiction noticed by Woodhams et al. [48] can, however, be elucidated.

### III.2.3. Neutron scattering

Neutron-scattering methods can yield information on the distribution of magnetic moment on atomic scale in magnetically ordering systems. Neutron-diffraction studies have been carried out on Pd-Fe alloys by Cable et al. [58] and by Phillips [22], and on Pd-Fe and Pd-Co alloys by Low and coworkers [59-61].

Cable et al. [58] investigated two disordered Pd-Fe specimens (3 and 7 at. % Fe) by means of diffuse neutron scattering in combination with magnetization measurements. Assuming that all Pd atoms carry the same moment it could be inferred from their experiments that the 3d-moment on the Fe atoms in both alloys is  $3.0 \pm 0.2 \mu_B$ , while the moment on the Pd atoms is  $0.15 \pm 0.01$  and  $0.26 \pm 0.02 \mu_B$ /Pd-atom for the 3 and 7 at. % alloys, respectively.

Low and coworkers [59,60] developed a special technique utilizing diffuse elastic scattering of long-wavelength neutrons ( $\lambda \approx 5 \text{ \AA}$ ) which enables the spatial distribution of magnetic-moment density in the vicinity of Fe or Co atoms dissolved in Pd to be examined. Polycrystalline specimens containing 0.25 to 4 at. % Fe or Co have been studied. At low concentrations the scattering cross-section shows a strong peak in the forward direction, whereas at higher concentrations a progressive loss of this peak is observed; for the 4 at. % alloys the cross-section has become independent of the scattering vector. Due to the largely different scattering form factors of Pd and Co or Fe the small-angle peak arises from the moments on the Pd atoms, whereas at higher scattering vectors the contribution from the 3d-moment on the Fe atoms dominates. The results have been interpreted as follows: at low concentrations the moment density pattern around each Fe or Co is assumed to be hardly distorted by overlap, and consequently reflects the pattern at 'infinite dilution'. When the amount of Fe or Co is increased effects arising from overlap of moment patterns become significant. At 4 at. % the moment distribution has become virtually uniform.

From their results on Pd-Fe 0.25 at. % and Pd-Co 0.3 at. % these workers obtained a diagram showing the 4d-moment density as a function of the distance from the solute site, as reproduced in fig. III.4, assuming the moment density to be spherically symmetric [60]. The long-range nature of the polarization is evident from the graph. On the other hand, as emphasized by the authors, the magnitude of the moment density is very small (about  $0.05 \mu_B$  on Pd atoms at nearest-neighbour distance  $\approx 2.75 \text{ \AA}$ ) and the giant moment arises from the large number of Pd atoms (about 300) involved in the polarization. Evidently, the observed polarization range accounts for the extremely low concentrations at which ferromagnetism has been found to persist in Pd alloys.

It is interesting to note here that Dunlap and Dash [49] and Trousdale et al. [50] have analysed their ME data of Pd-Co and Pd-Fe, respectively, in terms of probability distributions describing the effect of statistical variations of the

solute-atom concentration in the Pd-host. Assuming further the magnetization distribution about an Fe or Co atom to be given by a Gaussian function:  $\propto \exp(-r^2/\bar{r}^2)$  and assuming the magnetization to approach saturation according to the molecular field model, they deduced the following values for the range parameter  $\bar{r}$ . For Pd-Co alloys  $\bar{r} = 11.5 \pm 1.2 \text{ \AA}$  [49] and for Pd-Fe alloys  $\bar{r} = 4.2 \text{ \AA}$  [50], see also footnote 31 ref. 49. In view of the crudeness of the models these values agree reasonably well with the ranges obtained from neutron diffraction (Pd-Co:  $4 \text{ \AA} < \bar{r} < 5 \text{ \AA}$ ; Pd-Fe:  $2.8 \text{ \AA} < \bar{r} < 3.2 \text{ \AA}$ ).

The 3d-moments on each Fe and Co atom have been determined to be  $3.5 \pm 0.4 \mu_B$  and  $2.1 \pm 0.3 \mu_B$ , respectively.

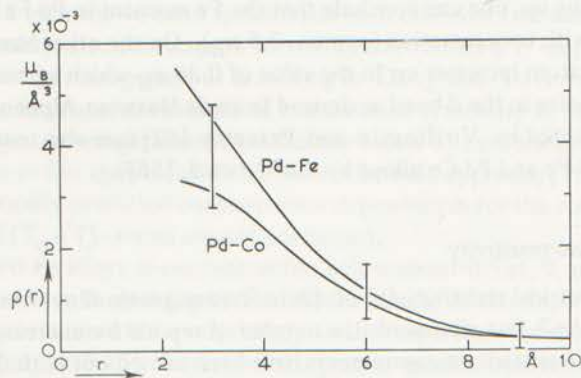


fig. III.4. Magnetic-moment density as a function of distance from solute site in dilute Pd-Fe and Pd-Co alloys. After Low and Holden [60].

In order to examine a possible anisotropy of the moment distribution in the matrix due to the highly anisotropic Fermi-surface of Pd, Hicks et al. [61] have studied a Pd-Fe 0.25 at. % single crystal in three directions by means of the same technique as used by Low and Holden [60]. Within the limits of experimental accuracy the scattering data in three different directions coincide. On the basis of a simple model the authors argue, however, that the lack of anisotropy does not necessarily indicate isotropy of the electronic properties of the alloys. Furthermore, the authors did not consider the possibility that statistical concentration variations might mask any anisotropy in the scattering data. Clearly, the experiments carried out by Low and coworkers have contributed much to the understanding of the phenomenon of ferromagnetism in dilute Pd alloys.

Phillips [22] has examined the magnetization distribution in a Pd-Fe 1.3 at. % single crystal, using polarized-beam neutron diffraction in combination with magnetization experiments. At the time the g-factors of Pd and Fe in Pd were not known. Assuming reasonable g-values the following moments per Fe atom could be deduced from the data: the 3d-moment localized on the Fe atoms is  $3.9 \pm 0.5 \mu_B$  and the (mean) 4d-moment associated with each atom is  $6.9 \pm 0.7 \mu_B$ . A negative conduction-electron (5s-) polarization (i.e. antiparallel to the 3d- and 4d- moments), amounting to  $-1.9 \pm 0.8 \mu_B$  per Fe atom, has been assumed in order to account for the discrepancy between the total d-moment calculated from the diffraction study ( $10.7 \mu_B/\text{Fe atom}$ ) and the total moment from magnetization experiments ( $8.8 \mu_B/\text{Fe atom}$ ). Both values have been inserted in fig.III.1. No other data are available which substantiate this negative conduction-electron polarization.

Summing up, one can conclude that the Fe moment in Pd-Fe alloys remains fairly constant with concentration (approx.  $3.5 \mu_B$ ). On the other hand, the mean moment per Pd atom increases up to the value of  $0.36 \mu_B$  which agrees well with the number of holes in the d-band as derived from de Haas-van Alphen effect data on pure Pd presented by Vuillemin and Priestly [62] (see also results for concentrated Pd-Fe and Pd-Co alloys by Cable et al. [58]).

#### III.2.4. Electrical resistivity

The electrical resistivity ( $\rho$ ) of dilute ferromagnetic alloys has hardly been studied before 1967, but afterwards the number of reports has increased rapidly [8,9,15,63-70]. Resistivity measurements have been carried out with different objectives such as determinations of  $T_C$ , the temperature dependence of  $\rho$  near  $T_C$  (critical behaviour) and the temperature dependence of  $\rho$  at  $T < T_C$  and  $T \ll T_C$ .

At low concentrations the resistivity and  $d\rho/dT$  generally increase with  $T$ ; in the vicinity of  $T_C$ , however, a marked decrease of  $d\rho/dT$  occurs when  $T$  increases. Qualitatively, the same description of the temperature dependence holds for the incremental resistivity,  $\Delta\rho(T) = \rho_{\text{alloy}} - \rho_{\text{Pd}}$ , and  $d(\Delta\rho)/dT$ . Some authors have determined  $T_C$  to be located at the point of inflection of the  $\Delta\rho$  versus  $T$  curve [15,63,65,69]. At higher concentrations, but for Pd-Co alloys even at fairly low concentrations (see below), the  $\rho$  versus  $T$  curve is rounded near  $T_C$ . Therefore, others [66-68] have obtained  $T_C$  for Pd-Fe alloys with Fe concentrations above 1 at. % assuming  $T_C$  to be located at the maximum of the  $d\rho/dT$  versus  $T$  curve; the relevance of this criterion would be supported by recent resistivity measurements near the critical temperature of pure Ni [71,72] and by theoretical arguments recently proposed by Fischer and Langer [73]. These authors, however, did not consider rounding effects due to e.g. concentration variations which may invalidate a precise determination of  $T_C$ . Likewise, an analysis of the critical behaviour of the resistivity in terms of power-laws (see ref. 74 for a recent review with emphasis on

transport properties) made by Longworth and Tsuei [67] and by Kawatra et al. [68] for Pd-Fe alloys should be considered as extremely questionable, since the results of such an analysis sensitively depend upon the value assumed for  $T_c$ . This point of view is supported by recent resistivity measurements on a Pd-Mn 1 at. % alloy and by calculations of the temperature dependence of the resistivity near  $T_c$ , incorporating a Gaussian distribution of  $T_c$ 's, which have been carried out by Nieuwenhuys \*).

The temperature and concentrations dependence of  $\Delta\rho$  has recently been studied by Williams and Loram for a number of Pd-Mn [15, see also 8], Pd-Fe [69] and Pd-Co alloys [70] over a wide range of temperatures below and above  $T_c$ . Fair agreement with the T-dependence at  $T \ll T_c$  predicted theoretically by Long and Turner [75] ( $\Delta\rho \propto T^{3/2}$  arising from s-electron scattering from spin waves in the coupled 3d-moment-4d-band system) has been observed (see also Theumann [76]). Commonly, electron-magnon scattering contributes a  $T^2$ -dependence at  $T \ll T_c$  in 'pure' ferromagnets, but according to Long and Turner the  $T^{3/2}$ -dependence arises from the absence of translational symmetry in random ferromagnetic alloys. At temperatures immediately below  $T_c$   $\Delta\rho$  varies proportionally to  $(T_c - T)$ , again in fair agreement with a molecular-field approach [75]. On the other hand, theoretically predicted concentration dependences for the coefficients of the  $T^{3/2}$ - and  $(T_c - T)$ -terms are not confirmed.

For Pd-Fe alloys at concentrations below about 0.5 at. % and Pd-Mn alloys at all concentrations studied (up to 3 at. %) the change of the slope of  $\Delta\rho$  versus T curves near  $T_c$  occurs within a surprisingly small temperature interval (in fact the transition is sharp) [69,15]. In view of the present specific-heat results (section IV.4) such a behaviour is not unexpected for Pd-Mn alloys, but it certainly is for Pd-Fe alloys of which the specific heat reflects a gradual magnetic transition. The resistivity transition of Pd-Co alloys, however, is not sharp at any concentration down to 0.098 at. % Co [70]. Instead, a gradual change of the T-dependence of  $\Delta\rho$  from  $\Delta\rho \propto T$  at  $T < T_c$  to  $\Delta\rho \approx \text{constant}$  at  $T > T_c$  has been observed. This behaviour is in agreement with the specific heat of Pd-Co alloys which shows a broad wedge-shaped transition which is, admittedly, comparatively wider than the corresponding transitions of Pd-Fe alloys at equal concentrations. Nevertheless the sharp resistivity transition of Pd-Fe alloys remains as yet difficult to understand.

$T_c$  values obtained from resistivity measurements are shown by crosses in fig.III.2 and fig. III.3; they clearly scatter around the lower curves.

---

\*) G.J. Nieuwenhuys, private communication.

### III.2.5. Specific heat

Some experiments have been reported on a number of Pd-Fe alloys by Veal and Rayne [77], by Montgomery and Cox [78] and, recently, on Pd-Co and Pt-Co alloys by Wheeler [79]. Results on 0.5 at. % solutions of Cr, Mn, Fe and Ni in Pt were published by Tsiovkin and Vol'kenshteyn [80]. All investigations, except Veal and Rayne's, have been carried out over a limited range of temperatures and consequently provide only fragmentary information. The magnetic-field dependence of the specific heat of a number of fairly concentrated Pd-Fe alloys has been studied by Montgomery and Cox [78].

The results of these investigations will often come up for discussion in the next chapters in connection with the present specific-heat studies. Consequently, a further discussion is postponed.

### III.2.6. Miscellaneous properties

The magnetization, ME, neutron scattering, resistivity and the specific heat of dilute ferromagnetic Pd (and Pt) alloys have been studied quite intensively. Measurements on some other properties have also been reported and will only be mentioned here. Reference to these reports will be made when pertinent to the present specific-heat studies.

Ferromagnetic resonance on a number of alloys has been reported by Bagguley et al. [81].  $T_C$  values obtained from these experiments have been indicated by triangles in fig. III.2 and fig. III.3; there is the same unsatisfactory feature in these  $T_C$  values in that they are considerably higher than those from other properties with the exception of the magnetization data. NMR studies have been reported by Skalski et al. [56] and EPR experiments by Shaltiel and coworkers [82, 83, 17]. Hyperfine fields acting on  $^{60}\text{Co}$  nuclei in Pd-Co alloys measured by means of anisotropy of  $\gamma$ -radiation from oriented nuclei have been studied by Cracknell et al. [84], by Parfenova et al. [85] and by Balabanov et al. [53]. Recently, Hörnfeldt et al. [86] reported de Haas-van Alphen effect studies on Pd-Co alloys which provide evidence of exchange splitting of the Fermi-surface, showing the existence of an itinerant contribution to the magnetization.

Finally, it should be stressed that by no means this review should be considered to be complete. Moreover, experiments on Pd-Ni alloys with concentrations below 2 at. % Ni have been left out (for experimental work on these alloys one is referred to ref. 87 and to references cited therein). Also the properties of the class of hydrogenated Pd alloys containing 3d-elements have not been discussed (see, however, Carlow and Meads [55] and references quoted in that paper).

### III.3. Some theoretical concepts

#### III.3.1. Ferromagnetism in metals

Since many years the problem of ferromagnetism in metals and alloys has been studied by a great many workers. Developments of microscopic theories have evolved along two lines, viz. those based upon the Heisenberg model (localized picture) and those based upon the band theory of metals (itinerant-electron theories). Besides, the molecular-field model introduced by Weiss [88] often provides a useful starting-point to the apprehension of the complex phenomena observed in ferromagnetic substances. An extensive recent review of the successes and deficiencies of localized models versus those of itinerant-electron models for ferromagnetism in metals has been given by Herring [89]; see also e.g. ref. 90. A short discussion is presented below.

In the Heisenberg model the moments are assumed to be localized on the atoms. The interaction of spins of different atoms is given by  $V_{ij} = -2(J_e)_{ij} S_i \cdot S_j$ , where  $(J_e)_{ij}$  is the exchange integral of electrons at atomic sites  $i$  and  $j$ . The exchange integral is only different from zero for nearest-neighbour atoms in this model. In order to obtain parallel coupling  $(J_e)_{ij}$  must be positive. Calculations have shown that with this model one cannot account e.g. for the transition temperatures of pure Fe, Co and Ni by one or two orders of magnitude [90]. Moreover, due to the atomic nature of the model, non-integral values of the saturation moments per atom as observed experimentally cannot be explained without making further assumptions [90]. For alloys consisting of magnetic and non-magnetic atoms, this model predicts ferromagnetism only at concentrations of magnetic atoms higher than a critical concentration,  $c_{\text{crit}}$  (see e.g. [91-93]). This concentration is of the order of  $1/(Z-1)$ , where  $Z$  is the number of nearest neighbours. For alloys with face-centred cubic structures  $c_{\text{crit}} \approx 0.09$ , which is substantially higher than the concentrations at which ferromagnetism is found in e.g. Pd-based alloys. Some calculations predict  $c_{\text{crit}}$  to be even higher (0.18 according to [93]).

The band theory of ferromagnetism has been developed by Stoner [94] within the framework of the electron theory of metals, and has been elaborated by many others. In Stoner's approach the interactions between the itinerant electrons, which are essential for ferromagnetism to occur, are taken into account by a molecular-field approximation. It shows that ferromagnetism is favoured by metals which possess a high density of states at the Fermi-level. In order to describe the influence of exchange interaction, states with 'spin-up' and 'spin-down' electrons are considered separately (the spin alignment being determined by some preference of direction due to secondary interactions with the lattice). In the ferromagnetic state the spin-up and spin-down bands are shifted in energy. If the number of electrons in the spin-up band exceeds that of electrons in the spin-down band by  $n$

per unit volume at  $T = 0$ , the molecular field is given by  $H_m = D\sigma = Dn\mu_B$ , where  $\sigma = n\mu_B$  is the saturation magnetization per unit volume and  $D$  is the molecular-field constant. Simple calculation then shows that the exchange energy is given by  $E_{\text{exch}} = -\frac{1}{2}Dn^2\mu_B^2$  and that the displacement at  $T = 0$  of the half-bands with respect to each other is given by  $Dn\mu_B^2$ .

The condition for ferromagnetism to occur is then determined by Fermi-Dirac statistics which takes full account of the Pauli-exclusion principle. Starting from the unmagnetized state, the decrease in energy by exchange interaction ( $\Delta E_{\text{exch}} = -\frac{1}{2}D\mu_B^2 n$ ) of one electron per unit volume which is transferred to an unoccupied state above the Fermi-level (Pauli-principle) should exceed its increase of kinetic energy  $\Delta E_{\text{kin}} = 2/N(E_F)$ .  $N(E_F)$  is the density of states per unit volume at the Fermi-energy of the unmagnetized state. Spontaneous magnetization arises when  $2D\mu_B^2 > 2/N(E_F)$  or  $DN(E_F)\mu_B^2 > 1$  (Stoner criterion). This expression shows that ferromagnetism is favoured by a high density of states at  $E_F$ . Equilibrium is reached when the Fermi-level of the spin-up band has shifted so far that additional transfer of an electron from the spin-down band becomes energetically unfavourable. The equilibrium condition is given by  $2D\mu_B^2 n = 1/N^+(E_m) + 1/N^-(E_m)$ , where  $N^+(E_m)$  and  $N^-(E_m)$  are the densities of states of the spin-up and spin-down bands respectively, at the Fermi-energy  $E_m$  of the ferromagnetic state. Clearly, knowledge of the band shape is required in order to calculate the equilibrium state.

Two situations may arise at  $T = 0$ . Firstly, it is possible that the spin-up band (majority band) is completely filled and the spin-down band (minority band) is filled up to  $E_m$ . Secondly, if the exchange energy is smaller, both the majority and the minority band may be partly filled up to  $E_m$ , with  $N^+(E_m) \neq N^-(E_m)$ . In 3d-metals the first situation seems to apply to Ni and Co, while the second one seems to occur in Fe. In order to calculate the temperature dependence of the magnetization the band structure must be known.

Stoner [95] has carried out such calculations assuming the bands to be parabolic (free-electron model). The calculated  $\sigma$  versus  $T$  curves are in broad qualitative agreement with experiment. Evidently, itinerant-electron models can simply account for the non-integral values of saturation moments, since these depend upon the shape of the density-of-states curve and upon the splitting of the band at  $T = 0$ .

In the Stoner model the effect of the exchange interactions is accounted for by the molecular-field constant  $D$ , and thus appears as an adjustable parameter. If, however, the exchange interaction is calculated from the wave functions it turns out that neither free-electron wave functions, nor wave functions of itinerant electrons constructed from more localized (atomic) wave functions provide, at present, a sound basis for the occurrence of ferromagnetism in metals. The difficulty is to account in a proper way for correlation effects arising from the Coulomb-repulsion between the electrons. For an extensive discussion see e.g. ref. 90.

Experimentally, as far as 3d-metals are concerned (and to a certain extent dilute ferromagnetic alloys as well) some properties can be accounted for by itinerant models, while other properties are described more satisfactorily in terms of local models. Theoretically, a similar picture has emerged, viz. in itinerant-electron models one has to allow for a certain degree of localization, and vice versa. Rhodes and Wohlfarth [96] have given a discussion of the properties of many ferromagnetic substances in terms of the localized and the so-called 'intermediate' model of ferromagnetism.

### III.3.2. Ferromagnetism in dilute Pd and Pt alloys

Theoretical interest in the properties of dilute Pd- and Pt-based alloys has mainly been focussed on the problem of the formation of the giant moment and the nature of the moment-density distribution in the matrix. Although many publications have been devoted to these problems, only a number of general ideas will be given below. Theories which account for the occurrence of a long-ranged polarization in Pd-based alloys have recently been reviewed by Anderson [97]. His exposition will be followed. Anderson first considers the response of a gas of free electrons to a space-dependent (exchange) field  $H(r)$ , generated by a localized moment. (This magnetic field measures the so-called s-d exchange interaction between a localized moment and the itinerant-electron moments). Introducing a susceptibility function  $\chi(r-r')$ , the induced moment  $\sigma(r)$  can be written in the linear response approximation as

$$\sigma(r) = \int \chi(r-r')H(r')dr' \quad (\text{III.1})$$

In order to calculate the moment distribution in the matrix around a local moment,  $\chi(r-r')$  should be calculated. This is usually done by Fourier-transformation, considering a susceptibility function  $\chi^\circ(q)$ , depending on the wave number  $q$ . For free electrons the magnetization at each wave number only responds to the corresponding field.

$$\sigma(q) = \chi^\circ(q)H(q), \quad \chi^\circ(q) = V^{-1} \int \chi(r-r') \exp[iq(r-r')]d(r-r').$$

For a free-electron gas  $\chi^\circ(q)$  has been calculated to be

$$\chi^\circ(q) = \sum_{\mathbf{k}} \frac{f_{\mathbf{k}+q} - f_{\mathbf{k}}}{\epsilon_{\mathbf{k}} - \epsilon_{\mathbf{k}+q}},$$

with  $f_{\mathbf{k}} = [1 + \exp(\epsilon_{\mathbf{k}}/k_B T)]^{-1}$ ,  $\epsilon_{\mathbf{k}} = \hbar^2 k^2 / 2m$ .

(In the present context the Boltzmann constant is denoted by  $k_B$ ).  $\chi^\circ(q)$  can be evaluated to

$$\chi^\circ(q) = \frac{\rho(0)}{2} \left[ 1 + \frac{4k_F^2 - q^2}{4k_F q} \ln \left| \frac{2k_F + q}{2k_F - q} \right| \right], \quad (\text{III.2})$$

with  $k_F$  the Fermi-momentum. Its Fourier transform is the Ruderman-Kittel-Kasuya-Yosida (RKKY) function [98-100]

$$F^\circ(r) = [\sin(2k_F r) - 2k_F r \cos(2k_F r)] / (2k_F r)^4, \quad (\text{III.3})$$

where  $r$  is the distance from the localized moment, see Anderson [101].

The functions  $\chi^\circ(q)$  and  $F^\circ(r)$  are shown in fig. III.5 as a function of  $q$  and  $r$ , respectively (full curves). As is evident from the figure  $F^\circ$  rapidly decreases ( $\propto 1/r^3$  at large  $r$ ) as a function of  $r$  and alternates in sign, the wavelength  $\pi/2k_F$  being of the order of the interatomic distance. The electron spin polarization induced by a local moment is highly localized in the vicinity of this moment. Due to the oscillatory character of  $F^\circ$ , interactions between local moments can lead to either parallel or anti-parallel coupling of these moments, depending on their mutual distance. This point has been emphasized first by Yosida [100], who considered the magnetic behaviour of dilute alloys of which Cu-Mn is a typical example. In these alloys the conduction electrons can in a good approximation be considered to be free. Due to the random distribution of solute atoms in the matrix the RKKY interaction leads to the complex ferromagnetic-antiferromagnetic behaviour of such alloys, discussed by many authors [100, 102-106].

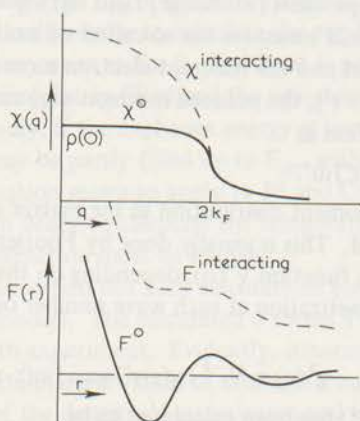


fig. III.5.  $\chi(q)$  versus  $q$  and  $F(r)$  versus  $r$ , as discussed in the text.

If the matrix is a transition metal, as e.g. in the case of Pd- or Pt-based alloys, the itinerant electrons can no longer be considered to be free electrons. In this case there can be considerable interaction between the host-metal d-electrons. Following again Anderson's discussion [97], suppose the electron gas has a moment density  $\sigma_d(r)$ . The exchange field is described by the relation  $h_{\text{exch}}(r) =$

$\int \bar{I}(\mathbf{r}-\mathbf{r}') \sigma_d(\mathbf{r}') d\mathbf{r}'$ , where  $\bar{I}$  measures the exchange interaction between the itinerant d-electrons (or holes). The effective field is given by  $h_{\text{eff}}(\mathbf{q}) = h(\mathbf{q}) + h_{\text{exch}}(\mathbf{q})$ , where  $h(\mathbf{q})$  is an external field (or a field due to a localized moment). Then

$$\sigma_d(\mathbf{q}) = \chi^\circ(\mathbf{q}) [h(\mathbf{q}) + \bar{I}(\mathbf{q}) \sigma_d(\mathbf{q})]$$

$$\sigma_d(\mathbf{q}) = \frac{\chi^\circ(\mathbf{q})}{1 - \bar{I}(\mathbf{q})\chi^\circ(\mathbf{q})} h(\mathbf{q})$$

or  $\chi_{\text{eff}} = \chi^\circ(\mathbf{q}) / [1 - \bar{I}(\mathbf{q})\chi^\circ(\mathbf{q})]$ . (III.4)

According to this equation the susceptibility  $\chi^\circ(\mathbf{q})$  is enhanced by a factor  $[1 - \bar{I}(\mathbf{q})\chi^\circ(\mathbf{q})]^{-1}$ . If  $\bar{I}(0)\chi^\circ(0)$  is large ( $\approx 1$ )  $\chi_{\text{eff}}$  becomes sharply peaked. As is seen from fig. III.5 (dashed curves) the shape of the susceptibility versus  $q$  and of the  $F$  versus  $r$  curves differ considerably from those of the free-electron case. Even in the absence of 3d-local moments the enhancement is large in such metals as Pd and Pt. Therefore these metals are sometimes called exchange-enhanced metals. The exchange-enhanced susceptibility at  $q = 0$  is given by

$$\chi_{\text{eff}}(0) = \chi^\circ(0) / [1 - \chi^\circ(0)\bar{I}(0)]. \quad (\text{III.5})$$

The enhancement factor  $[1 - \chi^\circ(0)\bar{I}(0)]^{-1}$  is about 10 for Pd. Ferromagnetism appears if  $\chi^\circ(0)\bar{I}(0)$  tends to 1. It is now believed that this condition is satisfied in Pd-Co and Pd-Fe alloys even at very low concentrations of Co or Fe atoms. In the case of Pd-Ni a minimum concentration of about 2 at. % Ni is apparently necessary to 'drive the alloy ferromagnetic' (see section III.1 and a recent report by Kim [107]). The spin polarization around a localized moment in exchange-enhanced metals is positive and long-ranged, as can be inferred from fig. III.5. Such a polarization appears to be corroborated by neutron-diffraction experiments on Pd-Fe and Pd-Co alloys as discussed in section III.2.3 (see fig. III.4). Calculations of the actual shape of the polarization have been published e.g. by Giovannini et al. [108] and by Kim and Schwartz [109].

Doniach and Wohlfarth [110] have also presented a treatment of the response of the Pd 4d-band electrons (or holes) to the spatially-dependent field generated by a localized moment on an Fe site. The calculation is based upon the s-d interaction model. In this model a localized moment has been assumed to exist in Pd-Fe and Pd-Co alloys (For a discussion of the occurrence of local moments one is referred to a recent article of Kim [107] and to references quoted therein).

The interaction between a set of localized spins  $S_i$  on the Fe sites  $X_i^{\text{Fe}}$  and the spin density  $(1/2)s(X_j)$  of the itinerant Pd holes (the interaction with 5s-electrons has not been considered) at  $X_j$  is described by the Hamiltonian

$$H = J_e \sum_i s(X_i^{\text{Fe}}) \cdot S_i, \quad (\text{III.6})$$

where  $J_e$  is the parameter measuring the exchange coupling. In order to calculate

the spatially-dependent induced moment, use has been made of the linear response approximation, as in Anderson's discussion (eq. (III.1)). As the authors point out the linear response does not seem to be unreasonable since the induced moment at nearest-neighbour distance is only  $0.06 \mu_B$  (see section III.2.3) as compared to the saturation moment of  $0.36 \mu_B$ /Pd-atom. Using essentially a molecular-field approximation the saturation moment per Fe atom (giant moment) was calculated to be

$$\mu = g\mu_B S(1 + \hat{J}_e \chi_{Pd}), \quad (\text{III.7})$$

where  $S$  is the maximum value of the Fe spin,  $\chi_{Pd}$  the static magnetic susceptibility of Pd and  $\hat{J}_e = 2J_e/Ng^2\mu_B^2$ .  $N$  is the number of Pd atoms. It may be noted that within the approximations made, the value of the giant moment is independent of the spatial distribution of the induced matrix polarization.

Relation (III.7) also applies to other strongly paramagnetic materials. In order to test this Doniach and Wohlfarth have plotted saturation moments per Fe atom for Fe dissolved in Pd and Pd-Ag, Pd-Rh and Pd-Pt alloys versus the matrix susceptibility of the latter materials. A reasonably good linear relationship was obtained. (Apparently,  $J_e$  depends only weakly upon the different matrices). From the fit to the experimental data the exchange parameter was found to be  $J_e = 0.15 \pm 0.02$  eV (or about  $k_B \times 1700$  K).

In order to account for the high-temperature susceptibility, relation (III.7) was generalized to

$$\mu(T) = g\mu_B S[1 + \hat{J}_e \chi_{Pd}(T)]. \quad (\text{III.8})$$

As mentioned earlier, the static susceptibility of Pd is markedly temperature dependent. According to eq. (III.8)  $\mu(T)$  may also be expected to be temperature dependent. Assuming the Pd spins to follow the Fe spins in their thermal motion (adiabatic approximation) the incremental susceptibility of the alloys can be shown to follow a Curie-Weiss law

$$\Delta\chi(T) = \chi_{\text{alloy}}(T) - \chi_{Pd}(T) = \frac{cN[\mu(T)]^2}{3k_B(T - T_c)} \frac{S+1}{S}. \quad (\text{III.9})$$

Hence,  $[(T - T_c)\Delta\chi(T)]^{1/2}$  should vary linearly with  $\chi_{Pd}(T)$ . Gerstenberg's [3] high-temperature susceptibility data on Pd-Fe 0.1 at. % have been used to test this relationship. At temperatures between 150 K and 750 K a reasonable linear fit was found. Above 750 K deviations occur which were ascribed to a break-down of the rigid coupling of the Pd spins to the Fe spin. The interaction parameter derived from this fit was in fair agreement with the one obtained from saturation data.

Two conclusions which are of importance for the interpretation of the entropy calculations presented in section IV.5 are suggested by this model. The form of eq. (III.7) suggests the thermal motion of the giant moments to be entirely determined by the proper Fe spin. Since, moreover, the giant moment apparently

persists at temperatures far beyond  $T_c$  the entropy associated with the ordering process of the giant moments corresponds to the multiplicity of the Fe spins only. As shown in section IV.5 this appears to be consistent with the data.

Theoretically, little is known about the specific heat of dilute ferromagnetic Pd and Pt alloys. Only recently, Cole and Turner [111] have reported a calculation of the specific heat (at  $H = 0$ ) of these alloys. Although the shape of the calculated  $C/T$  versus  $T$  curves resembles the experimental one, application of their formulae appears not to be feasible due to the complex temperature dependence of the calculated specific heat. The magnetic-field dependence of the specific heat has, as yet, not been studied theoretically.

A calculation, based on the Weiss molecular-field model, on the specific heat of dilute ferromagnetic alloys in the presence of strong magnetic fields is presented in chapter V\*). An analysis of the zero-field specific heat of Pd-Mn alloys is also given in that chapter.

## References

See references 1-112 of chapter IV, page 76.

---

\*) A similar calculation (for  $H = 0$ ) has previously been given by Takahashi and Shimizu [112].

## Chapter IV

### THE SPECIFIC HEAT OF DILUTE FERROMAGNETIC ALLOYS

#### IV.1. Introductory remarks

The present investigation into the specific heat of dilute ferromagnetic alloys has been initiated by experiments on a series of Pd-Co alloys. Because little was known at the time about the concentration dependence of  $T_c$  and about a possible lower bound for the occurrence of ferromagnetism in this system, a number of very dilute alloys were included in the series (see section IV.6). The facility to perform specific-heat measurements in external magnetic fields became available only in the course of the investigations, so that the field dependence of the specific heat has been studied only for part of the alloys. In order to allow a comparison between the specific heat of Pd-Co, Pd-Fe and Au-Fe alloys to be made, the specific heat of one Pd-Fe alloy and one Au-Fe alloy has been measured. The latter (Au-Fe), typified by a non-transition-metal base element does not exhibit ferromagnetism, but instead a complex ferromagnetic-antiferromagnetic ordering through the Ruderman-Kittel-Kasuya-Yosida (RKKY) mechanism (see section III.3.2). Both contain the same amount of Fe as one of the Pd-Co alloys contains Co (0.16 at. %). The specific heat of Pt-Co alloys and its magnetic field dependence has been studied primarily to investigate the effect upon these properties of the weaker exchange enhancement in Pt when compared to Pd. Finally, it seemed invertebrate that the system Pd-Mn would be an 'uninteresting' system in the series of Pd-alloys containing small amounts of Cr, Mn, Fe, Co and Ni, a conclusion which might have been drawn from available information (see section III.1). Unquestionably, this consideration has led to the most unexpected and remarkable results of this work, the temperature dependence of the specific heat of this system turning out to be entirely different from that of any other known dilute magnetic alloy, either transition-metal based or non-transition-metal based. The specific heat of the Pd-Mn system has, unfortunately, only been studied during the final stages of this work and, consequently, has not yet received the attention it deserves. However, various properties of these alloys are being studied at present more fully in the Metals Group of this laboratory.

The specific heat of the following specimens has been investigated:

Pd-Co: 0.017, 0.036, 0.075,	Au-Fe: 0.16 at. %
0.16, 0.24, 0.35 at. %	Pt-Co: 0.067, 0.5, 0.8 at. %
Pd-Fe: 0.16 at. %	Pd-Mn: 0.08, 0.19, 0.54, 1.35, 2.45 at. %.

A discussion of the preparation of the specimens has been given in Appendix I.

A number of preliminary results of the present specific-heat studies have already been published [113-117].

## IV.2. Presentation of specific-heat results on Pd, Pt and Au alloys containing Co or Fe

### IV.2.1. Pd-Co, Pd-Fe, Au-Fe

Fig. IV.1 shows the results obtained on Pd-Co 0.16 at. % in zero magnetic field and in two external magnetic fields. The data are given in a form in which specific-heat data on dilute magnetic alloys were commonly presented previously, viz. as a plot of  $C/T$  versus  $T$ . The lower curve shows the behaviour of pure Pd. The zero-field specific heat of this alloy (and of Pd-Co 0.24 at. %) has also been measured below 1 K in an apparatus described previously [118]\*).

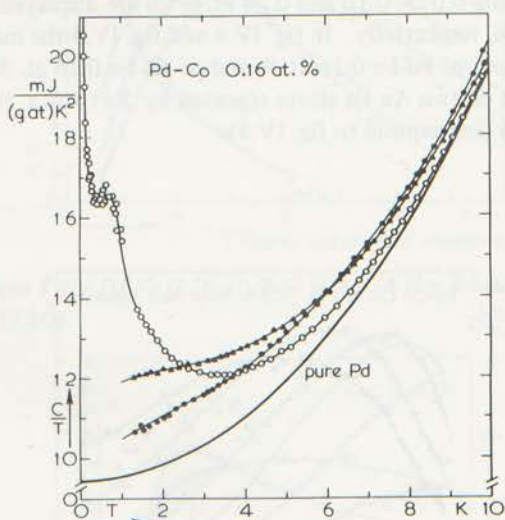


fig. IV.1.  $C/T$  versus  $T$  for Pd-Co 0.16 at. %.  $\circ H=0$ ,  $\blacktriangle H=9$  kOe,  $\bullet H=27$  kOe. The lower curves represent  $C/T$  of pure Pd. Note the shift of the ordinate scale.

\*) We are indebted to drs. E. Lagendijk and drs. H.W.J. Blöte, who measured the specific heat of these specimens and of one Pd-Mn alloy at  $T < 1$  K (figures IV.1, IV.6 and IV.12).

A number of features are immediately evident from this plot.

- The specific heat is strongly field dependent.
- In zero field  $C/T$  rises to very large values below 1 K, indicating that a large fraction of the magnetic entropy  $S_m$  is removed at these temperatures

$$(S_m(T)) = \int_0^T dT \{C - C_{Pd}\} / T.$$

- At the lowest temperatures, i.e.  $T < 0.3$  K, a hyperfine-field contribution is observed (see section IV.6).
- Although the magnetic contribution to the specific heat  $\Delta C = C_{\text{alloy}} - C_{Pd}$ , is large compared with  $C_{Pd}$  at the lowest temperatures and in zero field, an accurate determination of the shape of a  $\Delta C$  versus  $T$  curve makes high demands upon the accuracy of the measurements, due to the relative magnitude of  $\Delta C$  and  $C_{Pd}$  at higher temperatures and in applied magnetic fields. This is even more so when the specific heat of more-dilute alloys is studied.

As examples of  $\Delta C$  versus  $T$  plots from the series of Pd-Co alloys, obtained from measurements carried out in zero field and a number of external fields, results of the alloys containing 0.075, 0.16 and 0.24 at. % Co are displayed in fig. IV.2, fig. IV.3 and fig. IV.6, respectively. In fig. IV.4 and fig. IV.5 the magnetic contribution to the specific heat of Pd-Fe 0.16 at. % and of Au-Fe 0.16 at. % are shown, respectively. Results on two Au-Fe alloys reported by Béthoux et al. [119] have also been reproduced (see caption to fig. IV.5).

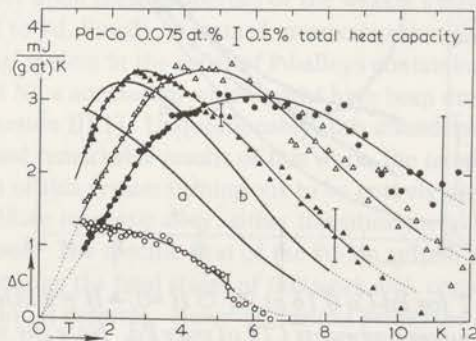


fig. IV.2.  $\Delta C$  versus  $T$  for Pd-Co 0.075 at.%.  $\circ H = 0$ ,  $\blacktriangle H = 9$  kOe,  $\triangle H = 18$  kOe,  $\bullet H = 27$  kOe. Curves a and b represent results obtained at  $H = 3$  kOe and  $H = 6$  kOe, respectively.

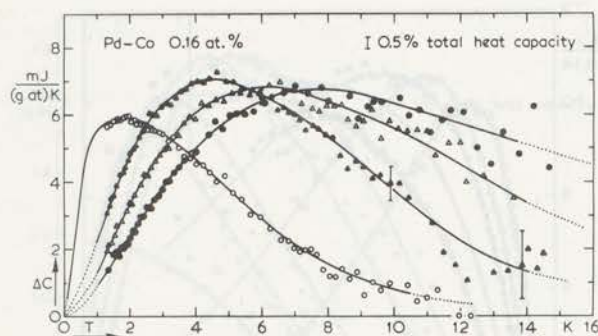


fig. IV.3.  $\Delta C$  versus  $T$  for Pd-Co 0.16 at.%.  $\circ H=0$ ,  $\blacktriangle H=9 \text{ kOe}$ ,  $\triangle H=18 \text{ kOe}$ ,  $\bullet H=27 \text{ kOe}$ . Points obtained at temperatures below 1 K at  $H=0$  have been omitted and are replaced by a full curve.

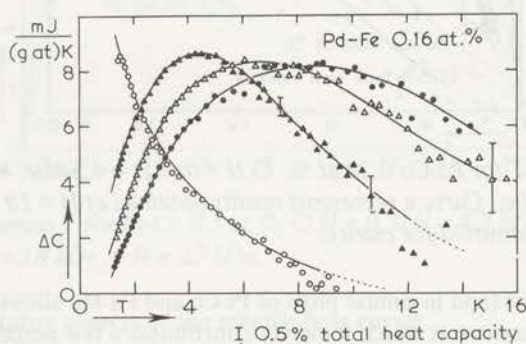


fig. IV.4.  $\Delta C$  versus  $T$  for Pd-Fe 0.16 at.%.  $\circ H=0$ ,  $\blacktriangle H=9 \text{ kOe}$ ,  $\triangle H=18 \text{ kOe}$ ,  $\bullet H=27 \text{ kOe}$ .

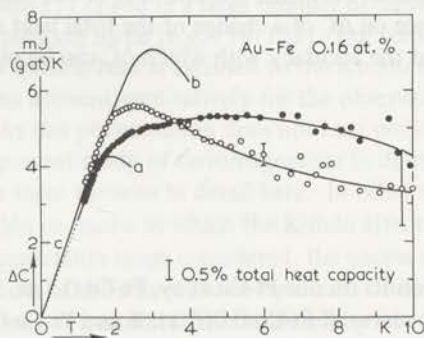


fig. IV.5.  $\Delta C$  versus  $T$  for Au-Fe 0.16 at.%.  $\circ H=0$ ,  $\bullet H=27 \text{ kOe}$ . Curves a and b represent data reported by Béthoux et al. [119] on Au-Fe 0.1 at.% and Au-Fe 0.2 at.%, respectively ( $H=0$ ). c represents the linear term of the Au-Fe alloys [119].

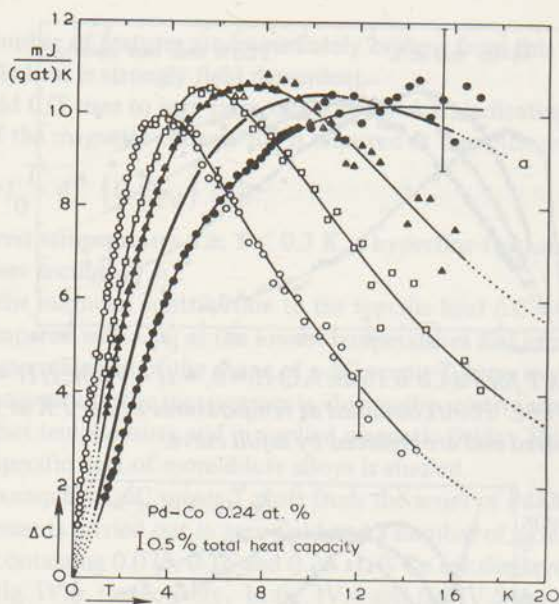


fig. IV.6.  $\Delta C$  versus  $T$  for Pd-Co 0.24 at. %.  $\circ H = 0$ ,  $\square H = 4.5$  kOe,  $\blacktriangle H = 9$  kOe,  $\bullet H = 27$  kOe. Curve a represents results obtained at  $H = 18$  kOe; points have been omitted for clarity.

In these plots (and in similar plots of Pt-Co and Pd-Mn alloys)  $\Delta C$  has been shown up to a temperature at which it merely contributes a few percents, or even less, to the total specific heat of the alloy. Above these temperatures the difference between the specific heat of an alloy and its base metal may vary wildly, although this difference rarely exceeds 1% of the specific heat of the base metal. In all figures bars indicate the influence on  $\Delta C$  of a change of the total heat capacity by 0.5%; it should be recalled that the accuracy with which  $\Delta C$  can be obtained is about 0.5% (see section II.6).

#### IV.2.2. Pt-Co

Specific-heat results on one Pt-Co alloy, Pt-Co 0.5 at. %, are shown in fig. IV.7. The specific-heat curves of Pt-Co 0.067 at. % and Pt-Co 0.8 at. % have not been shown because they are quite similar to those of Pt-Co 0.5 at. %, with the exception of the zero-field  $\Delta C$  versus  $T$  curve of Pt-Co 0.8 at. % which definitely reveals a maximum at 3.0 K.

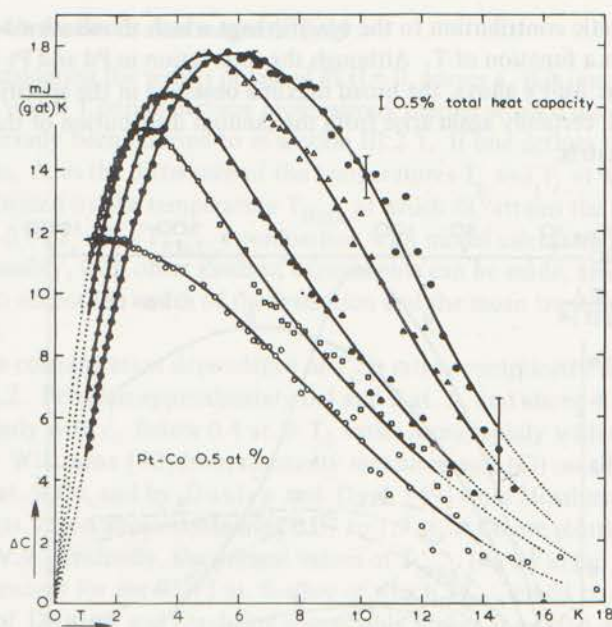


fig. IV.7.  $\Delta C$  versus  $T$  for Pt-Co 0.5 at. %.  $\circ H = 0$ ,  $\square H = 4.5$  kOe,  $\blacktriangle H = 9$  kOe,  $\triangle H = 18$  kOe,  $\bullet H = 27$  kOe.

### IV.3. Qualitative aspects of the specific-heat curves

A feature common to all the dilute magnetic alloys mentioned so far, is their gentle wedge-shaped  $\Delta C$  versus  $T$  curve. Such a behaviour has been observed previously in Pd-Fe alloys [77] and in a large number of dilute alloys of which the base metal is a non-transition metal [e.g. 119-123]. For some of the latter alloys, e.g. Cu-Fe, the excess specific heat is ascribed to the Kondo effect; in this case theoretical calculations account qualitatively for the observed specific heat [see e.g. the reviews 10-13]. As this phenomenon does not bear obvious resemblance in connection with the present study of ferromagnetism in dilute alloys, it is not expedient to consider these theories in detail here. In other non-transition-metal based alloys, e.g. Cu-Mn or Au-Fe in which the Kondo effect is ineffective in the temperature and concentration range considered, the excess specific heat arises from ordering of the moments of the solute atoms by means of the RKKY exchange interaction. On the basis of a model first considered by Marshall [103] and elaborated by Klein [104-106] one may readily understand this phenomenon. As the interaction strength among the solute atoms (RKKY) depends on their mutual distance and taking into account the random distribution of the solute atoms one

obtains a magnetic contribution to the specific heat which shows a broad maximum when plotted as a function of  $T$ . Although the interaction in Pd and Pt alloys differs from that in e.g. Au-Fe alloys, the broad maxima observed in the specific heat of these alloys will certainly again arise from the random distribution of the solute atoms in the matrix.

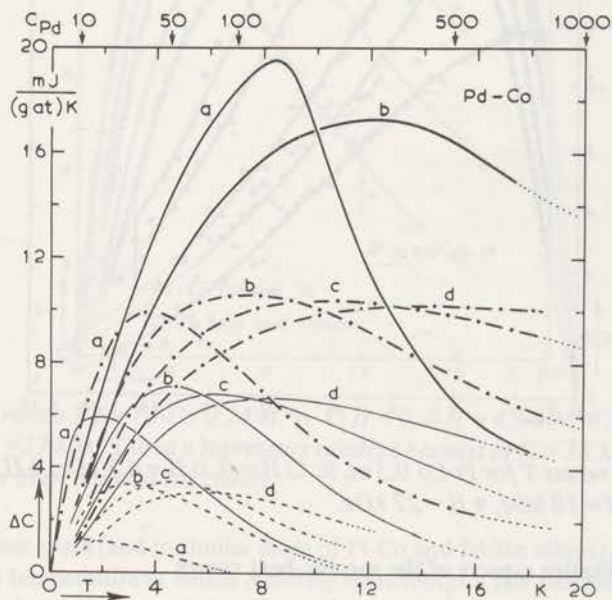


fig. IV.8.  $\Delta C$  versus  $T$  for Pd-Co alloys containing 0.075 at. % Co (----), 0.16 at. % Co (—), 0.24 at. % Co (-·-·-) and 0.35 at. % Co (—).  $a, b, c$  and  $d$  refer to measurements at  $H = 0, 9, 18$  and  $27$  kOe, respectively. Figures at the top of the graph indicate the specific heat of Pd in  $\text{mJ}(\text{g at})^{-1}\text{K}^{-1}$  at the marked temperatures.

In order to facilitate a comparison of the results of Pd-Co alloys, the curves from fig. IV.2, IV.3 and IV.5, together with those for Pd-Co 0.35 at. % have been redrawn in fig. IV.8.

#### IV.3.1. Pd-Co results in zero magnetic field

Considering the results obtained at  $H = 0$ , curves a, it is immediately evident that the  $\Delta C$  versus  $T$  curves become progressively sharper when  $c$  increases, a result which has already been referred to in section III.2.1. If one defines the relative width of the curves,  $\Delta$ , as the difference of the temperatures  $T_2$  and  $T_1$  at which  $\Delta C = \Delta C_{\max}/2$ , divided by the temperature  $T_{\max}$  at which  $\Delta C$  attains the maximal value  $\Delta C_{\max}$ , i.e.  $\Delta = (T_2 - T_1)/T_{\max}$ , a comparison with model calculations of the specific heat and, possibly, with other kinds of experiments can be made, assuming  $T_2 - T_1$  and  $T_{\max}$  to reflect the width of the transition and the mean transition temperature, respectively.

The concentration dependence of  $T_c$  is rather complicated as can be seen from fig. III.2. Between approximately 0.4 and 2 at. %, and above 4 at. %,  $T_c$  varies roughly linearly with  $c$ . Below 0.4 at. %  $T_c$  varies more rapidly with  $c$ .  $T_c$ -values obtained by Williams [70] from resistivity measurements (O) on alloys containing 0.1 to 1.05 at. % Co, and by Dunlap and Dash [49] from Mössbauer-effect (ME) measurements ( $\Delta$ ) on alloys containing 0.07 to 1.9 at. % Co are plotted as a function of  $c$  in fig. IV.9. Evidently, the present values of  $T_{\max}$  ( $\bullet$ ) are in fair agreement with the former, except for the 0.075 at. % alloy of which  $T_{\max}$  could be only estimated. The results of Dunlap and Dash are appreciably higher at  $c < 0.5$  at. %. From an analysis of his results Williams deduced  $T_c \propto c^{1.5}$ . As is evident, however, from the straight line in fig. IV.9, his data and the present values of  $T_{\max}$  can be represented more satisfactorily by  $T_c = T_0 c^2$ , with  $T_0 = (75 \pm 3) \text{ K}/(\text{at. \%})^2$ , in the concentration range at which the present measurements were carried out, that is below 0.5 at. %.

It appears from graphical analysis (fig. IV.10) that  $\Delta$  can be represented fairly well by  $\Delta = \Delta_0 c^{-1}$ , with  $\Delta_0 = (0.44 \pm 0.05) \text{ at. \%}$ . This implies that the width of the magnetic specific-heat curves increases proportionally to  $c$  according to  $T_2 - T_1 = (33 \pm 4)c \text{ K}$ ,  $c$  in at. %, in the range of concentrations considered.

Dunlap and Dash [49] have analysed the width of the transition from the ordered to the disordered state, as obtained from their ME experiments on alloys with 0.07 to 4.5 at. % Co, in terms of a molecular-field calculation and assuming the distribution of Co atoms around a particular Co atom to be Gaussian. It follows from their calculation that  $T_c$ , and the mean square deviation  $t^2$  of transition temperatures, are both proportional to  $c$ . According to the authors their experimental  $T_c$  and  $t$  values would be proportional to  $c$  and  $c^{0.5}$ , respectively, for  $c > 0.1$  at. % Co, in agreement with their calculation. However, as shown in fig. III.2, the concentration dependence is undoubtedly more complicated in the range up to 4.5 at. % Co. In fig. IV.10 (right-hand scale) their  $t/T_c$  data have been reproduced ( $\nabla$ ). Under the assumptions made  $t/T_c$  is proportional to  $\Delta$ . Below  $c = 0.5$  at. %  $t/T_c$  does seem to be approximately proportional to  $c^{-1}$ , rather than to  $c^{-0.5}$  as was

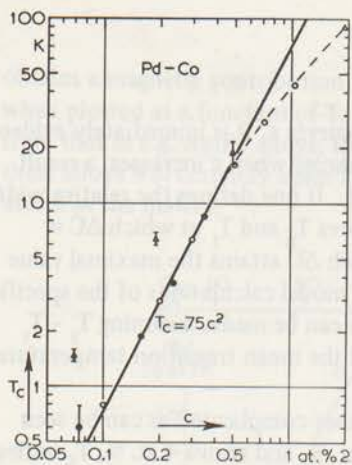


fig. IV.9. Transition temperatures of Pd-Co alloys as a function of concentration.  $\circ$ : resistivity measurements by Williams [70],  $\Delta$ : ME experiments by Dunlap and Dash [49]. Temperatures at which  $\Delta C$  attains its maximum are shown by black dots.

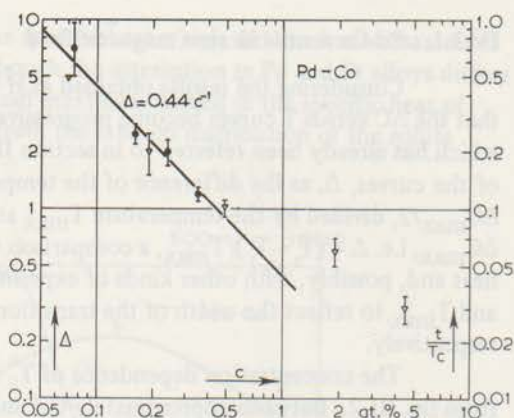


fig. IV.10. The relative width of the specific heat curves  $\Delta$ , (see text), versus concentration ( $\bullet$ ). The right-hand scale refers to ME data ( $\nabla$ ) reported by Dunlap and Dash [49]. The meaning of  $t/T_c$  is explained in the text.

stated by Dunlap and Dash. At higher concentrations  $t/T_c$  deviates from the  $c^{-1}$ -dependence, presumably due to the fact that  $T_c$  no longer varies proportionally to  $c^2$ .

It would, of course, be interesting to correlate the observed concentration dependences of  $T_{\max}$  and  $\Delta$  with theoretical predictions. Unfortunately, no theory exists, which deals with the statistical variation of effective fields in dilute ferromagnetic alloys. On the other hand, as mentioned earlier, such models do exist for systems in which magnetic ordering is governed by the oscillatory RKKY interaction. For lack of a theory more appropriate to the present system, it is tempting to compare the present results with those predicted by these theories. In no case, however, the concentration dependence of the width of the calculated specific-heat curves is stated by the authors. Plots of  $C/T$  versus  $T$  and  $C$  versus  $T$  have been given by Klein [105] and Liu [124]. From these the  $c$ -dependence of  $T_2 - T_1$  could be estimated and has been found to be proportional to  $c$ , using the model of Klein, but independent of  $c$  in the model of Liu. In both theories which are essentially effective-field approximations,  $T_{\max}$  varies proportionally to  $c$ . Consequently,  $\Delta$  is  $c$ -independent in Klein's and proportional to  $c^{-1}$  in Liu's model. According to Liu the main difference between his model and that of Klein is the temperature dependence of the field at the top of the probability function of internal fields  $P(H)$ ,

which decreases with  $T$  in his model and increases with  $T$  according to Klein. On physical grounds preference should be given to Liu's assumption. In both cases calculations have been carried out assuming the width of the  $P(H)$  curve to be proportional to  $c$ .

The  $c$ -dependences of the various quantities have been summarized in table IV.1. As can be seen, the relation for  $T_{\max}$ , as observed for Pd-Co alloys, is not predicted by theory. Consequently, any statement about the  $c$ -dependence of the width of the  $P(H)$  curve, of which one might have hoped to obtain some information, appears to be unjustified.

Table IV.1

Concentration dependence of  $T_{\max}$ ,  $T_2 - T_1$ ,  $\Delta$  and the width of the  $P(H)$  curve.

	$T_{\max}$	$T_2 - T_1$	$\Delta$	width $P(H)$
Klein [105]	$c^1$	$c^1$	$c^0$	$c^1$
Liu [124]	$c^1$	$c^0$	$c^{-1}$	$c^1$
Present work	$c^2$	$c^1$	$c^{-1}$	$c^?$

#### IV.3.2. Pd-Co results in applied magnetic fields

The influence of the magnetic field on the shape of the  $\Delta C$  versus  $T$  curves is shown in fig. IV.8 to follow a consistent pattern as a function of the concentration. At low Co concentration, i.e. when the zero-field curve is very broad,  $\Delta C_{\max}$  first rises as a function of  $H$ , attains a maximum and subsequently decreases slightly, as is most evident for Pd-Co 0.075 at. %. When  $c$  is increased, i.e. when the zero-field curve becomes sharper, the rise of  $\Delta C_{\max}$  diminishes; for the 0.24 at. % Co alloy  $\Delta C_{\max}$  appears to be almost independent of the applied field. On further increase of  $c$  the increase of  $\Delta C_{\max}$  disappears and a rapid initial decrease is observed instead, as could be inferred from measurements at  $H = 3$  and 6 kOe (not shown in fig. IV.8), followed by a slower decrease at higher fields. For Pt-Co alloys the same trend has been observed, although the pattern does not change as rapidly with  $c$  as it does in Pd-Co alloys.

This behaviour can be reproduced qualitatively by a molecular-field calculation of the specific heat in external magnetic fields, incorporating a Gaussian distribution of internal magnetic fields presented in sections V.2.3 and V.2.4. The pattern referred to above is then seen to be determined by the width of the internal-field distribution. It should be admitted, however, that a quantitative analysis failed to reproduce the present results.

### IV.3.3. Intercomparison of Pd-Co, Pd-Fe and Au-Fe alloys

In fig. IV.11 the results on Pd-Co, Pd-Fe and Au-Fe alloys each containing 0.16 at. % Co or Fe have been plotted on the same scale. The results of Pd-Co and Pd-Fe are very similar, although the curves of the Co alloy are comparatively broader, as is most evident for the zero-field curves. In view of the discussion given in section IV.3.1 this might be a manifestation of a broader distribution of internal fields in the Co alloy.

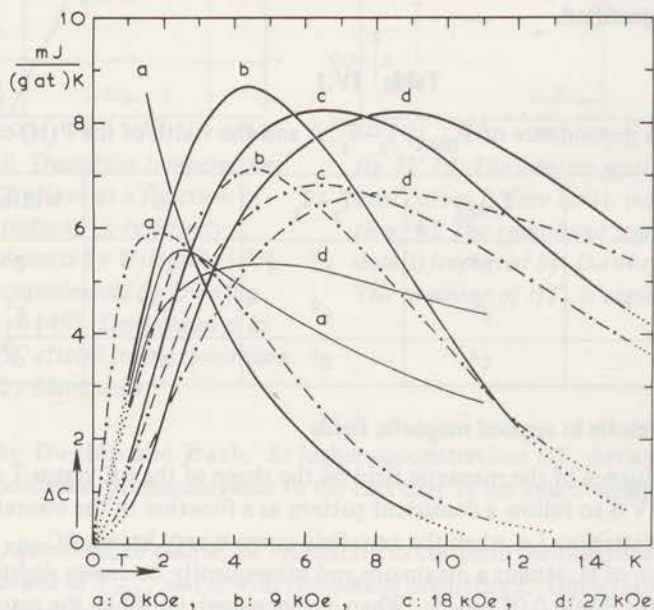


fig. IV.11.  $\Delta C$  versus  $T$  of Pd-Co, Pd-Fe and Au-Fe alloys, containing 0.16 at. % Co or Fe. Pd-Fe ———, Pd-Co - - - - -, Au-Fe - · - · - ·.

The specific heat of Au-Fe behaves rather differently. The most striking difference is the fact that the specific heat decreases only by 10% at the lowest temperatures at  $H = 27$  kOe when compared to the specific heat obtained at  $H = 0$ , whereas decreases of 75% are observed in Pd alloys at the lowest temperatures of the measurements and at the same field. Another difference is found for the shift of  $T_{\text{max}}$  towards higher temperatures when a magnetic field is applied. Comparing the data obtained at  $H = 0$  and  $H = 27$  kOe this shift is only 2.5 K for Au-Fe as contrasted to 6.6 K for Pd-Co and more than 7.5 K for Pd-Fe. This differing behaviour can be understood in principle if one remembers that  $T_{\text{max}}$  shifts towards higher temperatures in 'pure' ferromagnets and towards lower temperatures in 'pure'

antiferromagnets. In Au-Fe the spin density induced in the matrix is oscillatory and consequently the interactions among the solute atoms contain ferro- and antiferromagnetic aspects, apparently resulting in a net small shift of  $T_{\max}$  towards higher temperatures, in qualitative agreement with recent theoretical work of Klein [106]. In the Pd alloys the interactions are purely ferromagnetic, resulting in a much larger shift of  $T_{\max}$ .

#### IV.4. Presentation and discussion of the specific heat of Pd-Mn alloys

The excess specific heat of four Pd-Mn alloys is shown in fig. IV.12 and fig. IV.13. Experimental data on Pd-Mn 0.54 at. % have been reported earlier [116,117]. The results obtained for this alloy are very similar to those of the other four concentrations (see also fig. IV.14 and fig. V.5). For many dilute magnetic systems it is known that a concentration as low as 0.1 at. % of solute atoms is sufficient to give rise to a relatively large magnetic specific heat at temperatures above 1 K. In view of this experience the measurements on the series of Pd-Mn alloys were started with an alloy containing approximately this amount of Mn. As can be inferred from fig. IV.12 the zero-field specific heat of Pd-Mn 0.08 at. % hardly exceeds the specific heat of pure Pd at  $T > 1$  K ( $\Delta C < 3\%$  of  $C_{\text{Pd}}$ ). From this result one might have concluded that the Pd-Mn system is, apparently, non-magnetic, attributing the deviation at  $H = 0$  to some experimental error. However, experiments on more concentrated Pd-Mn alloys showed clear evidence of a magnetic transition occurring in this system.

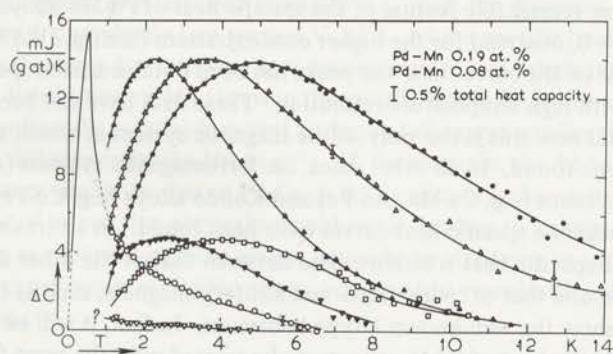


fig. IV.12.  $\Delta C$  versus  $T$  of Pd-Mn 0.08 at. % and Pd-Mn 0.19 at. %.  
 Pd-Mn 0.08 at. %:  $\nabla H = 0$ ,  $\blacktriangledown H = 13.5$  kOe,  $\square H = 27$  kOe.  
 Pd-Mn 0.19 at. %:  $\circ H = 0$ ,  $\blacktriangle H = 9$  kOe,  $\triangle H = 18$  kOe,  $\bullet H = 27$  kOe.  
 Experimental data obtained on Pd-Mn 0.19 at. % at  $T < 1$  K have been omitted for clarity.

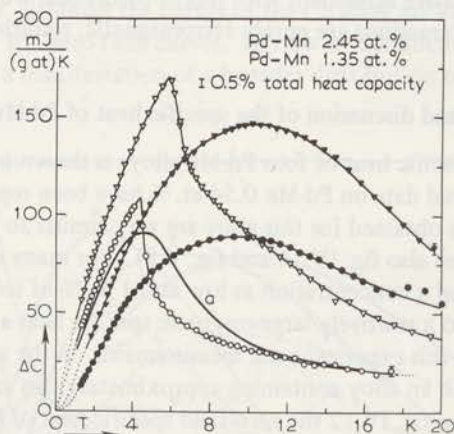


fig. IV.13.  $\Delta C$  versus  $T$  of Pd-Mn 1.35 at. % and Pd-Mn 2.45 at. %.  
 Pd-Mn 1.35 at. %:  $\circ$   $H = 0$ ,  $\bullet$   $H = 27$  kOe, curve a  $H = 2$  kOe.  
 Pd-Mn 2.45 at. %:  $\nabla$   $H = 0$ ,  $\blacktriangledown$   $H = 27$  kOe.

The most remarkable feature of the specific heat of Pd-Mn alloys is the sharp peak at  $H = 0$ , observed for the higher concentrations (see fig. IV.13 and IV.14). The precise shape of the curves near the peaks has been obtained from special measurements with high temperature-resolution. These data have not been plotted for clarity. Up till now this is the **only** dilute magnetic system in which such a behaviour has been found. In all other cases, i.e. ferromagnetic systems (e.g. Pd-Co, Pd-Fe), RKKY-systems (e.g. Cu-Mn, Au-Fe) and Kondo alloys (e.g. Cu-Fe) broad wedge-shaped magnetic specific-heat curves have been found. In a certain sense this type of magnetic specific heat is intermediate between that of the other dilute magnetic systems and that of 'pure' ferro- and antiferromagnets, such as Fe and Ni or MnO, which show the well-known  $\lambda$ -type behaviour. In fact, it will be shown that the zero-field specific heat of Pd-Mn alloys can be treated with the same formulae currently used to analyse  $\lambda$ -peaks (see eq. (V.27a,b)). As is evident from fig. IV.14 the specific-heat curves of dilute Pd-Mn alloys do not exhibit  $\lambda$ -peaks. However, the shape of the peaks is described by eq. (V.27a,b) with  $a < -1$ . This case has never been considered before because such a specific-heat behaviour has never been observed. The analysis of the zero-field specific heat is given in sections V. 3.1 - 4.

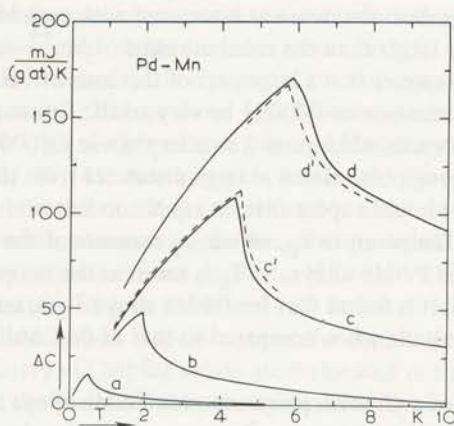


fig. IV.14.  $\Delta C$  versus  $T$  of Pd-Mn alloys containing 0.19 at. % (a), 0.54 at. % (b), 1.35 at. % (c) and 2.45 at. % Mn (d) at  $H = 0$ . Curves  $c'$  and  $d'$  represent measurements after 220 hours homogenization at  $1000^\circ\text{C}$  subsequent to the usual homogenization (24 hours at  $950^\circ\text{C}$ ).

Of course, this unexpected behaviour of the specific heat of Pd-Mn alloys gives rise to some speculations about the interactions involved in this phenomenon. It is important to note first that a sharp specific-heat maximum is only possible if the interactions among the magnetic carriers are uniform. It is easy to prove that even a small spread in interaction strengths will cause the sharpness of a specific-heat peak to vanish completely (see section V.2.1.). As the specific-heat maximum remains fairly sharp down to very low concentrations and taking into account the statistical distribution of Mn atoms in the matrix, one is forced to assume that the matrix is uniformly polarized, except perhaps at distances smaller than nearest-neighbour distance from the Mn sites \*). If, for example, the 4d-band polarization in Pd-Mn were similar to that of Pd-Co or Pd-Fe alloys (as shown in fig. III.4) a broad scale of interaction strengths would result, leading to a shape of the specific-heat curves as observed in those alloys. It might be clarifying to carry out neutron-scattering experiments on Pd-Mn alloys, which might reveal such a uniform polarization.

\*) It appears very unlikely that the sharp peaks are due to metallurgical clustering of Mn atoms since the peaks persist down to very low concentrations. Moreover, the solid-solubility limit of Mn in Pd is as high as 26 at. % at room temperature [see Appendix I].

As mentioned earlier, the moment associated with each Mn atom has been found to be only slightly larger than the usual moment of  $\text{Mn}^{++}$ -ions ( $5 \mu_B$ , see section III.2.1). If one assumes that a large part of this moment is localized at the Mn site the uniform polarization could only be very small. Consequently, the strength of the interactions should be much smaller than in e.g. Pd-Co alloys, in which occurs a fairly strong polarization at large distances from the Co sites. Under these circumstances one should expect that, at equal concentrations of Co and Mn in Pd, the mean transition temperature  $T_C$ , which is a measure of the strength of interaction, is much smaller in Pd-Mn alloys. If  $T_C$  is taken as the temperature at which  $\Delta C$  attains its maximum, it is found that for Pd-Mn alloys  $T_C$  is, indeed, smaller by at least an order of magnitude when compared to that of Pd-Co alloys of the same concentrations.

If the concept of a uniform polarization in Pd-Mn alloys is accepted one might proceed to describe the interactions in terms of a molecular field. Of course, the Weiss molecular-field (WMF) model is too simple a model to account for the zero-field specific heat, in view of the large contribution to the specific heat due to short-range ordering which is not considered in the WMF model. However, if an external magnetic field, sufficiently large compared to the molecular field (at  $T = 0$ ), is applied, the influence of short-range ordering will be highly suppressed and, consequently, the WMF model should then become a better approximation. Indeed, as will be shown in section V.2.2, the specific heat of Pd-Mn can be described quite satisfactorily in terms of the WMF model, sufficiently large external fields being available for some of the alloys.

Referring to the discussion on the magnetic-field dependence of the shape of the specific-heat curves of Pd-Co alloys in section IV.3.2, it should be noticed that if the distribution of internal fields in Pd-Mn alloys is sharply peaked, as assumed in the preceding paragraphs, the value of  $\Delta C_{\text{max}}$  should decrease with increasing field strength. From fig. IV.12 and fig. IV.13 it can be seen that the pattern described in section IV.3.2 for Pd-Co alloys evidently also applies in the extreme case of Pd-Mn.

The transition temperature  $T_C$  of Pd-Mn alloys as obtained from measurements of the magnetization and susceptibility [16], of the resistivity [8,15] and from the present specific-heat measurements has been plotted as a function of concentration in fig. IV.15. At the lowest concentrations agreement between the different experiments is fair. Below about 1 at. % Mn  $T_C$  varies proportionally to  $c$  ( $T_C = 3.6c$ ,  $c$  in at. %), in contrast to the concentration dependence found for Pd-Co in section IV.3.1 ( $T_C \propto c^2$ ). Above 1 at. % Mn differences between  $T_C$  values obtained from the different experiments occur, as was also found for Pd-Co and Pd-Fe alloys (see fig. III.2 and fig. III.3). According to the discussion presented in sections III.2.1 and III.2.4 this would imply that the interactions become less uniform at these concentrations. Indeed, there are indications from

the present specific-heat measurements that some broadening of the transition occurs at concentrations above 1 at. % Mn (see also section V.3.3). This broadening may, at least partly, be due to small-scale concentration variations in the matrix, because after homogenization for 220 h at about 1000°C subsequent to the usual heat treatment (48 h, 1000°C, see Appendix I) the specific-heat maximum became sharper (dashed curves in fig. IV.14). According to Rault and Burger [16]  $T_C$  decreases at concentrations above 2.5 at. %. As mentioned in section III.1 this may arise from direct Mn-Mn interactions because of the increased probability of finding a Mn atom at nearest-neighbour distance from a particular Mn atom. This probability is e.g. 11.5% at a concentration of 1 at. % Mn and 46% at 5 at. % Mn. If direct exchange interaction between Mn atoms leads to antiparallel coupling of their spins, as shown theoretically by Moriya [126] for solute atoms located in the middle of a series of transition metals in the periodic table, the decrease of  $T_C$  can be understood. Moreover, it also accounts for the antiferromagnetic behaviour observed at  $c > 8$  at. % Mn.

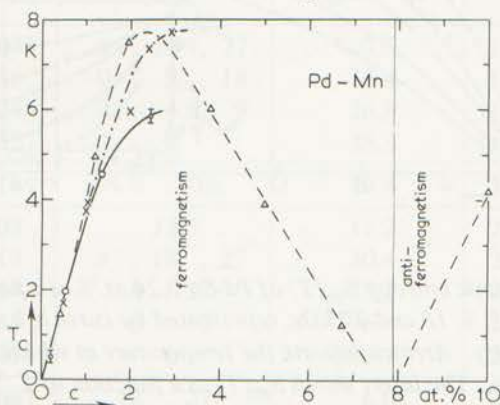


fig. IV.15. Transition temperatures of Pd-Mn alloys versus Mn concentration.  
 ○ Present specific-heat results, △ susceptibility and magnetization data [16], × resistivity data [8,15].

#### IV.5. Entropy and spin

The entropy of a system at temperature  $T'$  is given by the relation  $S(T') = \int_0^{T'} (C/T) dT$ , provided  $S(0) = 0$ . Thus, if  $C$  is known from  $T = 0$  to  $T = T'$  the entropy at  $T'$  can be evaluated. Considering only the entropy involved in the magnetic ordering process it follows from general arguments, i.e. independent of any model calculation, that the high-temperature limit of the magnetic entropy per magnetic carrier with a moment of momentum  $J\hbar$ , is equal to  $k \ln (2J + 1)$ . Thus, the total magnetic entropy,  $S_m$ , of a system consisting of  $cN$  magnetic carriers per gram-atom is given by

$$S_m = cNk \ln(2J + 1) = cR \ln(2J + 1), \quad (\text{IV.1})$$

where  $N$  is the number of atoms per gram-atom. For the present alloys it has been assumed that the magnetic carriers may be identified as the solute atoms and, accordingly,  $c$  is the atomic fraction of the latter. Assuming that the orbital momentum of the solute atoms is quenched,  $J$  equals the spin  $S$ .

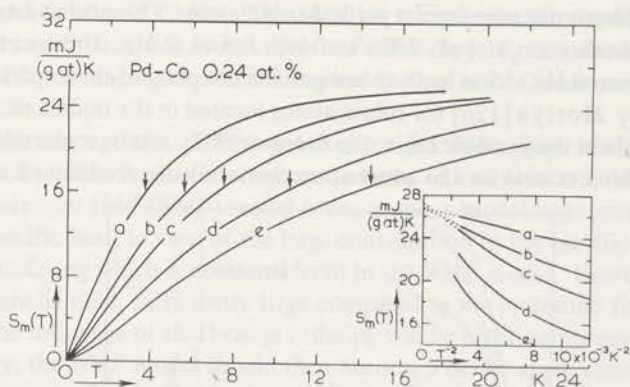


fig. IV.16. The magnetic entropy  $S_m(T)$  of Pd-Co 0.24 at. % as a function of  $T$  at  $H = 0, 4.5, 9, 18$  and  $27$  kOe, represented by curve  $a, b, c, d$  and  $e$ , respectively. Arrows indicate the temperature at which  $\Delta C$  attains its maximum. The insert shows  $S_m(T)$  as a function of  $T^{-2}$ .

As an example, the magnetic part of the entropy of Pd-Co 0.24 at. % as obtained from graphical integration of a  $\Delta C/T$  versus  $T$  plot, is shown in fig. IV.16. The accuracy of  $S_m$  depends upon the accuracy of the extrapolations of  $\Delta C/T$  to low and high temperatures. For almost all specimens a large fraction of the magnetic entropy is removed at temperatures at which  $\Delta C$  could be readily obtained for one or a number of applied fields (or  $H = 0$ ). Extrapolations to  $T = \infty$  have been made by plotting  $S_m(T)$  versus  $T^{-2}$  for temperatures sufficiently far beyond  $T_{\text{max}}$ . If  $C \propto T^{-2}$  at high temperatures, as is found for many magnetic systems,  $S_m(T)$  also varies proportionally to  $T^{-2}$ . In many cases the high-temperature dependence of  $S_m(T)$  can indeed be represented fairly by a straight line in a  $S_m(T)$  versus  $T^{-2}$  plot, as for instance for Pd-Co 0.24 at. % at  $H = 0, 4.5$  and  $9$  kOe (insert, fig. IV.16). The curves for  $H = 18$  and  $27$  kOe are convex to the  $T^{-2}$ -axis as they should if the temperature is not sufficiently high. Extrapolations to  $T = 0$  have only been carried out if fairly

reliable extrapolations of  $\Delta C$  to  $T = 0$  could be made.

Entropy values, obtained from measurements which allowed a sufficiently accurate estimate of the contributions outside the temperature range of the measurements to be made, are shown in the fourth column of table IV.2. The quoted  $S_m$  value is based upon measurements at fields given in the preceding column. Spin values calculated from  $S_m$  are listed in the fifth column. As no systematic dependence of  $S_m$  has been found either upon concentration or upon applied magnetic field for any system, a mean spin value is given in the last column. The latter value has been calculated assigning little weight to less precise results.

Table IV.2

Alloy	Conc.	Field	$S_m$	S	Mean S
	at. %	kOe	$\text{mJ}(\text{g at})^{-1} \text{K}^{-1}$		
Pd-Co	0.075	9, 18, 27	7.5	1.2	$1.35 \pm 0.05$
	0.16	0, 9, 18	17.4	1.35	
	0.24	0, 4.5, 9	26.9	1.44	
	0.35	0	38.1	1.35	
Pd-Fe	0.16	9, 18	19.4	1.58	$1.6 \pm 0.1$
Pd-Mn	0.08	13.5	11.2	2.2	$2.35 \pm 0.1$
	0.19	9, 18, 27	30.4	2.9	
	0.54	0, 27	77.2	2.31	
	1.35	0, 2	196	2.37	
	2.45	0	353	2.33	
Pt-Co	0.067	18, 27	6.05	0.98	$1.0 \pm 0.05$
	0.5	4.5, 9, 18	44.1	1.05	
	0.8	4.5, 9	69.5	0.92	
Au-Fe	0.16	0	14.6	1.03	$1.0 \pm 0.2$

In view of the well-established existence of giant moments associated with Fe or Co in Pd and Pt it is, at first sight, striking that rather 'normal' spin values are derived from entropy calculations, as was noticed previously by other workers [77,78]. The more so, while, as discussed in sections III.1 and III.2.2, several workers were able to derive giant spin values from ME experiments [43, 46, 51] on very dilute alloys (paramagnetic state) and from magnetization experiments [25,26]. This apparent discrepancy will be discussed below.

The H/T dependence of the hyperfine field derived from ME experiments could be represented by Brillouin curves, whereas the magnetization data have been

analysed in terms of Brillouin functions with arguments incorporating an internal field proportional to the magnetization, i.e.  $B_J \{g\mu_B J(H + D\sigma)/kT\}$ . The giant spin value has been deduced from a fit to such curves. As such it seemed possible to describe the behaviour of the giant moment by

$$\mu = g\mu_B J \quad (\text{IV.2})$$

with  $g = 2$ . According to ferromagnetic resonance experiments carried out by Bagguley et al. [81]  $g$  is indeed close to 2 for Fe and Co in Pd. If this interpretation were correct the entropy should be expected to reflect a multiplicity corresponding to, for example,  $J = 6$ , which obviously contradicts the experimental evidence presented above. Other evidence suggesting that  $J$  may be considerably lower comes from ME experiments by Craig et al. [21] on Pd-Fe 2.65 at. % at  $T < T_C$  and at  $H = 0$  (see also [48]). Comparing the  $H_j/H_{\text{sat}}$  versus  $T$  data with a molecular-field calculation the authors note that the data can be fitted fairly to the Brillouin curve for  $J = 1$ , although it was admitted that this result might be fortuitous. In an external field no agreement with molecular-field theory is obtained, except at  $T \gg T_C$  (paramagnetic state) where the data seemed to be consistent with  $J = 4$ .

The following explanation of the present results is suggested. It is assumed that the Pd 4d-moments are rigidly coupled to the central Co moment in the range of temperatures at which the measurements were made. Thus, due to this rigid coupling of the induced moment to the Co moment the entropy removed in the transition simply corresponds to the multiplicity of the Co spin, i.e. the giant moment can only assume those quantal orientations appropriate to the Co spin. If this assumption is correct one should expect that the giant moment still persists at  $T > T_C$  which seems to be confirmed by susceptibility measurements [17,19,23], see section III.2.1. Alternatively, if the 4d-moments were decoupled from the Co moment in the temperature range of the measurements a certain amount of entropy would be involved in this process and, consequently, observed in the specific heat. Further evidence for the existence of the giant moment at  $T > T_C$  comes from a calculation of Doniach and Wohlfarth [110] discussed in section III.3.2, which accounts fairly for the high-temperature susceptibility of Pd-Co and Pd-Fe alloys. A suggestion put forward by Kitchens and Craig [47], viz. the possibility that specific-heat measurements at high fields might yield entropies corresponding to larger spin values as could have been inferred from Craig's ME experiments [21] discussed in the preceding paragraph, is unlikely to be correct from this point of view. Indeed, no field dependence could be perceived from the present experiments.

Obviously, eq. (IV.2) no longer relates moment and spin of the giant-moment complex properly. Doniach and Wohlfarth [110] derived a relation for the giant moment from a linear response approximation (see section III.3.2) which strongly suggests the assumption made above. The giant moment is given by

$$\mu = g\mu_B S(1 + \hat{J}_e \chi_m), \quad (\text{IV.3})$$

where  $\hat{J}_e = 2J_e/Ng^2\mu_B^2$ . In these expressions  $J_e$  represents the exchange parameter between the Co moment and the Pd 4d-moments and  $S$  represents the proper Co spin. From this expression it is not hard to assume that the dynamical behaviour of the giant moment is governed by the Co spin.

Of course, it remains to be explained why ME experiments and magnetization measurements seem to be consistent with high spin values. Such an explanation cannot be easily given. It should, however, be emphasized that in order to obtain spin values from such experiments the system has been assumed to satisfy some particular model (simple paramagnetic behaviour or molecular-field approximation), whereas  $S$  can be evaluated directly from specific-heat measurements. According to the experiments of Craig et al. [21] the application of molecular-field theory in external fields is doubtful. A simple molecular-field calculation of the specific heat in external fields (section V.2.4) strongly supports this observation. It seems likely that the extremely long-range nature of the polarization and the statistical distribution of effective fields which have not been considered in the analysis of hyperfine-field and magnetization experiments, may have a large influence on the properties of these alloys.

Spin values from specific-heat measurements on Pd-Fe and Au-Fe alloys have been reported previously by Veal and Rayne [77] ( $S = 1.1 \pm 0.3$ ) and by du Chatenier et al. [120,121] ( $S = 0.65$ ), respectively. For both systems the spin values presented in table IV.2 are higher. The differences may be due to the higher precision with which  $\Delta C$  can be obtained in the present work, especially at higher temperatures. A comparison with spin values derived from other kinds of measurements on Au-Fe alloys, which is not significantly altered by the present result, can be found in the paper of du Chatenier et al. [121]. Recently, Wheeler [79] reported  $S = 0.8$  for Co in Pt, which is only slightly smaller than the value obtained in this work. Again, the difference may be ascribed to the less uncertain extrapolations in this work.

#### IV.6. Some other details of the specific heat

In this last section of this chapter a discussion is presented concerning

- 1) the specific heat of two extremely dilute Pd-Co alloys,
- 2) the temperature dependence of  $\Delta C$  as  $T \rightarrow 0$  for more concentrated alloys and
- 3) the hyperfine-field contribution to the specific heat of Pd-Co 0.16 at. %. Finally,
- 4) the influence of non-magnetic effects on the specific heat upon alloying is briefly discussed.

1) Specific-heat data of Pd-Co 0.017 at. % and Pd-Co 0.036 at. % are presented in fig. IV.17 in a  $C/T$  versus  $T^2$  plot. As mentioned in section II.6 the specific heat of metals and alloys at sufficiently low temperatures can, in general, be represented by

$C = \gamma T + \beta T^3$ . Hence, it should be possible to represent the data by a straight line in such a plot. If, however, other mechanisms contribute to the specific heat in the range of temperatures considered, deviations from a straight line may occur. Although the data on the dilute alloys can indeed be represented satisfactorily by straight lines for  $T^2 > 3 \text{ K}^2$  (full lines), a rise is found at the lowest temperatures which might indicate the occurrence of a magnetic transition below 1 K. If this conjecture is correct one merely observes the high-temperature tail of the magnetic contribution to the specific heat; the specific heat of pure Pd (Appendix II) is shown by the dashed line. As can be inferred from the plot the magnetic specific-heat contribution is small at  $T > 1.5 \text{ K}$ , while at  $T > 3.5 \text{ K}$  the specific heat of the alloys can hardly be distinguished from that of pure Pd.

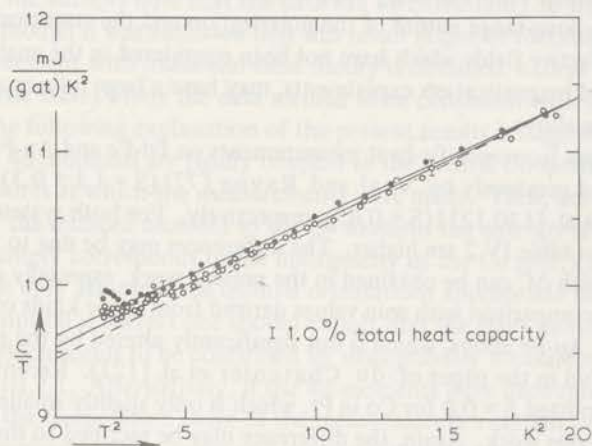


fig. IV.17.  $C/T$  versus  $T^2$  for Pd-Co 0.017 at. % (○) and Pd-Co 0.036 at. % (●).  
The dashed line represents the specific heat of pure Pd.

The data on these alloys suggest a possible explanation of the various values of  $\gamma$  and the characteristic Debye temperature  $\theta_D(0)$  reported for pure Pd ( $\beta = (12\pi^4/5)R/\theta_D^3(0)$ ), see e.g. [113,126,127]. These values of  $\gamma$  and  $\theta_D(0)$ , which were generally higher than those found more recently, could be due to Fe impurities which used to be present in commercially available Pd. Deviations arising from these impurities may have remained unnoticed e.g. due to a larger scattering of the data. Considering the present data on the two very dilute Pd-Co alloys, and attributing the rise at the lowest temperatures to some experimental error, one finds from the straight lines through the data  $\gamma = 9.53$  and  $9.62 \text{ mJ}(\text{g at})^{-1}\text{K}^{-2}$  and  $\theta_D(0) = 275$  and  $280 \text{ K}$ . These values are higher than those found presently for high-purity Pd,

viz.  $\gamma = 9.45 \pm 0.04 \text{ mJ}(\text{at})^{-1} \text{K}^{-2}$  and  $\theta_{\text{D}}(0) = 271 \pm 2 \text{ K}$ . It appears, therefore, reasonable to suppose the high values found previously to be, at least partially, due to Fe (Co) impurities in the Pd specimens.

2) For less dilute alloys it is interesting to consider the temperature dependence of  $\Delta C$  as  $T$  tends to zero. Several authors calculated this temperature dependence for dilute alloys in which the mutual interactions of the localized moments are governed by the RKKY interaction, e.g. for Cu-Mn (see section III.3.1). The effective field acting on a particular local moment sensitively depends upon the distribution of local moments in its environment (see also chapter V). Marshall [103] showed qualitatively that for such systems the effective field has a quasi-continuous probability distribution  $P(H)$ , where  $P(H)$  measures the number of moments experiencing a field between  $H$  and  $H + dH$ . Owing to the RKKY mechanism the distribution is symmetrical with respect to  $H = 0$ . Marshall's qualitative arguments have been confirmed by a number of statistical analyses by Klein and Brout [104] and Klein [105,106]. As to the temperature and concentration dependence of the specific heat as  $T \rightarrow 0$  these models predict  $\Delta C = \gamma_{\text{m}} T$ , with  $\gamma_{\text{m}}$  independent of  $c$ , provided  $P(0) \propto c^{-1}$ . This behaviour has been found experimentally for many systems of which the base metal is a noble metal, see e.g. [119, 120, 123].

For the dilute ferromagnetic alloys measured in this investigation the temperature dependence of  $\Delta C$  at very low temperatures turned out to be difficult to analyse. In those cases at which the measurements (at  $H = 0$ ) were extended to temperatures below 1 K, the temperature dependence of  $\Delta C$  is masked by a hyperfine-field-splitting contribution (hfs). Such contributions have been observed previously by du Chatenier and Miedema [123,120] for Mn dissolved in Au, Ag and Cu. These authors were able to represent their data reasonably well by the relation  $\Delta C = \gamma_{\text{m}} T + \delta T^{-2}$ , the second term being the high-temperature tail of the nuclear Schottky specific heat. The data obtained on Pd-Co 0.16 at. % at  $T \ll 1 \text{ K}$  can also be represented by such a relation (see below).

Fig. IV.18 shows  $\Delta C/T$  versus  $T$  curves for measurements at  $H = 0$  on three Pd-Co alloys. The hfs contribution has been subtracted, assuming for Pd-Co 0.24 at. % this contribution to be proportionally higher than the one derived for Pd-Co 0.16 at. % (see below). Results obtained on Pd-Co 0.24 at. % at two external fields are also shown in the figure. As can be seen, for high fields definite maxima of  $\Delta C/T$  are found at  $T > 1 \text{ K}$ . The dotted extrapolations to  $T = 0$  have been obtained from the corresponding  $\Delta C$  versus  $T$  plot by a 'smooth' extrapolation, assuming  $\Delta C$  is proportional to  $T$  as  $T$  tends to zero. This assumption seems reasonable for the curves at  $H = 0$ . However, the data obtained at  $H \neq 0$  do not exclude the possibility that  $\Delta C \propto T^n$ ,  $n > 1$ , or even proportional to a Boltzmann factor, as  $T \rightarrow 0$ . (The latter case occurs when a gap exists between the ground state and the first excited state of the system).

Contrary to the case of the RKKY systems the extrapolated values of  $\Delta C/T$  at  $T = 0$  are not concentration independent. For instance, one obtains from the measurements carried out on Pd-Co 0.16, 0.24 and 0.35 at. % at  $H = 0$ ,  $\gamma_m = 6.4$ , 5.4 and 3.5  $\text{mJ}(\text{g at})^{-1} \text{K}^{-2}$ , respectively.

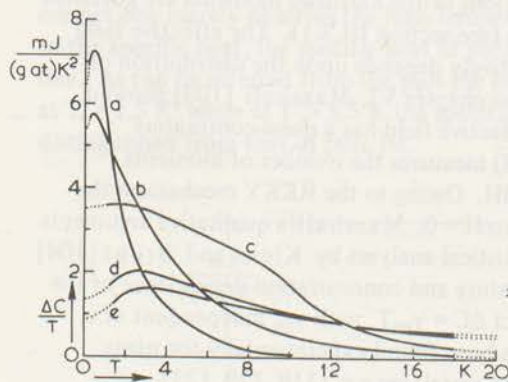


fig. IV.18.  $\Delta C/T$  versus  $T$  for measurements at  $H = 0$  on Pd-Co 0.16 at. % (a), Pd-Co 0.24 at. % (b) and Pd-Co 0.35 at. % (c). Curves d and e represent data on Pd-Co 0.24 at. % at  $H = 18$  and  $27 \text{ kOe}$ , respectively.

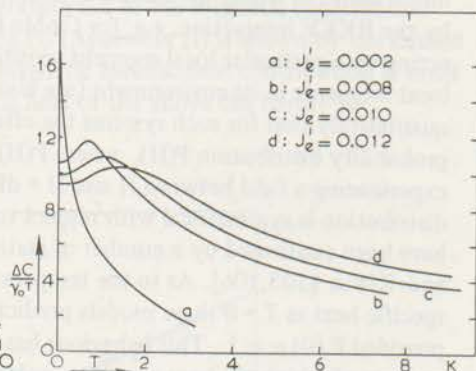


fig. IV.19. Specific-heat curves calculated for Gd at different values of  $J'_e$  (cf. the text). After Cole and Turner [128,111].

Fig. IV.19 shows a number of specific-heat curves from a paper by Cole and Turner [128,111], in which they attempted to interpret the low-temperature specific heat of Gd ( $T_c = 291.2 \text{ K}$ ). The calculated specific heat arises from spin-wave type excitations of the localized moments which are coupled indirectly by the RKKY mechanism. The curves have been calculated for different values of the parameter  $J'_e$  which is related to the s-d interaction parameter.  $\gamma_0 T$  is the unenhanced low-temperature specific heat, as derived from band-structure calculations. According to the authors similar curves could be calculated for dilute ferromagnetic Pd alloys. The similarity between the experimental  $\Delta C/T$  versus  $T$  curves and the theoretical curves both for results obtained at zero field on alloys with different concentrations and for results obtained at different fields on one alloy, is remarkable.

However, according to the authors, their calculation is only valid at very low temperatures at which interactions between the spin-waves can be neglected. But the observed maxima of  $\Delta C/T$  at  $H = 0$  are found at temperatures which can

hardly be considered to be low as compared to the transition temperature. Bearing in mind the uncertainty in the extrapolations of the  $\Delta C/T$  versus  $T$  curves, further application of Cole and Turner's theory at this stage must be considered to be speculative. It might, however, present a starting-point for a microscopic description of the specific heat of these weakly ferromagnetic systems.

3) As mentioned before, the specific heat of Pd-Co 0.16 at. % can be represented by  $C = \gamma_m T + \delta T^{-2} + C_{Pd}$  at sufficiently low temperatures. The measurements on Pd-Co 0.24 at. % were not carried out at sufficiently low temperatures to yield an independent determination of  $\delta$ . As can be inferred from fig. IV.20 the relation holds for Pd-Co 0.16 at. % at  $0.07 \text{ K} < T < 0.2 \text{ K}$ , with  $\gamma_m = 6.4 \pm 0.5 \text{ mJ}(\text{g at})^{-1} \text{ K}^{-2}$  and  $\delta = (7 \pm 1) \times 10^{-3} \text{ mJ}(\text{g at})^{-1} \text{ K}$ .

The nuclear specific heat  $C_N = \delta T^{-2}$  arises from interactions between the electronic and the nuclear moments of Co, represented by the Hamiltonian  $H = AS \cdot I$ , which describes the action of an effective field  $H_{\text{eff}} = SA/g_I \mu_N$  on the nucleus.  $\mu_N$  is the nuclear magneton and  $g_I$  the splitting factor associated with the nuclear spin  $I$ .  $C_N$  can be calculated to be  $C_N = cR [I(I+1)/3](\theta/T)^2$ , at temperatures high compared to the splitting temperature  $\theta = AS/k = g_I \mu_N H_{\text{eff}}/k$ .

From the experiments one derives  $\theta = 0.010 \pm 0.001 \text{ K}$ . For  $^{59}\text{Co}$  the nuclear moment is  $4.62 \mu_N$  and  $I = 7/2$ . Using these figures the hyperfine field is  $210 \pm 20 \text{ kOe}$ . Contributions to the specific heat arising from Pd nuclei have been estimated using nuclear data obtained by Seitchik et al. [129] from NMR experiments on Pd. As the moments induced on the Pd atoms in Pd-Co alloys depend upon their distance from the Co atoms (section III.2.3), the Pd nuclei will experience different hyperfine fields. For simplicity the total induced moment was assumed to be uniformly spread over some 300 Pd atoms around each Co atom. Taking into account the natural abundance (22.2%) of the only Pd nucleus which has a moment,  $^{105}\text{Pd}$ , the specific heat arising from these nuclei is estimated to be less than 0.5% of the contribution of the  $^{59}\text{Co}$  nuclei, despite the large ratio of the number of Pd atoms to the number of Co atoms!

The calculated value of  $H_{\text{eff}}$  may be compared with those derived from NMR measurements [130], from measurements of  $\gamma$ -radiation from oriented nuclei [84,85] and from Mössbauer-effect measurements [44,49] on Pd-Co alloys. Ehara [130] (NMR) obtained  $H_{\text{eff}} = 213 \text{ kOe}$  on Pd-Co 0.5, 1 and 2 at. %, while Cracknell et al. [84] (oriented nuclei) derived  $128 \pm 20 \text{ kOe}$  for Pd-Co 5 ppm and  $205 \pm 25 \text{ kOe}$  for Pd-Co 0.05 at. %. Such a sharp decrease as  $c$  tends to zero has also been observed by Parfenova et al. [85] (oriented nuclei). These workers obtained  $130 \pm 10 \text{ kOe}$  at  $c = 0.03 \text{ at. \% Co}$ , while  $H_{\text{eff}}$  attains a maximum ( $280 \pm 20 \text{ kOe}$ ) at  $c = 0.1 \text{ at. \% Co}$ . Good agreement of the present value of  $H_{\text{eff}}$  with Ehara's and Cracknell's can be noticed.

Mössbauer-effect measurements on Pd-Co have been carried out using

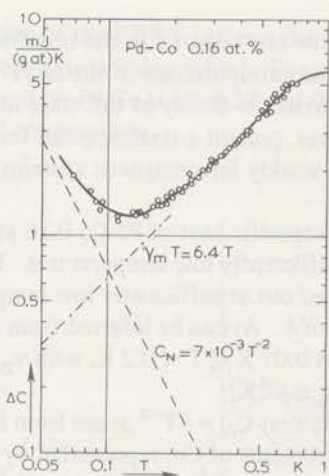


fig. IV.20.  $\Delta C$  versus  $T$  of Pd-Co 0.16 at. % at  $T < 1$  K. The dashed line represents the nuclear specific heat  $C_N$ . The dash-dotted line represents the electronic magnetic contribution to the specific heat at  $T < 0.2$  K.

$^{57}\text{Fe}$  [44,49]. The hyperfine fields derived from such measurements are about 310 kOe. This value is presumably more characteristic of the field acting on Fe nuclei in Pd than on Co nuclei in Pd, since a  $^{57}\text{Fe}$  nucleus in Pd-Fe alloys experiences approximately the same field [43,45,51,54]. Finally, it is interesting to note, that the present value of  $H_{\text{eff}}$  is about equal to those derived from the specific heat of Co metal (see e.g. Dixon et al. [131]), though  $H_{\text{eff}}$  is known to vary appreciably with alloy composition in concentrated Pd-Co alloys [53].

An erroneously calculated value of  $\theta$  has been suggested in a preliminary report [113]; this value should be discarded.

4) So far, it has tacitly been assumed that the magnetic specific heat could be derived from  $\Delta C = C_{\text{alloy}} - C_{\text{bm}}$ , where  $C_{\text{bm}}$  is the specific heat of the base metal. If, however, upon alloying the specific heat changes by non-magnetic effects, erroneous results can be expected. Such changes may arise from a change of the electronic specific heat by ordinary band-filling effects and from a change of the lattice specific heat if the elastic constants and the lattice parameter undergo a change. The former will obviously be more important at lower temperatures, the latter at higher temperatures.

As to the electronic contribution the increase or decrease per at. % is in first approximation proportional to the difference of the valencies of the metals. Especially for Pd and Pt the change of  $\gamma$  can be expected to be fairly large as the Fermi-level is located in the vicinity of a sharp peak of the density-of-states curve

( $\gamma \propto N(E_F)$ ). No data on elastic constants of the alloys are available so that the change of the lattice specific heat cannot be estimated.

Nevertheless, an impression of these effects can be obtained from specific-heat measurements of Hoare and coworkers [132,133] on Pd-Ag and Pd-Rh alloys. (Note that Rh and Co are iso-electronic). The difference of the valency of Ag and of Rh with Pd is one. At low Ag and Rh concentrations the following changes of  $\gamma$  and  $\theta_D(0)$  can be derived from the data:

Pd-Ag:  $\Delta\gamma/\gamma_{Pd} = -1.9\%/at. \%$ ,  $\Delta\theta/\theta_{Pd} = +0.2\%/at. \%$ .

Pd-Rh:  $\Delta\gamma/\gamma_{Pd} = +1.0\%/at. \%$ ,  $\Delta\theta/\theta_{Pd} = -1.1\%/at. \%$ .

Taking the values of the Pd-Rh alloys one obtains the following changes of  $C_{alloy}$  at 10 K and 20 K for Pd-Co 0.35 at. %:

T = 10 K:  $\Delta C_{el}/C_{Pd} = 0.15\%$ ,  $\Delta C_{latt}/C_{Pd} = 0.5\%$ ,  $\Delta C_{alloy}/C_{Pd} = 0.7\%$ .

T = 20 K:  $\Delta C_{el}/C_{Pd} = 0.05\%$ ,  $\Delta C_{latt}/C_{Pd} = 0.9\%$ ,  $\Delta C_{alloy}/C_{Pd} = 1.0\%$ .

At  $T \gg T_{max}$  the specific heat of all Pd-Fe and Pd-Co alloys differs less than 0.5% with  $C_{Pd}$ , indicating that non-magnetic contributions are negligibly small.

On the other hand,  $C_{Pd}$  may possibly be changed by a few percents in Pd-Mn 1.35 at. % and 2.45 at. %. The magnetic contribution to the specific heat is, however, so large in these cases that no significant error should be expected in e.g. entropy calculations. The same holds for Pt-Co alloys, although in this case the difference of the specific heat of the 0.5 at. % and the 0.8 at. % alloys with  $C_{Pt}$  is negative and slightly more than 1% above 20 K.

## References

1. P. Lederer and A. Blandin, *Phil.Mag.* 14(1966)363.
2. T. Takahashi and M. Shimizu, *J.Phys.Soc.Jap.* 20(1965)26.
3. D. Gerstenberg, *Ann.Physik* 2(1958)236.
4. J. Crangle, *Phil.Mag.* 5(1960)335.
5. R.M. Bozorth, P.A. Wolff, D.D. Davis, V.B. Compton and J.H. Wernick, *Phys. Rev.* 122(1961)1157.
6. J. Crangle, *Phys.Rev.Lett.* 13(1964)569.
7. J. Crangle and W.R. Scott, *J.appl.Phys.* 36(1965)921.
8. M.P. Sarachik and D. Shaltiel, *J.appl.Phys.* 38(1967)1155.
9. C.W. Chen, L.R. Edwards and S. Legvold, *Phys.Stat.Sol.* 26(1968)611.
10. J. Kondo, *Sol.State Physics*, Vol. 23, ed. F. Seitz, D. Turnbull and H. Ehrenreich, Academic Press, New York, 1969, p.183.
11. A.J. Heeger, *Sol.State Physics*, Vol. 23, p.283.
12. A.A. Abrikosov, *Usp.Fiz.Nauk* 97(1969)403, *Soviet Phys.Uspekhi* 12(1969)168.
13. J.E. van Dam and G.J. van den Berg, *Phys.Stat.Sol.* to be published.
14. see e.g. N.F. Berk and J.R. Schrieffer, *Phys.Rev.Lett.* 17(1966)433.  
P. Lederer and D.L. Mills, *Phys.Rev.* 165(1968)837.  
S. Engelsberg, W.F. Brinkman and S. Doniach, *Phys.Rev.Lett.* 20(1968)1040.
15. G. Williams and J. Loram, *Sol.State Comm.* 7(1969)1261.
16. J. Rault and J.P. Burger, *C.R.Acad.Sc.(Paris)* 269, Serie B (1969)1085.
17. D. Shaltiel, J.H. Wernick, H.J. Williams and M. Peter, *Phys.Rev.* 135(1964)A1346.
18. R.M. Bozorth, D.D. Davis and J.H. Wernick, *J.Phys.Soc.Jap.* 17, Suppl.B1(1962)112.
19. A.M. Clogston, B.T. Matthias, M. Peter, H.J. Williams, E. Corenzwit and R.C. Sherwood, *Phys.Rev.* 125(1962)541.
20. J.P. Burger, thesis, Paris 1964; *Ann. Physique* 9(1964)345.
21. P.P. Craig, R.C. Perisho, R. Segnan and W.A. Steyert, *Phys.Rev.* 138(1965)A1460.
22. W.C. Phillips, *Phys.Rev.* 138(1965)A1649.
23. T.H. Geballe, B.T. Matthias, A.M. Clogston, H.J. Williams, R.C. Sherwood and J.P. Maita, *J.appl.Phys.* 37(1966)1181.
24. J.I. Budnick, J. Lechaton, J.H. Wernick, S. Foner, E.J. McNiff Jr., D.J. Kim and B.B. Schwartz, *J.appl.Phys.* 39(1968)960.
25. M. McDougald and A.J. Manuel, *J.appl.Phys.* 39(1968)961.
26. M. McDougald and A.J. Manuel, *J.Phys.C* 3(1970)147.
27. T.F. Smith, W.E. Gardner and J.I. Budnick, *Phys.Lett.* 27A(1968)326.
28. M. Gibson and D.E. Moody, *Phys.Lett.* 30A(1969)194.
29. S. Foner, E.J. McNiff Jr. and R.P. Guertin, *Phys.Lett.* 31A(1970)466.
30. R.P. Guertin and S. Foner, *J.appl.Phys.* 41(1970)917.

31. S.Foner, *J.appl.Phys.* 39(1968)411.
32. P. Weiss and M. Forrer, *Ann.Physique* 5(1926)153.
33. A. Arrott, *Phys.Rev.* 108(1957)1394.
34. J.S. Kouvel, C.D. Graham Jr. and J.J. Becker, *J.appl.Phys.* 29(1958)518.
35. K.P. Belov, *Magnetic Transitions*, Consultants Bureau, New York, 1961.
36. S. Foner, R.Doclo and E.J. McNiff Jr., *J.appl.Phys.* 39(1968)551.
37. M. Shimizu, T. Takahashi and A. Katsuki, *J.Phys.Soc.Jap.* 18(1963)240.
38. E.W. Elcock, P. Rhodes and A. Teviotdale, *Proc.roy.Soc.(London)* A221(1954)53.
39. C.J. Schinkel, F.R. de Boer and J. Biesterbos, *Phys.Lett.* 26A(1968)501.
40. F.R. de Boer, C.J. Schinkel, J. Biesterbos and S. Proost, *J.appl.Phys.* 40(1969)1049.
41. F.R. de Boer, thesis, Amsterdam, 1969.
42. T.J. Hicks, B. Rainford, J.S. Kouvel, G.G. Low and J.B. Comly, *Phys.Rev.Lett.* 22(1969)531.
43. P.P. Craig, D.E. Nagle, W.A. Steyert and R.D. Taylor, *Phys.Rev.Lett.* 9(1962)12.
44. D.E. Nagle, P.P. Craig, P. Barrett, D.F.R. Cochran, C.E. Olsen and R.D. Taylor, *Phys.Rev.* 125(1962)490.
45. P.P. Craig, B. Mozer and R. Segnan, *Phys.Rev.Lett.* 14(1965)895.
46. T.A. Kitchens, W.A. Steyert and R.D. Taylor, *Phys.Rev.* 138(1965)A467.
47. T.A. Kitchens and P.P. Craig, *J.appl.Phys.* 37(1966)1187.
48. F.W.D. Woodhams, R.E. Meads and J.S. Carlow, *Phys.Lett.* 23(1966)419.
49. B.D. Dunlap and J.G. Dash, *Phys.Rev.* 155(1967)460.
50. W.L. Trousdale, T.A. Kitchens and G. Longworth, *J. appl.Phys.* 38(1967)922.
51. M.P. Maley, R.D. Taylor and J.L. Thompson, *J.appl.Phys.* 38(1967)1249.
52. N.A. Alekseevskii, Yu.A. Samarskii, A.P. Kirjanov and V.I. Tsebro, *Zh.ETF Pis.Red.* 8(1968)650, *Soviet Phys.JETP Lett.* 8(1968)403.
53. A.E. Balabanov, N.N. Delyagin, A.L. Yezinkyan, V.P. Parfenova and V.S. Shpinel', *Zh.Eks. Teor.Fiz.* 55(1968)2136, *Soviet Phys.JETP* 28(1969)1131.
54. N.A. Blum and R.B. Frankel, *J.appl.Phys.* 39(1968)965.
55. J.S. Carlow and R.E. Meads, *J. Phys.C.2*(1969)2120.
56. S. Skalski, J.I. Budnick and J. Lechaton, *J.appl.Phys.* 39(1968)965.
57. R.E. Watson and A.J. Freeman, *Phys.Rev.* 123(1961)2027.
58. J.W. Cable, E.O. Wollan and W.C. Koehler, *Phys.Rev.* 138(1965)A1649.
59. G.G. Low, *Proc.int.Conf.Magnetism*, Nottingham 1964, I.P.P.S., London, 1965, p. 133.
60. G.G. Low and T.M. Holden, *Proc.phys.Soc.* 89(1966)119.
61. T.J. Hicks, T.M. Holden and G.G. Low, *J.Phys.C 1*(1968)528.
62. J.J. Vuillemin and M. Priestly, *Phys.Rev.Lett.* 14(1965)307.
63. B.R. Coles, J.H. Waszink and J. Loram, *Proc.int.Conf.Magnetism*, Nottingham 1964, I.P.P.S., London, 1965, p.165.
64. R. Schwaller and J. Wucher, *C.R. Acad.Sc.(Paris)* 264(1967)1007.
65. M.D. Wilding, *Proc.phys.Soc.* 90(1967)801.

66. J.A. Mydosh, J.I. Budnick, M.P. Kawatra and S. Skalski, *Phys.Rev.Lett.* 21(1968)1346.
67. G. Longworth and C.C. Tsuei, *Phys.Lett.* 27A(1968)258.
68. M.P. Kawatra, S. Skalski, J.A. Mydosh and J.I. Budnick, *J.appl.Phys.* 40(1969)1202.
69. G. Williams and J. Loram, *J.Phys.Chem.Solids* 30(1969)1827.
70. G. Williams, *J.Phys.Chem.Solids* 31(1970)529.
71. P.P. Craig, W.I. Goldburg, T.A. Kitchens and J.I. Budnick, *Phys.Rev.Lett.* 19(1967)1334.
72. I. Nagy and L. Pál, *Phys.Rev.Lett.* 24(1970)894.
73. M.E. Fischer and J.S. Langer, *Phys.Rev.Lett.* 20(1968)665.
74. P.P. Craig and W.I. Goldburg, *J.appl.Phys.* 40(1969)964.
75. P.D. Long and R.E. Turner, *J.Phys.C* 2(1970)S127.
76. A. Theumann, *Phys.Rev. B* 1(1970)4400.
77. B.W. Veal and J.A. Rayne, *Phys.Rev.* 135(1964)A442.
78. H. Montgomery and A.A. Cox, *Proc. Xth int.Conf.low Temp.Phys., Vol.IV, Moscow, Viniti, 1967, p.211.*
79. J.C.G. Wheeler, *J. Phys.C* 2(1969)135.
80. Yu.N. Tsiovkin and N.V. Vol'kenshteyn, *Fiz. Metal. Metalloved.* 19(1965)133, and *Fiz. Tverdogo Tela* 7(1965)543, *Sov.Phys.Solid State* 7(1965)432.
81. D.M.S. Bagguley, W.A. Crossley and J. Liesegang, *Proc.phys.Soc.* 90(1967)1047.  
D.M.S. Bagguley and J.A. Robertson, *Phys.Lett.* 27A(1968)516.
82. M. Peter, D. Shaltiel, J.H. Wernick, H.J. Williams, J.B. Mock and R.C. Sherwood, *Phys.Rev.* 126(1962)1395.
83. D. Shaltiel and J.H. Wernick, *Phys.Rev.* 136(1964)A245.
84. M.F. Cracknell, J.C. Gallop and G.V.H. Wilson, *Phys.Lett.* 24A(1967)719.
85. V.P. Parfenova, N.E. Alekseevskii, A.L. Erzinkyan and V.S. Shpinel', *Zh.Eksp.Teor.Fiz.* 53(1967)492, *Soviet Phys.JETP* 26(1968)324.
86. S. Hörnfeldt, J.B. Ketterson and L.R. Windmiller, *Phys.Rev.Lett.* 23(1969)1292.
87. J.T. Schriempf, A.I. Schindler and D.L. Mills, *Phys.Rev.* 187(1969)959.
88. P. Weiss, *J.Phys.Radium* 4(1907)661.
89. C. Herring, *Magnetism, Vol. IV, ed. G.T. Rado and H. Suhl, Academic Press, New York, 1966, Chapter VI.*
90. D.H. Martin, *Magnetism in Solids, Iliffe Books Ltd, London, 1967, Chapter 6.*
91. H. Sato, A. Arrott and R. Kikuchi, *J.Phys.Chem.Solids* 10(1959)19.
92. J.S. Smart, *J.Phys.Chem.Solids* 16(1960)169.
93. R.J. Elliott, B.R. Heap, D.J. Morgan and G.S. Rushbrooke, *Phys.Rev.Lett.* 5(1960)366.
94. E.C. Stoner, *Proc.roy.Soc. (London)* A154 (1936) 656.
95. E.C. Stoner, *Proc.roy.Soc. (London)* A165(1938)372; *Rep.Progr.Phys.* 11(1947)43.
96. P. Rhodes and E.P. Wohlfarth, *Proc.roy.Soc.(London)* A273(1963)247.
97. P.W. Anderson, *Many Body Physics, ed. C. deWit and R. Balian, 1967 Lecture Notes Les Houches Summer School, Gordon and Breach, New York, 1968, p. 229.*
98. M.A. Ruderman and C. Kittel, *Phys.Rev.* 96(1954)99.

99. T. Kasuya, *Progr.Theor.Phys.* 16(1956)45.
100. K. Yosida, *Phys.Rev.* 106(1957)893.
101. P.W. Anderson, *Concepts in Solids*, W.A. Benjamin Inc., New York, 1963.
102. A. Blandin and J. Friedel, *J. Phys. Radium* 20(1959)160.
103. W. Marshall, *Phys.Rev.* 118(1960)1519.
104. M.W. Klein and R. Brout, *Phys.Rev.* 132(1963)2412.
105. M.W. Klein, *Phys.Rev.* 136(1964)A1156; *Phys.Rev.* 173(1968) 552.
106. M.W. Klein, *Phys.Rev.* 188(1969)933.
107. D.J. Kim, *Phys.Rev. B* 1(1970)3725.
108. B. Giovannini, M. Peter and J.R. Schrieffer, *Phys.Rev.Lett.* 12(1964)736.
109. D.J. Kim and B.B. Schwartz, *Phys.Rev.Lett.* 20(1968)201.
110. S. Doniach and E.P. Wohlfarth, *Proc. roy.Soc.(London)*A296(1967)442.
111. H.S.D. Cole and R.E. Turner, *J.Phys.C* 2(1969)124.
112. T. Takahashi and M. Shimizu, *J. Phys.Soc.Jap.* 23(1967)945.
113. B.M. Boerstael, F.J. du Chatenier and G.J. van den Berg, *Low Temp. Phys.- LT9 (part B)*, Plenum Press, New York, 1965, p.1071.
114. B.M. Boerstael, G.J. Nieuwenhuys and G.J. van den Berg, *Phys.Lett.* 29A(1969) 526.
115. B.M. Boerstael and C. van Baarle, *J.appl.Phys.* 41(1970)1079.
116. B.M. Boerstael, J.J. Zwart and C. van Baarle, *Phys.Lett* 31A(1970)378.
117. B.M. Boerstael and R.F. Wielinga, *Phys.Lett.* 31A(1970)359.
118. A.R. Miedema, R.F. Wielinga and W.J. Huiskamp, *Physica* 31(1965)1585, *Comm. Leiden* No. 345a.
119. O. Béthoux, J.A. Careaga, B. Dreyfus, K. Gobrecht, J.Souletie, R. Tournier, J.J. Veyssié and L. Weil, *Proc. Xth int.Conf.low Temp.Phys., Vol.IV, Moscow, Vinit, p. 290.*
120. F.J. du Chatenier, thesis, Leiden, 1964.
121. F.J. du Chatenier, J. de Nobel and B.M. Boerstael, *Physica* 32(1966)561, *Comm. Leiden*, No. 347a.
122. F.J. du Chatenier and J. de Nobel, *Physica* 32(1966)1097, *Comm.Leiden* No. 347c.
123. F.J. du Chatenier and A.R. Miedema, *Physica* 32(1966)403, *Comm.Leiden* No. 343b.
124. S.H.Liu, *Phys.Rev.* 157(1967)411.
125. T. Moriya, *Proc. int. School Physics 'Enrico Fermi'*, Academic Press, New York, 1967, Course 37, p. 206.
126. G. Chouteau, R. Fourneaux, K. Gobrecht and R. Tournier, *Phys.Rev.Lett.* 20(1968)193.  
G. Chouteau, R. Fourneaux, R. Tournier and P. Lederer, *Phys.Rev.Lett.* 21(1968)1082.
127. B.M. Boerstael, to be published.
128. H.S.D. Cole and R.E. Turner, *Phys.Rev.Lett.* 19(1967)501.
129. J.A. Seitchik, A.C. Gossard and V. Jaccarino, *Phys.Rev.* 136(1964)A1119.
130. S. Ehara, *J.Phys.Soc.Jap.* 19(1964)1313.
131. M. Dixon, F.E.Hoare, T.M. Holden and D.E. Moody, *Proc.roy.Soc.(London)* A285(1965)561.
132. F.E. Hoare and B. Yates, *Proc.roy.Soc.(London)* A240(1957)42.
133. D.W. Budworth, F.E. Hoare and J. Preston, *Proc.roy.Soc. (London)* A257(1960)250.

## Chapter V

### MOLECULAR FIELD CALCULATION OF THE SPECIFIC HEAT IN EXTERNAL MAGNETIC FIELDS; CRITICAL BEHAVIOUR OF PD-MN ALLOYS

#### V.1. Introduction

In the first part of this chapter the specific heat in external magnetic fields is calculated on the basis of the Weiss molecular-field (WMF) model. The calculated curves will be compared with the results obtained on Pd-Mn alloys. In an attempt to describe also the specific heat of Pd-Co and Pd-Fe alloys in external magnetic fields, the calculations have been extended, introducing a distribution of molecular fields. It will be shown that quite fair agreement is obtained between the specific heat of Pd-Mn alloys and that calculated from the WMF approximation while, on the other hand, agreement is poor in the case of Pd-Co and Pd-Fe alloys.

#### V.2.1. Derivation of the specific heat

In the WMF approximation the specific heat in the presence of an external magnetic field can be calculated from the basic equations [1]:

$$\sigma = \sigma(T) = \sigma(0) B_S(x) \quad (V.1)$$

$$B_S(x) = \frac{2S+1}{2S} \coth\left(\frac{2S+1}{2S}x\right) - \frac{1}{2S} \coth\left(\frac{x}{2S}\right) \quad (V.2)$$

$$\text{where } x = g\mu_B S (H + H_m)/kT \quad (V.3)$$

$$\text{and } H_m = H_m(T) = D\sigma(T). \quad (V.4)$$

In these equations  $\sigma(0) = Ng\mu_B S$  is the saturation magnetization per gram-atom,  $H$  the external magnetic field,  $H_m$  the molecular field and  $D$  the molecular-field constant.  $N$  is the number of atoms per gram-atom, while  $B_S(x)$  is the well-known Brillouin function with  $S$  the spin of the magnetic carriers \*).

The magnetic energy in the presence of a constant external field is given by

$$U_m = - \int H_{\text{tot}} d\sigma = - \int (H + H_m) d\sigma.$$

\*) Since the magnetization of dilute ferromagnetic alloys is very small, contributions to the total magnetic field acting on the magnetic carriers arising from demagnetization effects [2] may be neglected (see also footnote in section III.2.1).

Using eq. (V.4) one obtains

$$C = dU/dT = -(H + H_m) d\sigma/dT. \quad (V.5)$$

In order to obtain the specific heat  $\sigma$  has to be calculated as a function of  $T$ . This problem leads to the well-known set of implicit equations

$$\sigma(T)/\sigma(0) = B_S(x) \quad (V.6)$$

$$\sigma(T)/\sigma(0) = \{NkT/D\sigma(0)^2\} x - H/D\sigma(0) \quad (V.7)$$

which have to be solved simultaneously. This can be done either graphically or numerically [1].

It is useful to introduce a dimensionless parameter

$$b = \{Nk/D\sigma(0)^2\} T \quad (V.8)$$

and to define  $p$  as the ratio of the external magnetic field and the molecular field at  $T = 0$ :

$$p = H/H_m(0) = H/D\sigma(0). \quad (V.9)$$

When calculating the specific heat per gram-atom ( $Nk = R$ ) one obtains from eq. (V.5), using eq. (V.8) and eq. (V.9)

$$\frac{C}{R} = - \{B_S(x) + p\} \frac{dB_S(x)}{db} = - \{B_S(x) + p\} \frac{dB_S(x)}{dx} \frac{dx}{db}. \quad (V.10)$$

The relation between  $x$  and  $b$ , and hence  $T$ , can be easily obtained from eqs. (V.6) . . . (V.9):

$$b = \{B_S(x) + p\} / x. \quad (V.11)$$

The specific heat can now be calculated from eq. (V.10) and eq. (V.11).

The calculations have been carried out on a computer. The procedure is as follows. For fixed values of  $S$  and  $p$  a suitable set of  $x$  values is chosen.  $B_S(x)$  is calculated for each  $x$ . Then  $b$  is found from eq. (V.11) and finally  $C/R$  is obtained straightforwardly at each value of  $b$ , the derivatives occurring in eq. (V.10) being calculated from eq. (V.2) and eq. (V.11).

As an example a set of specific-heat curves calculated for  $S = 5/2$  and  $p$  ranging from 0 to 10 has been plotted as a function of  $b$  in fig. V.1. It is found that at  $p \gg 1$  the Schottky specific heat, i.e. the specific heat of a paramagnetic system in an applied magnetic field, is obtained. This was to be expected, of course, since the external field dominates the molecular field at these  $p$  values. This might be phrased as follows: at sufficiently large applied magnetic fields the interacting system is forced to behave paramagnetically. In fig. V.1 the dashed line denotes the maximum value,  $(C/R)_{\max} = 0.85$ , of the Schottky curve for  $S = 5/2$ . As can be seen, application of a magnetic field has a large influence on the specific heat;

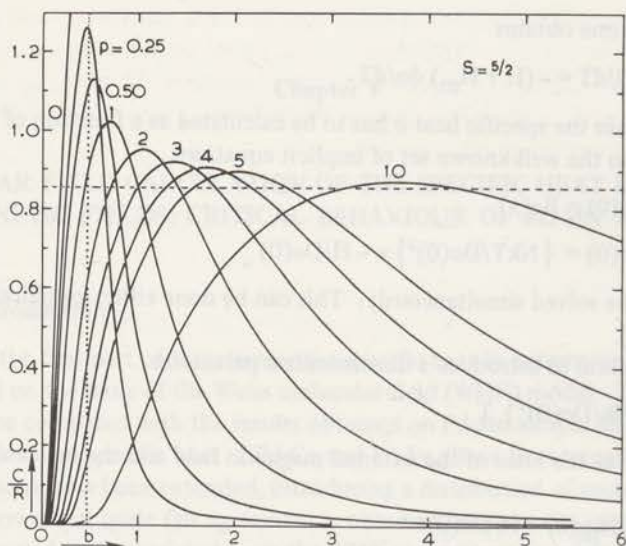


fig. V.1.  $C/R$  versus  $b$  at different values of  $p = H/H_m(0)$ . Values of  $p$  have been indicated near the top of the appropriate specific-heat curve. The dashed line is explained in the text.

$(C/R)_{\max}$  rapidly decreases with  $p$  from 2.365 (at  $p = 0$ ) to values close to 0.85. (Note that at  $p = 0$   $(C/R)_{\max}$  is almost twice as high as the upper bound of the ordinate scale in fig. V.1).

It is interesting to consider the dependence upon  $p$  of the  $b$ -value ( $b_{\max,p}$ ) at which  $C/R$  attains its maximum. From fig. V.1 values of  $b_{\max,p}$  were taken and subsequently plotted in fig. V.2 as a function of  $p$ . As can be inferred from fig. V.2,  $b_{\max,p}$  varies almost linearly with  $p$  at  $p \geq 2$  approximately; that is within the accuracy with which the numerical computations and the graphical analyses were carried out ( $\approx 1\%$ ). A very remarkable feature should be noted: the straight line also passes through  $b_{\max,0}$  which is, of course, related to the Curie temperature  $\theta$ . The Curie temperature is given by  $\theta = \{D\sigma(0)^2/3Nk\} (S+1)/S$  [1]. Using eq. (V.8) and  $S = 5/2$  one obtains  $b_{\max,0} = 7/15$ . At  $0 < p < 2$  the variation of  $b_{\max,p}$  with  $p$  is more complicated; at very small  $p$ -values  $b_{\max,p}$  even passes through a small minimum. After extrapolation, the straight line is found to intersect the  $p$ -axis at  $-1.50$ . For  $S = 5/2$ ,  $p = 0$  and  $p \geq 2$ , approximately, one can now write

$$b_{\max,p} = b_{\max,0}(1 + p/1.50) \quad (\text{V.12a})$$

or 
$$T_{\max,H} = \theta (1 + H/1.50 H_m(0)). \quad (\text{V.12b})$$

These relations have been obtained graphically.

For other values of  $S$  similar relations for  $b_{\max,p}$  can be obtained. The importance of eq. (V.12a,b) follows from the fact that the same type of relationship is observed experimentally, as is shown in the next section. Moreover, it may be stressed that according to eq. (V.12b) the only adjustable parameter of the model, viz. the molecular-field  $H_m(0)$ , can be derived from a plot of  $T_{\max,H}$  versus  $H$ .

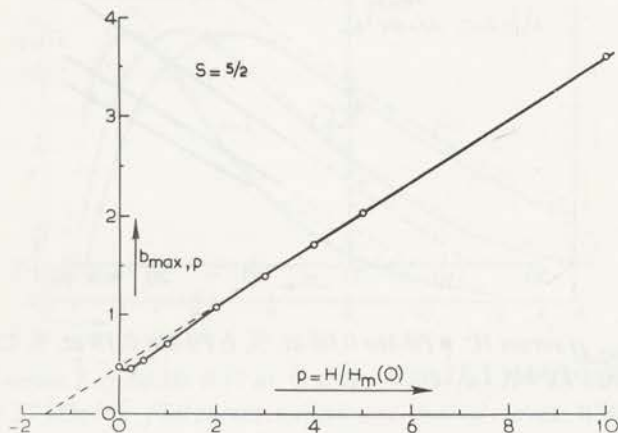


fig. V.2.  $b_{\max,p}$  versus  $p$  for  $S = 5/2$ .  $b_{\max,p}$  and  $p$  have been defined in the text.

### V.2.2. Application to Pd-Mn alloys

As discussed in section IV.4 there are a number of indications that interactions in the Pd-Mn system are, to a high degree, spatially uniform. However, one cannot expect that the WMF approximation provides a good description of the specific heat of Pd-Mn alloys at low external magnetic fields (i.e. low compared to  $H_m(0)$ ), since short-range fluctuations are not considered in this approximation. By neglecting these fluctuations one calculates a specific heat which drops to zero discontinuously at  $T = \theta$  (dotted line in fig. V.1), whereas, according to fig. IV.14 the specific heat of Pd-Mn alloys exhibits a large short-range-order contribution. At higher fields, however, one may expect the WMF model to become more applicable, short-range fluctuations then being quenched by these fields.

In order to verify the applicability of the WMF model, it is useful to first consider the magnetic-field dependence of  $T_{\max,H}$ . A plot of  $T_{\max,H}$  versus  $H$  is given in fig. V.3 for four Pd-Mn alloys. Only on Pd-Mn 0.19 at. % and 0.54 at. % measurements have been carried out at three values of  $H \neq 0$ . Nevertheless, for both these alloys the data lie on straight lines which, moreover, are approximately parallel

to each other. Both points obtained for Pd-Mn 0.08 at. % lie on a line which is almost parallel to the former ones.

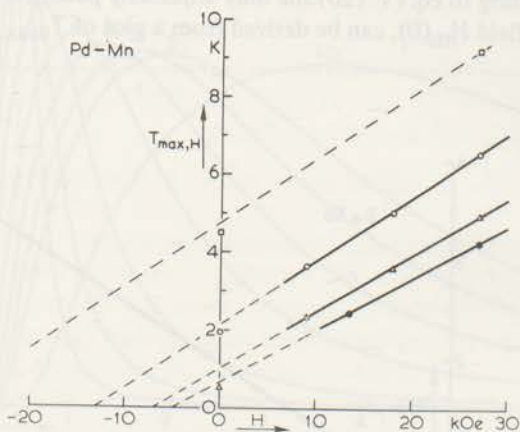


fig. V.3.  $T_{max,H}$  versus  $H$ . ● Pd-Mn 0.08 at. %,  $\Delta$  Pd-Mn 0.19 at. %,  $\circ$  Pd-Mn 0.54 at. %,  $\square$  Pd-Mn 1.35 at. %.

At sufficiently high external fields, the field dependence of  $T_{max,H}$  may be described by the relation

$$T_{max,H} = T_{max,0} (1 + H/|H^{\circ}|). \quad (V.13)$$

$H^{\circ}$  is the intersection of the lines with the  $H$ -axis. Evidently, relation (V.13) is structurally equivalent to eq. (V.12a,b) derived from the WMF model.  $T_{max,0}$  may now be interpreted as the Curie temperature fitting to the WMF model at  $H = 0$ ; the real transition temperatures are always lower, as expected (note the points at  $H = 0$ ).

Values of  $H^{\circ}$  deduced from fig. V.3 have been listed in table V.1. For Pd-Mn 1.35 at. %  $H^{\circ}$  has been obtained assuming the line through the point at  $H = 27$  kOe to be parallel to the one for Pd-Mn 0.54 at. %, as shown. If the WMF model is considered to be appropriate for the analysis of the specific heat of Pd-Mn alloys, one can proceed by calculating  $H_m(0)$  from  $H_m(0) = |H^{\circ}|/1.50$ , which also determines  $p = H/H_m(0)$  at each  $H$ . Values of  $H_m(0)$  are given in the third column of table V.1. As noted in the preceding section the only adjustable parameter in the WMF calculation is  $H_m(0)$  (or  $D$ ). Thus, if  $H_m(0)$  is known,  $\theta = T_{max,0}$  can be calculated from the expression for  $\theta$  and hence,  $T_{max,H}$  can be evaluated from eq. (V.13). If this is actually done the calculated value of  $T_{max,0}$  is always smaller than the one

derived directly from experiment. This implies that two different values of the molecular field (or  $D$ ) can be obtained. This inconsistency will be discussed at the end of this section. In practice, the calculated specific-heat curves were fitted to the experimental curves by matching  $b_{\max,0}$  to the value of  $T_{\max,0}$ , obtained experimentally for each specimen.

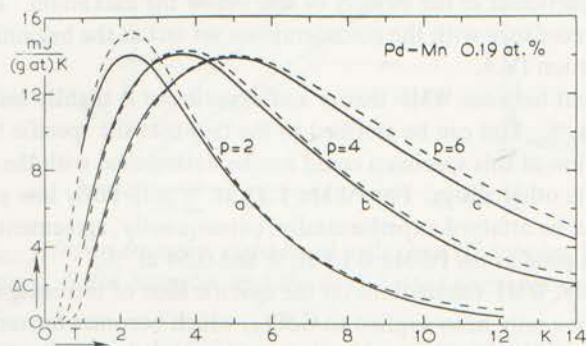


fig. V.4.  $\Delta C$  versus  $T$  of Pd-Mn 0.19 at. % at  $H = 9$  kOe (a),  $H = 18$  kOe (b) and  $H = 27$  kOe (c). Full curves: experiment, dashed curves: WMF-model calculation.  $p$  has been defined in the text.

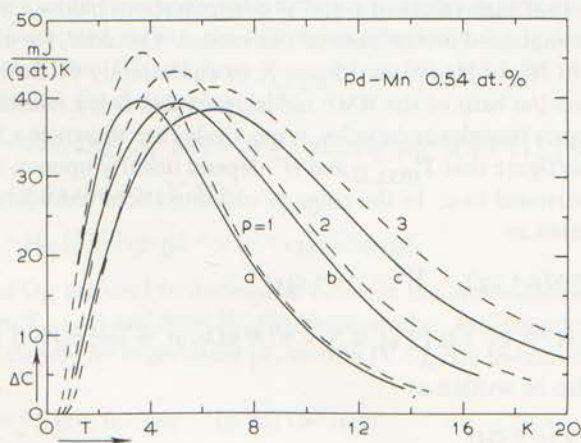


fig. V.5.  $\Delta C$  versus  $T$  of Pd-Mn 0.54 at. % at  $H = 9$  kOe (a),  $H = 18$  kOe (b) and  $H = 27$  kOe (c). Full curves: experiment, dashed curves: WMF-model calculation.  $p$  has been defined in the text.

In fig. V.4 and fig. V.5 the specific heat is shown for Pd-Mn 0.19 at. % and Pd-Mn 0.54 at. % at  $H = 9, 18$  and  $27$  kOe. The experimental results are shown by drawn curves, the theoretical results by dashed lines in the figures. Theoretical curves have been calculated by multiplying  $C/R$  by  $c$  and deriving the appropriate  $p$  from  $H_m(0)$ . Taking into account the uncertainty in  $c$  and the possible experimental error in the specific heat, agreement between WMF theory and experiment is surprisingly good, especially at higher  $p$ -values. For  $p < 2$  agreement becomes less, in particular in the vicinity of and below the maximum. This behaviour is in accordance with the considerations set out at the beginning of this section and in section IV.4.

Agreement between WMF theory and experiment is slightly less satisfactory for Pd-Mn 0.08 at. %. This can be ascribed to the fact that the specific heat as well as the concentration of this specimen could not be determined with the same accuracy as for the other alloys. For Pd-Mn 1.35 at. % only fairly low  $p$ -values (up to 1.35) could be attained experimentally; consequently, agreement cannot be expected to be as good as for Pd-Mn 0.19 at. % and 0.54 at. %.

Previously, WMF calculations on the specific heat of ferromagnets in external magnetic fields have only been applied to  $GdCl_3$ , which becomes ferromagnetic at 2.20 K (Garton et al. [3]). Their measurements have been carried out at fields up to 8.4 kOe, enabling comparison between theory and experiment to be made at  $p$ -values up to  $p = 0.66$ . Nevertheless, these authors also noted that agreement with experiment improved at higher  $p$ -values.

Although the WMF model can be used successfully to represent the specific heat of Pd-Mn alloys at high values of  $p$  and at concentrations below 1 at. %, some features cannot be explained on the basis of this model. Consider, for example, the  $c$ -dependence of  $H^\circ$ , or  $H_m(0)$ , and  $T_{max,0}$ , or equivalently  $\theta$ . Both should be proportional to  $c$  on the basis of the WMF model, provided  $D$  is a constant. In fig. V.6  $T_{max,0}$  and  $H^\circ$  (open triangles and circles, respectively) are shown as a function of  $c$ . It follows from this figure that  $T_{max,0}$  and  $H^\circ$  depend linearly upon  $c$ , instead of simply being proportional to  $c$ . In the range of concentrations considered  $T_{max,0}$  and  $H^\circ$  can be written as

$$T_{max,0} = x(c + c_T), \quad H^\circ = y(c + c_H) \quad (V.14,15a)$$

where  $x = 3.27$  K/at. %,  $c_T = 0.12$  at. %,  $y = 17.9$  kOe/at. % and  $c_H = 0.19$  at. %.

Eq. (V.15a) can also be written as

$$H_m(0) = y'(c + c_H) \quad (V.15b)$$

where  $y' = 11.9$  kOe/at. % and  $c_H = 0.19$  at. %. As was discussed in section IV.4 (see also fig. IV.15) the  $T_C$  derived from the actual specific-heat maximum at  $H = 0$ , is proportional to  $c$ . This is shown in fig. V.6 by the solid triangles.

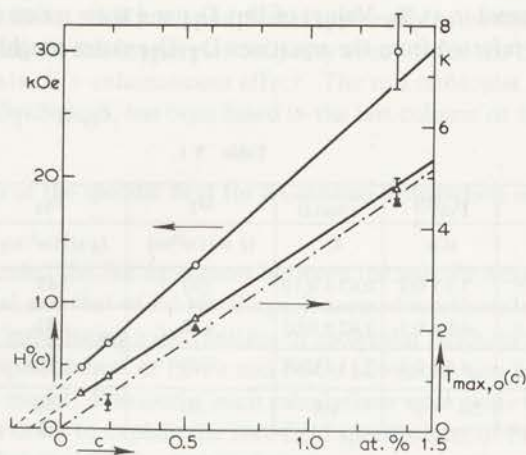


fig. V.6.  $T_{\max,0}$  (open triangles, right-hand scale) and  $H^0$  (circles, left-hand scale) versus  $c$ . Solid triangles and the dash-dotted line represent  $T_c$  as a function of  $c$ .

Extrapolation of the full lines in fig. V.6 to  $c = 0$  leads to a result which is difficult to understand physically. On the other hand, considering the accuracy of the data, it cannot be denied that  $T_{\max,0}$  and  $H^0$  closely follow relations (V.14) and (V.15a) in the range of concentrations at which the measurements were carried out. It is, of course, possible that  $T_{\max,0}$  tends to zero for  $c < 0.08$  at. %. However, in order to verify this possibility extremely accurate measurements are required.

As mentioned earlier, the discrepancy between the molecular-field constant derived from  $H^0$  and from  $\theta$  remains to be explained. Using eq. (V.14) and the expression for  $\theta$  one obtains \*)

$$D_T = 3k\theta/cNg^2\mu_B^2 S(S+1) = \{3k/cNg^2\mu_B^2 S(S+1)\} \{x(c+cT)\}$$

and from eq. (V.4) and eq. (V.15b)

$$D_H = H_m(0)/cNg\mu_B S = y'(c+c_H)/cNg\mu_B S$$

where  $D_T$  and  $D_H$  are used to distinguish between the molecular-field constant obtained from  $T_{\max,0}$  and from  $H_m(0)$ , respectively. Assuming  $g = 2$  and  $S = 5/2$ , as confirmed closely by experiment [4, section IV.5], one obtains from these equations

$$D_T = 75(c+0.12)/c \quad (\text{g at}) \text{ Oe}^2/\text{erg} \quad (\text{V.16})$$

$$D_H = 43(c+0.19)/c \quad (\text{g at}) \text{ Oe}^2/\text{erg} \quad (\text{V.17})$$

\*) Note that the number of magnetic carriers is  $cN$ . Hence, in all preceding equations  $N$  should be replaced by  $cN$ .

where  $c$  is expressed in at.%. Values of  $D_T$ ,  $D_H$  and their ratios are shown in table V.1. As can be inferred from the equations  $D_T/D_H$  varies roughly between 1.0 and 1.75.

Table V.1.

Alloy	$ H^0 $	$H_m(0)$	$T_{max,0}$	$D_T$	$D_H$	$D_T/D_H$	$D_{T0}(0)$
at. %	kOe	kOe	K	(g at) Oe <sup>2</sup> /erg	(g at) Oe <sup>2</sup> /erg		kOe
0.08	$4.8 \pm 0.5$	$3.2 \pm 0.3$	$0.67 \pm 0.10$	190	145	1.31	$4.2 \pm 0.4$
0.19	$6.8 \pm 0.2$	$4.5 \pm 0.1$	$1.02 \pm 0.05$	120	85	1.41	$6.3 \pm 0.1$
0.54	$13.0 \pm 0.2$	$8.7 \pm 0.1$	$2.15 \pm 0.05$	90	60	1.50	$13.0 \pm 0.2$
1.35	$30 \pm 3$	$20 \pm 2$	4.8	80	50	1.60	$32 \pm 3$

In order to account for the difference between  $D_T$  and  $D_H$  the following suggestion is made. From theoretical considerations Doniach [5] has pointed out that the effect of an external magnetic field may be increased appreciably by exchange enhancement in Pd alloys. If this were so, an external field  $H$  may act on the magnetic carriers in a specimen as if it were equal to  $nH$ . The situation which now arises has been presented graphically in fig. V.7. For the analysis of  $T_{max,H}$  as a function of  $H$  the nominal values of  $H$  have been used. Hence  $H^0$  has been derived. Actually, the molecular-field constant  $D$  is determined by  $nH^0$  so that in order to find  $D$ ,  $nH$  and hence  $nH^0$  should have been used. On the other hand,  $T_{max,0} = \theta$  is independent of  $n$ , as will be evident from the plot. Thus, if this suggestion is correct,  $D_T$  should be considered to be the real molecular-field constant. From fig. V.3 it follows that the enhancement factor  $n$  is independent of the applied field and it can be easily verified that  $n$  is equal to the ratio  $D_T/D_H$ :

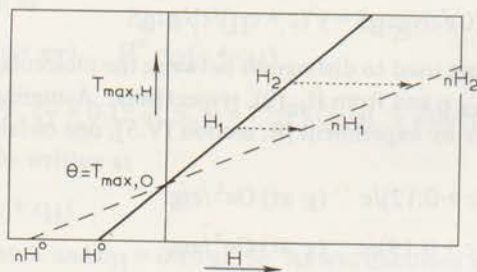


fig. V.7. Influence of field enhancement on  $T_{max,H}$ .

see table V.1. Note that  $n > 1$  if  $c > 0$  and that  $n$  apparently saturates rapidly at higher concentrations. In this interpretation  $n$  may account for the concentration dependence of Doniach's enhancement effect. The real molecular field at  $T = 0$ , given by  $D_T\sigma(0) = D_TcNg\mu_B S$ , has been listed in the last column of table V.1.

### V.2.3. Calculation of the specific heat for a Gaussian distribution of molecular fields

Bearing in mind the fair agreement between the specific heat calculated from the WMF model and that of Pd-Mn alloys, it seemed worthwhile to carry out similar calculations, introducing a distribution of molecular fields, in an attempt to verify, whether the specific heat of Pd-Fe and Pd-Co alloys can also be described in terms of this simple model. Previously, such calculations were made by Takahashi and Shimizu [6] in order to explain the zero-field specific heat of Pd-Fe and Pd-Co alloys, available at that time [7,8]. Although these authors considered agreement between theory and experiment to be rather satisfactory, it certainly is less impressive than in the case of the Pd-Mn alloys at high external fields. As a matter of fact, this is not so surprising because the WMF model is also unable to account for the zero-field specific heat of Pd-Mn alloys.

For a uniform internal field the specific heat is given by

$$C/R = - \{ B_S(x) + p \} \{ dB_S(x)/dx \} dx/db. \quad (V.10)$$

For the present calculation the distribution of molecular fields is assumed to be Gaussian at  $T = 0$ . It can be imagined to arise from the statistical distribution of magnetic carriers in the matrix and from inhomogeneities in the specimen, remembering that the interaction strength depends upon the distance. The 'most probable' internal field at  $T = 0$  is denoted by  $\bar{H}_m(0)$ . The parameter  $p$  is now defined as the ratio of the external field and the 'most probable' field

$$p = H/\bar{H}_m(0) = H/\bar{D}\sigma(0), \quad (V.18)$$

where  $\bar{D}$  is the 'most probable' molecular-field constant. The distribution of molecular fields at  $T = 0$  can be represented by a distribution of molecular-field constants.

The Gaussian distribution function is given by

$$P(D) \propto \exp \left\{ -\frac{1}{2} \left( \frac{D/\bar{D} - 1}{F} \right)^2 \right\} \quad (V.19)$$

where  $\bar{D}$  is the width of the distribution function. The parameter  $x$  is more complicated than in eq. (V.3):

$$x = \frac{g\mu_B S}{kT} (H + H_m) = \frac{g\mu_B S}{kT} \left\{ \frac{H}{\bar{D}\sigma(0)} + \frac{D\sigma(T)}{\bar{D}\sigma(0)} \right\} \bar{D}\sigma(0) =$$

$$= (\bar{D}/D') \{ p + (D/\bar{D}) B_S(x) \}, \quad (V.20)$$

where  $D' = RT/\sigma(0)^2$ ; according to eq. (V.8)  $b = D'/\bar{D}$ .

In order to calculate the specific heat the range of  $D$  values is divided into  $l$  discrete steps which are chosen to be suitably small. The lower bound is taken to be  $D = 0$ , which applies to isolated magnetic carriers, and the upper bound is determined by the interaction strength of magnetic carriers at nearest-neighbour distance. For dilute alloys the upper bound is chosen to be much larger than  $\bar{D}$ ; the computed specific-heat curves then turn out to be rather insensitive to the value actually chosen for the upper bound.

As explained in section V.2.1 the specific heat can be calculated by choosing a suitable set of  $x$  values at fixed  $S$  and  $p$ . However, for each  $x$  the distribution of  $D$  should be taken into account, as follows from eq. (V.20). Thus, at each  $x$  a set of  $x_m$  values corresponding to the set of  $D$  values, should be calculated. Due to the presence of  $B_S(x)$  in eq. (V.20) this cannot be done straightforwardly. This problem has been solved by iteration, carrying out the following procedure. At each  $x$  the value of  $b = D'/\bar{D}$  is obtained from eq. (V.20), taking  $D = \bar{D}$ , by which the corresponding temperature  $T$  has been determined apart from a constant factor. At each  $x$  one can now proceed by evaluating  $x_m$ , corresponding to a particular value  $D_m$  from the set of  $D$ 's. As a first step it is assumed that  $B_S(x_{m,1}) = B_S(x)$ . Then  $x_{m,1}$  can be calculated from eq. (V.20)

$$x_{m,1} = (\bar{D}/D') \{ p + (D_m/\bar{D}) B_S(x) \}.$$

Thereupon,  $B_S(x_{m,1})$  is evaluated from  $x_{m,1}$ . The second step is, obviously,

$$x_{m,2} = (\bar{D}/D') \{ p + (D_m/\bar{D}) B_S(x_{m,1}) \}.$$

Hence, the iterative procedure is based upon the relation

$$x_{m,n} = (\bar{D}/D') \{ p + (D_m/\bar{D}) B_S(x_{m,n-1}) \}, \quad (V.21)$$

and is completed when  $x_{m,n}$  satisfies the criterion  $|x_{m,n} - x_{m,n-1}|/x_{m,n} < a$ , where  $a$  is chosen in advance. The approximation turns out to converge rapidly, as it never took more than two successive steps to satisfy the criterion with  $a$  as small as 0.3%.

Once  $x_m = x_{m,n}$  is known for each  $D_m$ , at each value of  $x$ , it is straightforward to evaluate the specific heat at each  $x$  (or  $b$ ) from

$$(C/R)_x = \sum_{m=0}^l P(D_m) C(x_m)/R, \quad (V.22)$$

using eqs (V.10) and (V.19). The number of steps,  $l$ , has been chosen to be one hundred at least.

As an example, results calculated for  $S = 1.5$  at different values of  $p$  and  $F$  are shown in fig. V.8. The parameter  $F$  corresponds to the width of the molecular-field distribution expressed in units of  $\bar{H}_m(0)$ .

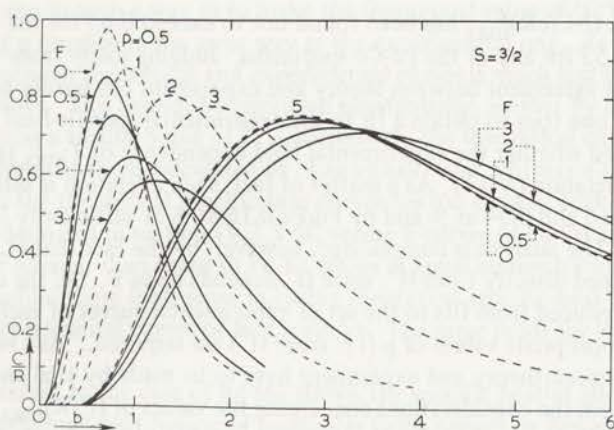


fig. V.8. Calculated specific-heat curves for  $S = 1.5$  and  $p = 0.5, 1, 2, 3$  and  $5$ .  
 At  $p = 0.5$  and  $p = 5$  a set of curves for  $F = 0.5, 1, 2$  and  $3$  is given.  
 At  $p = 1, 2$  and  $3$  only curves for  $F = 0$  are presented. All curves for  $F = 0$  have been plotted as dashed curves.

The influence of  $F$  on the specific heat can be summarized as follows.

- At low external fields the specific-heat maximum rapidly decreases with increasing  $F$ , provided  $F$  is not too large. Meanwhile the specific-heat curve broadens appreciably. At larger values of  $F$  the decrease of the specific-heat maximum becomes less pronounced.
- At high external fields the decrease of the specific-heat maximum and the broadening of the curves with increasing  $F$  is much less marked.
- For a given value of  $F$  the  $p$ -dependence of  $b_{\max,p}$  can be described by a linear relation similar to eq. (V.12a). Both  $H^\circ$  and  $b_{\max,0}$  increase with increasing  $F$ , as can be inferred from the shift of  $b_{\max,p}$  towards higher  $b$ -values at constant  $p$  and increasing  $F$ .
- Generally large values of  $F$  are required in order to obtain an appreciable decrease of  $(C/R)_{\max}$ .

#### V.2.4 Application to Pd-Fe, Pd-Co and Pt-Co alloys

According to the entropy as determined in section IV.5, the spin of Fe and Co in Pd is close to  $3/2$ . In order to get a rough idea of the applicability of the theory for  $S = 3/2$  to the experimental curves of Pd-Fe and Pd-Co alloys, it is useful to consider the values of the specific-heat maxima. Theoretically,  $(C/R)_{\max}$  is found between about 0.85 and 0.65 at  $p > 1$  and  $F$  ranging from 0 to 3.

Experimentally,  $(\Delta C/cR)_{\max}$  has been found not to exceed 0.63 for the Pd-Fe specimen and 0.53 for any of the Pd-Co specimens. Judging solely from this discrepancy, fair agreement between theory and experiment can hardly be expected.

Yet, if one tries to obtain a fit to the experimental specific-heat curves, it should be verified whether the experimental field dependence of  $T_{\max,H}$  can be represented by relation (V.13). As a matter of fact, such a relation is satisfied by Pd-Co 0.075, 0.16 and 0.24 at.% and by Pd-Fe 0.16 at.% at sufficiently large external fields. The analysis is complicated, however, by the fact that  $\bar{H}_m(0)$  (or  $D$ ) cannot be obtained directly from  $H^\circ$ , since  $H^\circ$  depends upon  $F$ . On the other hand,  $F$  can only be deduced from fits to the set of experimental curves of each specimen, for which the appropriate values of  $p$  (i.e. from  $H^\circ$ ) are required. As a result comparisons between theory and experiment have to be made by trial and error. As is obvious from the considerations concerning the values of  $(C/R)_{\max}$  given above, agreement between theory and experiment can be expected to be more satisfactory for Pd-Fe than for Pd-Co. It turns out that rather large values of  $F$  are required. A precise determination of  $F$  cannot be expected as the specific heat appears to be rather insensitive to changes of  $F$ .

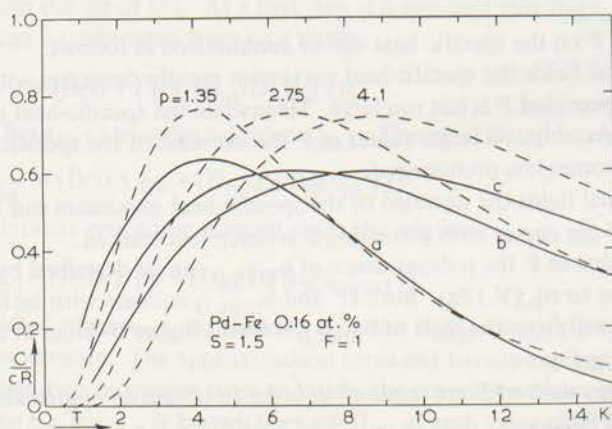


fig. V.9. Pd-Fe 0.16 at.%. Comparison between experimental (—) and theoretical (----) specific-heat curves. a, b and c represent results obtained at  $H = 9, 18$  and  $27$  kOe, resp. Theoretical curves were obtained for  $S = 3/2$ ,  $F = 1$  and  $p = 1.35, 2.75$  and  $4.1$ , resp.  $H_m(0) = 6.6$  kOe.

In spite of these rather discouraging considerations, the result of an attempt to fit the specific heat of Pd-Fe 0.16 at.% is presented in fig. V.9. The value of  $F$

has been chosen in such a way as to make the theoretical value of  $(C/R)_{\max}$  vary as a function of  $p$  roughly in the same way as the experimental one. As can be seen, agreement between theoretical and experimental curves is much less satisfactory than for Pd-Mn alloys. This cannot be improved substantially, neither by choosing a larger nor by choosing a smaller value of  $F$ . Qualitatively the theoretical curves exhibit the same deficiencies as those calculated by Takahashi and Shimizu [6] for  $H = 0$ . In both cases the theoretical specific-heat curves are too sharply peaked.

As discussed in section IV.3.3  $\Delta C$  versus  $T$  curves of Pd-Co alloys are considerably broader than those of Pd-Fe alloys at equal concentration of solute atoms. Therefore there is no sense in fitting theoretical specific-heat curves for  $S = 3/2$  to experimental curves of Pd-Co alloys. The same holds for Pt-Co alloys, using  $S = 1$ .

Contrary to the case of Pd-Mn alloys, the specific heat of alloys which exhibit a continuous distribution of molecular fields cannot be described quantitatively in terms of the present calculation. Therefore, it is advisable to reconsider the shape of the distribution function (of  $D$ ) at  $T = 0$ . Once this distribution function has been chosen the temperature dependence of the internal fields follows within the framework of the WMF approximation from eq. (V.4) and eq. (V.20). In the calculations the shape of the distribution function at  $T = 0$  has so far been assumed implicitly to remain unchanged by application of an external field. Two possibilities arise if, for any reason, a change of the shape does occur. If the field merely causes a change of the width of the distribution function one cannot expect to obtain better agreement with the data for obvious reasons. One can also imagine as a possibility that the distribution becomes skew-symmetrical. Actually, some calculations have been carried out using skew-symmetrical distribution functions at  $T = 0$ . The shape of the specific-heat curves was changed, but the value of  $(C/R)_{\max}$  turned out to be hardly affected and, consequently, no improvement has been obtained. To conclude, the present calculations have suggested that WMF theory is much too simple to account for the specific heat of Pd-Fe, Pd-Co and Pt-Co alloys, even at moderately high fields. If this is so the applicability of WMF theory to the specific heat of Pd-Mn alloys, becomes the more unique.

Finally, it should be remembered that for Pd-Co alloys  $T_c \propto c^2$  at  $c < 0.5$  at.% and  $H = 0$  (section IV.3.1), in disagreement with  $T_c \propto c$  which follows from the WMF model. This empirical fact could have been incorporated artificially in the calculations, assuming  $\theta \propto (D_m/\bar{D})^2$ . Better agreement between such calculations and experiment can be expected, since the specific heat at  $T \ll T_{\max}$  and at  $T \gg T_{\max}$  will be enhanced, whereas at  $T \approx T_{\max}$  the specific heat is expected to decrease.

Although no quantitative agreement with experiment could be obtained it is still possible to make some remarks about the magnetic-field dependence of the calculated specific heat. In order to make this point clear, three sets of curves,

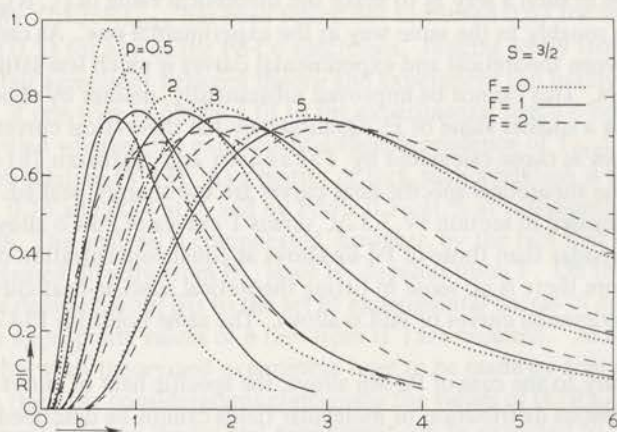


fig. V.10. Calculated specific-heat curves for  $S = 3/2$  at  $p = 0.5, 1, 2, 3$  and  $5$ . At each value of  $p$  curves for  $F = 0, 1$  and  $2$  have been plotted.

calculated for  $p = 0.5, 1, 2, 3$  and  $5$  and for  $F = 0, 1$  and  $2$  are shown in fig. V.10. As is evident from the graph  $(C/R)_{\max}$  decreases with increasing  $p$  at small values of  $F$ . The opposite behaviour is found at large values of  $F$ . The width of the specific-heat curves increases considerably with increasing  $F$ , provided  $p$  is not too large. As mentioned in section IV.3.2, and as shown in fig. IV.8, the specific heat of a number of Pd-Co alloys qualitatively exhibits a similar behaviour. As already suggested, the width of the distribution of internal fields is large at low concentrations and decreases at higher concentrations of Co.

#### V.2.5. Concluding remarks

Up till now, no theory on the specific heat of dilute ferromagnetic alloys in the presence of an external magnetic field has been reported in the literature. In order to account for the experimental results of Pd-Mn, Pd-Co, Pd-Fe and Pt-Co alloys, it seemed worthwhile to carry out calculations using the WMF model. The method used is outlined in section V.2.1. The WMF model should be considered as the simplest approximation to the problem of ferromagnetism. One should therefore not expect very good agreement with experiment, except perhaps in very strong external fields. Although for the specific heat of dilute Pd-Mn alloys in rather strong external fields agreement between WMF theory and experiment turns out to be surprisingly good, there are some features which cannot be interpreted by this theory. These have been discussed in section V.2.2.

An extension of the WMF calculations, using a distribution of molecular

fields, has been given in section V.2.3. As is shown, however, such an extension does not lead to a satisfactory description of the specific heat of dilute Pd-Fe, Pd-Co and Pt-Co alloys, though it seems possible to account qualitatively for the magnetic-field dependence of the specific heat of these alloys by a proper choice of the width of the internal-field distribution.

One can now conclude that the WMF model is apparently much too simple a model to give a proper description of the specific heat of dilute Pd-Co, Pd-Fe and Pt-Co alloys. However, a more elaborate theory, which e.g. takes into account spin-wave type excitations, will not only have to interpret the behaviour of these alloys, but also why just the specific heat of dilute Pd-Mn alloys can be described rather satisfactorily by means of the WMF model. For instance, there are so far no reasons to assume that the type of interaction in these alloys is essentially different from that of e.g. Pd-Co alloys.

### V.3. Analysis of the specific-heat cusp of Pd-Mn alloys

#### V.3.1. Introduction

Since the specific heat of dilute ferromagnetic Pd-Mn alloys at  $H = 0$  exhibits a remarkably sharp peak (see section IV.4), it seemed worthwhile to consider its temperature dependence in more detail in the light of modern theories on the critical behaviour of the specific heat near continuous phase transitions. A phase transition is termed 'continuous' whenever all first-order derivatives of the Gibbs-free-energy function are continuous, while higher-order derivatives may change discontinuously or diverge at the transition point as a function of the relevant variables (Fischer [9]). In most theories concerning the properties near the critical point, power-law behaviour is assumed to be valid in the asymptotic (or critical) region. Detailed calculations based upon certain models, e.g. the Ising or the Heisenberg model, have confirmed this either in an exact or in an approximate way. Although, so far, none of these models was found to be fully applicable in the case of Pd-Mn alloys, it has been tried to fit the specific-heat data to 'power-laws'. This proved to be possible within the experimental accuracy and the results of the analyses reveal that the specific-heat behaviour of Pd-Mn alloys does not fit to the theoretical models proposed so far. Therefore the analyses should be considered as being purely phenomenological; for the time being, it merely presents a description of the specific heat near the transition temperature.

Recent reviews on critical phenomena have been given by Domb and Miedema [10], Fischer [9,11,15], Heller [12], Kadanoff et al. [13] and Wielinga [14], to which one may be referred for detailed information.

The temperature dependence of the specific heat near  $T_C$  is currently described in terms of the relations [12,15]

$$C_{\pm} = (A_{\pm}/a_{\pm})(\epsilon^{-a_{\pm}} - 1) + B_{\pm} \quad (\text{V.23a,b})$$

$$\text{where } \epsilon = |T - T_c|/T_c \quad (\text{V.24})$$

and the subscripts + and - refer to the temperature regions above and below  $T_c$ , respectively. In the limit where  $a_{\pm} \rightarrow 0$  the specific heat is described by

$$C_{\pm} = a_{\pm} \ln \epsilon + b_{\pm} \quad (\text{V.25a,b})$$

which diverges logarithmically as  $T \rightarrow T_c$ .

In view of the results of the analyses presented below it is interesting to consider the behaviour of these functions for different values of the 'critical exponent'  $a$ , allowing  $a$  to assume positive as well as negative values (see, however, section V.3.4). Up till now, values of  $a$  which have been found experimentally range from positive ones down to e.g.  $a_- = -0.25$  for EuS [16],  $a_- = -0.262$  for Ni [17],  $a_- = -0.265$  for  $\text{ErCl}_3 \cdot 6\text{H}_2\text{O}$  [18] and  $a_- = -0.32$  for Gd [19], the last value being the lowest one found in the literature.

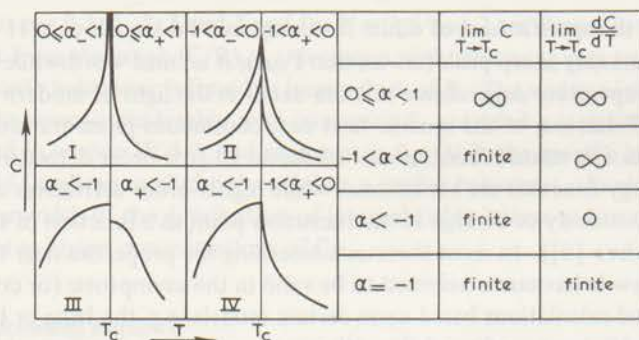


fig. V.11. Qualitative behaviour of the specific heat near  $T_c$  for several ranges of  $a$ .

It is easily verified that for  $0 \leq a < 1$  both  $C$  and  $dC/dT$  diverge as  $T \rightarrow T_c$ ; the specific heat is said to exhibit a  $\lambda$ -peak. For  $-1 < a < 0$   $C$  attains a finite value at  $T_c$ , while  $dC/dT$  diverges as  $T \rightarrow T_c$ . As mentioned above both cases have been found experimentally. If  $a < -1$   $C$  remains finite as  $T \rightarrow T_c$ , but  $dC/dT$  tends to zero; in this case only higher-order derivatives may diverge. Whenever the specific heat attains a finite maximum at  $T_c$  ( $a < 0$ ) the peak is called a cusp. The qualitative behaviour of  $C$  as a function of  $T$  is shown in fig. V.11 for several ranges of  $a$ . (Note that  $C$  may be either continuous or discontinuous at  $T_c$ , dependent upon the values of the coefficients in eqs (V.23a,b)). Specific-heat curves as sketched in cases III and IV

have never been observed experimentally up till now, nor predicted by any theoretical calculation as can be inferred from a tabulation of predicted values of  $a$ , recently given by Lewis [19]. Nevertheless, it should be stressed that these cases follow quite naturally from eqs (V.23a,b). It will be shown that case IV appears to be appropriate to dilute Pd-Mn alloys.

### V.3.2. Analysis of a rounded specific-heat peak

High temperature-resolution measurements carried out near  $T_C$  unambiguously revealed rounding of the specific-heat curves of Pd-Mn alloys. It has been conjectured that this arises from slight variations of the transition temperature throughout the specimen; the specimen is assumed to contain a large number of small regions  $i$ , each having its own transition temperature  $t_{c,i}$  depending on local conditions. The possible origin for these variations will be discussed in section V.3.4. The analysis of the specific-heat data has been carried out by means of an iterative method developed by Wielinga. This method was only briefly outlined in ref. 20 and 21; see also ref. 22.

The local variations of  $t_{c,i}$  have been assumed to have a Gaussian distribution

$$P(t_{c,i}) \propto \exp [-(t_{c,i} - T_C)^2 / 2(FT_C)^2], \quad (\text{V.26})$$

where  $T_C$  is the centre of the Gauss curve and  $FT_C$  is the width of the distribution of transition temperatures. The calculations have been carried out using a modification of eqs (V.23a,b) as proposed by Wielinga [22,14]

$$C_{\pm} = (P_{\pm}/a_{\pm}) (1 - \epsilon_{\pm}^{-a_{\pm}}) + Q_{\pm}, \quad (\text{V.27a,b})$$

$$\text{where } \epsilon_{\pm} = 1 - (T_C/T)^{\pm 1}. \quad (\text{V.28a,b})$$

Apart from the sign of  $P_{\pm}$  this function is the same as (V.23b) for  $T < T_C$ . Above  $T_C$  the function has the advantage that it may be developed into a high-temperature series.

The calculations are carried out essentially in two steps. In the first step, trial values for  $F$  and  $T_C$  are chosen to fit the data obtained at temperatures above and below  $T_C$  to eq. (V.27a) and (V.27b), respectively, by means of the least-square method. Data obtained at temperatures close to  $T_C$  are excluded from the fit as these data are affected by rounding effects. As was shown by Wielinga [22] rounding is negligibly small for  $\epsilon_{\pm} > 4F$ . Points with  $\epsilon_{\pm}$  larger than some (chosen) outer bound are also excluded from the fit as these points may lay outside the critical region of the transition. Least-square fits are made for different values of  $a_{\pm}$  and  $a_{-}$ ,  $a_{+}$  and  $a_{-}$  varying in a prescribed way. The 'best' fit is obtained at those values of  $a_{+}$  and  $a_{-}$  at which the standard deviation is a minimum.

In the second step the rounded specific-heat curve across the transition region is calculated from

$$C(T, T_C, F) = K \int_i dt_{c,i} [C_{-} \theta(t_{c,i} - T) + C_{+} \theta(T - t_{c,i})] P(t_{c,i}), \quad (\text{V.29})$$

using the parameters obtained from the best fits. In these expressions  $K$  is a normalizing constant and  $\theta(x)$  is a unit step-function;  $\theta(x) = 0$  if  $x < 0$  and  $\theta(x) = 1$  if  $x > 0$ . The computed values of  $T_{\max}$  and  $C_{\max}$  have been used as a criterion. If these are not equal to the ones obtained from experiment within prescribed limits,  $F$  and  $T_c$  are changed slightly in such a way as might lead to better agreement with experiment. The second step is then repeated, keeping  $a_{\pm}$ ,  $P_{\pm}$  and  $Q_{\pm}$  fixed, and hence new values for  $T_{\max}$  and  $C_{\max}$  are computed which are compared again with the data. If necessary, the second step is repeated four times. After the fifth calculation the first step is repeated again, using the last values obtained for  $F$  and  $T_c$ . This provides new values for  $a_{\pm}$ ,  $P_{\pm}$  and  $Q_{\pm}$ . In this way the whole procedure is repeated until the criterion is satisfied. When this occurs the first and the second step are repeated once more in order to obtain final values for  $F$ ,  $T_c$ ,  $a_{\pm}$ ,  $P_{\pm}$  and  $Q_{\pm}$ .

A similar calculation has recently been reported by Lewis [19], but his version is not a set-search procedure.

### V.3.3. Results

Data obtained from the analysis \*) have been summarized in table V.2. The standard fractional deviations are given under the caption St.D. Two sets of data are presented on Pd-Mn 1.35 at.%, one being obtained from measurements after homogenization for 65 h and the other one after homogenization for 285 h at about 1000°C. As an example,  $a$ ,  $P$  and  $Q$  values, obtained from fits calculated when the inner bound, which is commonly  $4F$ , is chosen to be  $2F$ ,  $6F$  and  $8F$ , are shown for Pd-Mn 1.35 at.%, 65 h (in italics). As can be seen those obtained for  $6F$  and  $8F$  agree fairly well with those for  $4F$ , while for  $2F$  agreement is slightly less only for  $T > T_c$ . This implies that rounding effects are indeed excluded using a cut-off  $4F$ . The value of  $a$ , at which the standard deviation is a minimum, is approached in the computer program from below. Hence, only lower limits of  $a$ ,  $P$  and  $Q$ , which are consistent with the data, are found. For instance, for Pd-Mn 1.35 at.%, 65 h, these lower limits are:  $a_- = -1.46$ ,  $P_- = -179$  and  $Q_- = -14.5$ ,  $a_+ = -0.26$ ,  $P_+ = -26.8$  and  $Q_+ = 18.3$ .

Little weight should be given to the data on Pd-Mn 0.54 at.% since these were derived from only a small number of experimental points. The results given in the table will be discussed further in the next section.

The results of the analyses are also shown in a semi-logarithmic plot, fig. V.12, and in a linear plot, fig. V.13. In fig. V.12 the left-hand scale refers to the measurements on Pd-Mn 1.35 at.% at  $T > T_c$  and the lower right-hand scale to those on the same specimen at  $T < T_c$ . (Note the scales are different). The upper right-hand scale refers to Pd-Mn 2.45 at.%. Small arrows indicate the temperature regions in which the fits to the data were made. In both figures the full curves represent the computed rounded specific heat. The 'asymptotic' behaviour (in the absence of rounding) is represented by dashed curves, in so far as they deviate from the full curves.

\*) We are very much indebted to dr. R.F. Wielinga who carried out the computer analyses.

Table V.2

Data defined by eqs. (V.26) and (V.27a,b), obtained from the analysis of the specific heat of dilute Pd-Mn alloys near  $T_c$ .  $F$  is expressed in units  $T_c$  and  $P_{\pm}$  and  $Q_{\pm}$  are given in  $\text{mJ} (\text{g at})^{-1} \text{K}^{-1}$ .

Specimen at. % Mn	$T_c$ K	$F$	$a_-$	$P_-$	$Q_-$	St.D %	$a_+$	$P_+$	$Q_+$	St.D %
0.54	1.98	0.02	-1.78	-122.7	-21.7	0.25	-0.14	-10.97	9.05	1.0
1.35 (65 h)	4.477	0.011	-1.359	-146.7	-0.878	0.19	-0.201	-23.43	21.48	0.26
		$2F$	-1.31	-132.6	7.45	0.20	-0.09	-18.3	26.5	0.35
		$6F$	-1.30	-130.7	8.31	0.19	-0.19	-22.8	22.0	0.27
		$8F$	-1.40	-157.5	-4.14	0.18	-0.17	-22.0	22.7	0.28
1.35 (285 h)	4.541	0.0071	-1.416	-179.8	-15.81	0.25	-0.121	-20.69	27.95	0.43
2.45 (250 h)	5.783	0.0092	-1.175	-162.2	28.94	0.12	-0.41	-58.4	46.1	1.0

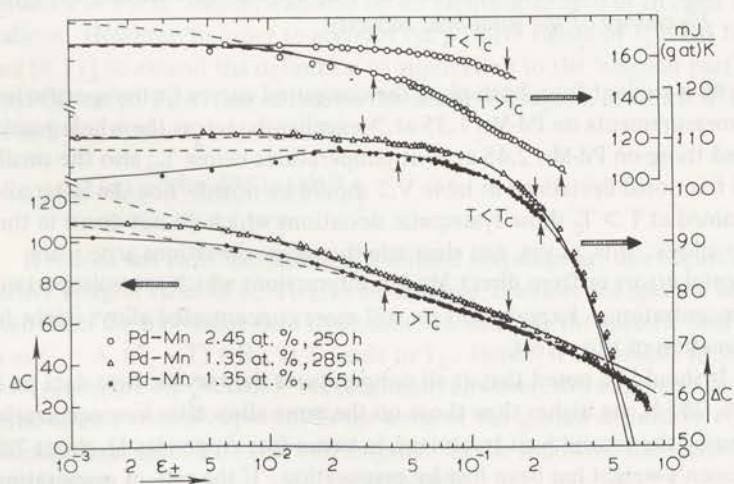


fig. V.12.  $\Delta C$  versus  $\epsilon_{\pm}$  for Pd-Mn 1.35 at.%, 65 h ( $\bullet$ ), Pd-Mn 1.35 at.%, 285 h ( $\Delta$ ) and Pd-Mn 2.45 at.%, 250 h ( $\circ$ ). The full curves represent the computed rounded specific heat. The asymptotic behaviour is shown by dashed curves. The small arrows are explained in the text.

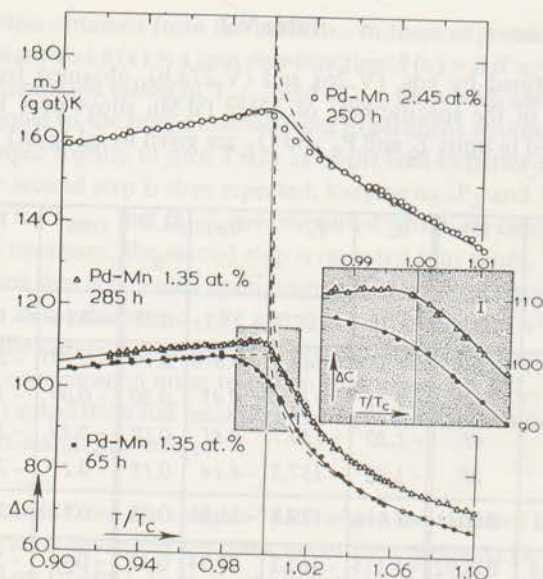


fig. V.13.  $\Delta C$  versus  $T/T_c$  for Pd-Mn 1.35 at. % and Pd-Mn 2.45 at. %, cf. the caption to fig. V.12. The insert shows the results on Pd-Mn 1.35 at. %, 65 h and 285 h at temperatures within 1.5% of  $T_c$ ; the bar indicates the effect of a 1% change of the total heat capacity.

As is evident from both plots the computed curves fit the specific-heat data of both measurements on Pd-Mn 1.35 at. % excellently across the whole transition region and those on Pd-Mn 2.45 at. % at temperatures below  $T_c$ ; also the small standard fractional deviations in table V.2 should be noted. For the latter alloy the data obtained at  $T > T_c$  show systematic deviations which do not occur in those of the other alloys. It is, as yet, not clear whether these deviations arise from experimental errors or from direct Mn-Mn interactions which are unimportant at lower concentrations. Experiments on still more concentrated alloys might further the explanation of this effect.

It should be noted that at all temperatures the specific-heat data on Pd-Mn 1.35 at. %, 285 h, are higher than those on the same alloy after homogenization for 65 h. During the second heat treatment, in vacuo (see Appendix I), about 7% of the specimen's weight has been lost by evaporation. If the rate of evaporation of Pd atoms has been higher than that of Mn atoms, the concentration of the latter has increased. The total entropy is found to be larger by about 3% which can be considered as a measure of the increased Mn concentration. Using this figure and the fact that  $dT_c/dc = 2.1 \text{ K(at.}\%)^{-1}$  at  $c = 1.35 \text{ at.}\%$ , fig. IV.15, one calculates  $T_c$  to be increased by 85 mK, while 64 mK was found experimentally. In view of the

uncertainty in both figures, the assumption that the higher specific heat arises from an increased Mn concentration seems to be reasonable.

As is evident from fig. V.13 the peak of Pd-Mn 1.35 at.% is much sharper after prolonged homogenization at about 1000°C. This also occurs for the 2.45 at.% specimen, see fig. IV.14, of which the peak was rounded, initially, in such a way as to make an analysis impossible.

Finally, one may have noticed that the specific heat is represented to within 1% by the calculated curves up to  $\epsilon_{\pm} \approx 0.3 - 0.45$  (fig. V.12), which is far out of the regions in which the fits were made.

#### V.3.4. Discussion

Since in all cases  $a$  was found to be negative, i.e. the specific heat attains a finite value at  $T = T_c$ , it is worthwhile to consider more precisely the definition of a critical exponent. A general definition of a critical exponent  $\lambda$  which describes the singular behaviour of the function  $F(x) = x^\lambda + a$ , as  $0 \leftarrow x$ , i.e.  $x$  approaching zero from positive values of  $x$ , is given by (see e.g. Fischer [9,11])

$$\lambda = \lim_{0 \leftarrow x} \left[ \frac{\ln F(x)}{\ln x} \right] \quad (\text{V.30})$$

On the basis of this definition one obtains  $\lambda$  to be zero whenever  $F(x)$  approaches the constant  $a$  at  $x = 0$ . Hence,  $a$  should be set identical to zero in all cases found in Pd-Mn alloys. However, in order to account for positive values of  $\lambda$ , it has been proposed [9,11] to extend the definition to application to the 'singular part' of the function  $F(x)$  only. First, one calculates the smallest integer  $n$  at which  $d^n F(x)/dx^n$  diverges as  $0 \leftarrow x$ . Then  $\lambda_s$  is defined by

$$\lambda_s = n + \lim_{0 \leftarrow x} \left[ \frac{\ln d^n F(x)/dx^n}{\ln x} \right]. \quad (\text{V.31})$$

If  $n$  does not exist the function is termed non-singular; this occurs e.g. for any positive integral value of  $\lambda$ . To give an example, consider the specific heat as calculated from the molecular-field treatment. In this case the specific heat can be written as  $C_- = A_-(T_c - T) + B_-$ , as  $T$  tends to  $T_c$ . Hence, it is possible to formally set  $a_s = -1$ , compare eq. (V.23,b). As is evident, however, this exponent cannot be considered to be a critical exponent in the sense of the second definition, eq. (V.31); the molecular-field specific heat is non-singular. In the following the second definition is used; the subscript  $s$  will be dropped.

As mentioned in the introduction one should not expect the results on the present alloys to be interpretable in terms of current model calculations. For instance, calculations based upon the Heisenberg model do not predict ferromagnetism to occur at the degree of dilution of magnetic atoms as in the Pd-Mn alloys considered

(section III.3.1). On the other hand, the Weiss molecular-field model predicts the specific heat to exhibit a discontinuity at  $T_C$ , while at  $T > T_C$  the specific heat is zero.

The alloys under consideration may be characterized as a system of fairly localized spins, widely separated in space, with long-range interactions through a system of non-localized (itinerant) electrons. According to a number of calculations [e.g. 23] one expects the molecular-field treatment to become more appropriate as the range of the interactions and/or the co-ordination number increases. Considering the values of  $a$  obtained for  $T < T_C$  (table V.2) it is interesting to note that  $a_-$  seems to approach the molecular-field value ( $a_- = -1$ ) as the Mn concentration increases. (This trend may be conjectured to be a manifestation of an increase of the co-ordination number). In fact, the value found from the computer analysis for Pd-Mn 2.45 at.%,  $a_- = -1.18$ , is so close to minus-unity that the curvature of a  $\Delta C$  versus  $T/T_C$  plot, fig. V.13, can hardly be noticed. In the other cases definite curvature is found at  $T < T_C$ .

In this context it is, however, worth noticing that the specific-heat maxima are relatively low as compared to the molecular-field value. In the Weiss approximation  $(C/R)_{\max} = 2.365$  for  $S = 5/2$ , while for Pd-Mn alloys containing 0.19, 0.54, 1.35 and 2.45 at.% Mn the value of  $(C/cR)_{\max}$  is found to be  $0.96 \pm 0.06$ ,  $1.05 \pm 0.05$ ,  $0.98 \pm 0.04$  (mean value) and  $0.82 \pm 0.03$ , respectively. The last values are within the experimental error equal to the calculated non-rounded values of  $C_-/cR$  at  $T = T_C$ , which are obtained from  $C_- = (P_-/a_-) + Q_-$  (provided  $a < 0$ ), using the data given in table V.2. It is also interesting to calculate the entropy gains  $S_C$  and  $S_\infty - S_C$  involved in the magnetic transition at temperatures below  $T_C$  and above  $T_C$ , respectively. These are given in table V.3 as fractions of the total entropy  $S_\infty$ . Likewise the energies  $E_C - E_0$  and  $-E_C$  released below  $T_C$  and above  $T_C$ , respectively, are given as fractions of the total energy  $-E_0$ . These values may be compared with theoretical predictions of e.g. the Heisenberg model for a 3-dimensional f.c.c. lattice with  $S = 5/2$  [10] and with the Weiss molecular-field predictions for  $S = 5/2$ .

Table V.3

Critical entropy and energy values for Pd-Mn alloys and theoretical predictions of the Heisenberg model for a 3-dim. f.c.c. lattice and the Weiss model, with  $S = 5/2$ .

	0.54 at. %	1.35 at. %	2.45 at. %	Heisenberg 3-dim., f.c.c.	Weiss model
$S_C/cR$	68%	69%	64%	83%	100%
$(S_\infty - S_C)/cR$	32%	31%	36%	17%	0%
$S_\infty/cR$	1.72	1.75	1.73	1.792	1.792
$(E_C - E_0)/cR$	37%	33%	—	67%	100%
$-E_C/cR$	63%	67%	—	33%	0%
$-E_0/cR$	1.59	1.71	—	1.37	1.071

As is evident the entropy gain at  $T > T_c$  appreciably exceeds the Heisenberg-model prediction. As to the critical energy values this disagreement is even more obvious. The percentages given in table V.3 show that a trend towards the predictions of molecular-field theory, as mentioned above, is not found. They might even suggest that the interactions are compatible with a co-ordination number lower than the one for f.c.c. Pd.

As to the critical exponent  $a_+$ , several recent Heisenberg-model calculations predict negative values for  $a_+$  ranging from  $-0.07$  to  $-0.20$  (see e.g. a recent tabulation by Lewis [19]), which are comparable to those found for Pd-Mn 0.54 at.% and 1.35 at.%. However, in view of the considerations presented in this section, it is not clear whether this formal agreement has any significance.

As mentioned in the introduction the results of the 'power-law' analyses, however excellent the fits to the data may be, should be considered merely as a phenomenological way to describe the specific heat near the phase transition. The theoretical relevance of these results will, of course, only become clear when calculations for the Pd-Mn system become available. As was mentioned also in section V.2.5, such calculations should also explain why the sharp transition of dilute Pd-Mn alloys is, up till now, unique among dilute Pd-based and all other known dilute magnetic alloys.

Rounding of specific-heat curves is commonly observed in high temperature-resolution measurements. Just to quote a few illustrative examples, see the work of Skalyo and Friedberg [24] on  $\text{CoCl}_2 \cdot 2\text{H}_2\text{O}$  ( $T_N = 2.289$  K), of Maher and McCormick [17] and Handler et al. [25] on Ni ( $T_c = 629.6$  K), of Lewis [19] on Gd ( $T_c = 291.2$  K) and Wielinga et al. [26], see also Wielinga [22, p.57,59] on  $\text{CoCs}_3\text{Cl}_5$  ( $T_N = 0.527$  K). The analyses of the present specific-heat data were based upon the assumption that rounding arises from local variations of  $T_c$ . The results of the measurements on Pd-Mn 1.35 at.% and 2.45 at.% suggest a mechanism which, at least partially, can explain such a distribution. As was shown, fig. IV.14 and fig. V.13, prolonged homogenization at  $1000^\circ\text{C}$  reduces the width of the distribution of  $T_c$ 's. Since the specimens were quenched in water in the same way after both the first and the second heat treatment (Appendix I), the reduction of  $F$  may be supposed to arise from improvement of homogeneity alone. Provided the interaction depends only weakly upon the Mn-Mn distance, the low values of  $F$  can be understood, the local variation of  $T_c$  being determined by slightly different values of the interaction strength. In the case of Pd-Mn 1.35 at.%, a decrease of  $F$  from 0.011 to 0.007 was found after the second heat treatment; for the 2.45 at.% specimen a much larger decrease must have occurred.

It is of course questionable, whether the homogeneity can still be improved appreciably by homogenization for periods largely exceeding 250 h. Therefore, in order to account for the rounding which remained, the following suggestion is made. A certain distribution of  $T_c$ 's should be expected to persist, resulting from the

inescapable statistical distribution of Mn atoms over the lattice. As the spatial shape of the induced electron polarization, which determines the strength of the interaction, is not known for Pd-Mn alloys, an estimate of such a 'residual' distribution of  $T_C$ 's can hardly be made.

A number of other mechanisms which might explain rounding have been suggested in the literature. Wielinga [22], for instance, discussed mechanisms arising from crystal imperfections of physical origin. His calculation showed that neither the 'finite size effect', which arises from a division of the crystal into a large number of small parts by cracks, nor domain structure can account for the observed values of  $F$  by one or two orders of magnitude. Finally, the specimens presumably contained a high density of vacancies as their equilibrium distribution at  $1000^\circ\text{C}$  was quenched in. In order to eliminate a possible influence on  $T_C$  by strains arising from vacancies (and dislocations), it seems worthwhile to repeat measurements on e.g. the Pd-Mn 1.35 at.% specimen after annealing at about  $500^\circ\text{C}$  and careful cooling down to room temperature.

To conclude, it might be desirable to investigate whether the unique behaviour of the specific heat of Pd-Mn alloys also occurs in other dilute alloys. One immediately realizes Pt-Mn to be a candidate. However, a recent experiment revealed that, though a large magnetic contribution was found, the specific heat of a 0.9 at.% Pt-Mn specimen does not exhibit a sharp peak\*). As mentioned in section III.1, the main difference between Pd-Mn and other ferromagnetic Pd-based alloys is the occurrence of giant moments in the latter ones, while in Pd-Mn alloys the moment per Mn-atom is approximately equal to the one for a  $\text{Mn}^{++}$ -ion. Purely on the basis of this experimental fact, remembering its tentative interpretation given in section IV.4, one may suggest to investigate Pd-Gd (and Pt-Gd), since the moment per Gd atom is only slightly lower than the moment of a  $\text{Gd}^{3+}$ -ion. The specific heat of the Pd-Gd system is under investigation\*).

---

\*) We are indebted to J.J. Zwart for this communication.

## References

1. A.H. Morrish, *The physical Principles of Magnetism*, J. Wiley and Sons, New York, 1965, p. 261.
2. ref. 1, p.8.
3. G. Garton, M.J.M. Leask, W.P. Wolf and A.F.G. Wyatt, *J. appl.Phys.* 34(1963)1083.
4. D. Shaltiel, J.H. Wernick, H.J. Williams and M. Peter, *Phys.Rev.* 135(1964)A1346.
5. S. Doniach, *J.Phys.Chem.Solids* 29(1968)2169.
6. T. Takahashi and M. Shimuzu, *J.Phys.Soc.Jap.* 23(1967)945.
7. B.W. Veal and J.A. Rayne, *Phys.Rev.* 135(1964)A442.
8. B.M. Boerstael, F.J. du Chatenier and G.J. van den Berg, *Proc. IXth. int. Conf. low Temp. Phys. LT-9, part B*, Plenum Press, New York, 1965, p. 1071.
9. M.E. Fischer, *Rep. Progr. Phys.*, Vol. XXX, part II, 1967, p. 615.
10. C. Domb and A.R. Miedema, *Progr. Low Temp. Phys.*, ed. C.J. Gorter, North-Holland Publ. Comp., Amsterdam, 1964, Vol. IV, Chapter V.
11. M.E. Fischer, *J. appl. Phys.* 38(1967)981.
12. P. Heller, *Rep. Progr. Phys.*, Vol. XXX, part II, 1967, p. 731.
13. L.P. Kadanoff, W. Götze, D. Hamblen, R. Hecht, E.A.S. Lewis, V.V. Palciauskas, M. Rayl, J. Swift, D. Aspnes and J. Kane, *Rev. mod. Phys.* 39(1967)395.
14. R.F. Wielinga, *Progr. Low Temp. Phys.*, ed. C.J. Gorter, North-Holland Publ. Comp., Amsterdam, 1970, Vol. VI, Chapter 8.
15. M.E. Fischer, *Lectures in Theoretical Physics*, ed. W.E. Brittin, University of Colorado Press, Boulder, Vol. VII C, 1965, p. 1.
16. B.J.C. van der Hoeven, D.T. Teany and V.L. Moruzzi, *Phys. Rev. Lett.* 20(1968)719.
17. W.E. Maher and W.D. McCormick, *Phys. Rev.* 183(1969)573.
18. E. Lagendijk, R.F. Wielinga and W.J. Huiskamp, *Phys. Lett.* 31A(1970)375.
19. E.A.S. Lewis, *Phys. Rev. B* 1(1970)4368.
20. B.M. Boerstael and R.F. Wielinga, *Phys. Lett.* 31A(1970)359.
21. R.F. Wielinga and C.J. Gorter, *Comments Sol. State Phys.*, to be published.
22. R.F. Wielinga, thesis, Leiden, 1968.
23. G.A. Baker Jr., *Phys. Rev.* 122(1961)1477.  
C. Domb and N.W. Dalton, *Proc. phys. Soc.* 89(1966)859, 873.
24. J. Skalyo, Jr. and S.A. Friedberg, *Phys. Rev. Lett.* 13(1964)133.
25. P. Handler, D.E. Mapother and M. Rayl, *Phys. Rev. Lett.* 19(1967)356.
26. R.F. Wielinga, H.W.J. Blöte, J.A. Roest and W.J. Huiskamp, *Physica* 34(1967)233.

## Appendix I

### AI. Preparation of specimens

Two furnaces were available for the preparation of specimens of the metals and alloys described in this thesis, viz. a furnace with radiation heating by means of a tungsten resistance coil and an induction furnace. The pure Cu and Au specimens were melted in vacuo in the radiation furnace. All other specimens have been prepared inside the induction coil because the highest operation-temperature of the radiation furnace was not sufficient to melt the fairly large Pd and Pt specimens. An induction furnace has the important advantage of intensive stirring of the melt, effecting rapid mixing of the components of an alloy. On the other hand, melting in vacuo was unfeasible with the existing equipment. Therefore the melting process was carried out under a flow of argon gas.

It will be obvious from the discussion of the specific heat of the pure metals in chapter II that much attention had to be paid to handling of specimens before, during and after the melting process in order to preclude contamination. To a certain extent this pertains also to the alloys. Therefore the crucible and starting-materials (except when available in the form of sponge) were cleaned by means of an appropriate etchant, usually aqua regia. Subsequently the etchant was removed by ultrasonic cleaning in distilled water, followed by the same treatment in alcohol in order to remove the water. Finally the crucible and metals were dried in a drying oven. Whenever the specimen had been machined after the melting procedure the whole treatment was repeated.

Alumina crucibles (Morgan Purox Recrystallised Alumina, 99.7%  $\text{Al}_2\text{O}_3$ ) have been used throughout. These crucibles were preferred because of their better thermo-mechanical and electrical properties at temperatures up to  $1900^\circ\text{C}$  in comparison with other crucible materials. Moreover, in most cases (see however Pd-Mn, below) the metals and alloys remained unaffected by these crucibles.

As mentioned above, the Cu and Au specimens have been prepared in the radiation furnace which was evacuated to below  $10^{-5}$  torr before the melting procedure was started. During the melting procedure the metals were heated slowly. Whenever the vacuum deteriorated due to degassing, the temperature increase was stopped until the pressure was again below  $10^{-5}$  torr. After melting the copper rods (supplied by Asarco) and subsequent solidification, some graphite powder was found as a thin layer on top of the specimen; it could be rubbed off easily. Presumably graphite had been used by the manufacturer as a lubricant when drawing the rods. As graphite does not dissolve into copper it is not present in solid solution but

merely in the form of small particles. The batch of copper was remelted several times until no more graphite was released.

Before melting in the induction furnace, the crucible was put into a mullite cylinder, thoroughly flushed with argon gas. In order to remove air the melting process was started after an amount of gas equal to 60 to 100 times the volume of the cylinder had flown through the cylinder. After liquefaction of the metals the melt was kept liquid for some time in order to let the components of the alloy mix thoroughly. The mixing time, however, was kept short in order to avoid appreciable oxidation of the metal by traces of oxygen or by the crucible (see below). Moreover, the mixing time had to be kept short to avoid undue evaporation of the sample. After cooling down to room temperature, screw-holes were tapped into the specimen, and crucible material, if any, was removed from the specimen.

Little is known about the homogeneity of the (alloy) specimens achieved after solidification from the melt. According to Hansen [1] and Elliott [2] Pd and Pt form continuous series of solid solutions with Co, while the solid-solubility limit of Fe and Mn in Pd is about 20 at.% and 26 at.%, respectively, at room temperature. For Fe dissolved in Au this limit is approximately 10 at.% at room temperature. Consequently, one may expect that specimens with a reasonable degree of homogeneity can be prepared, because precipitation is not likely to occur at concentrations below e.g. 1 at.%. Gravitational segregation is also unlikely in specimens prepared by induction heating due to intensive motion of the melt. Yet, on a small scale (e.g. grain size) concentration variations may always be present. Therefore, as a precaution, the alloys have been homogenized in vacuum for at least 24 hours at about 1000°C. The heat treatment was terminated by quenching in water, whereby the specimens cooled to room temperature within 30 s. One specimen, Pt-Co 0.067 at.% was measured both before and after heat treatment. Although the difference in the specific heat proved to be small, preference has been given to the heat treatment outlined above, because there is no certainty that sufficient homogeneity has been obtained after melting in all cases. Two Pd-Mn alloys have been homogenized for a much longer time in order to investigate its influence on the specific-heat peaks of these alloys (see chapters IV and V).

The concentrations of the specimens were determined by dr. H.A.Das of the Reactor Centrum Nederland by means of neutron-activation analysis [3] and chemically at this laboratory by means of spectrophotometry using a Bausch and Lomb Spectronic 20. The accuracy of the determinations was generally a few percents for both methods. An impression of the macroscopic homogeneity could be obtained from analyses on samples taken from the top and the bottom of the specimen. Mostly, agreement between these determinations is fair. Co concentrations obtained from analyses are commonly slightly below the nominal ones. This may be due to oxidation or evaporation of Co during the melting process. Indeed, sometimes a blue colouring of the crucible has been observed, presumably

due to cobaltous oxide.

The nominal concentrations of the Pd-Mn alloys containing 0.08, 0.19 and 0.54 at. % Mn are much higher than the concentrations obtained from chemical analysis. However, in this case a rather strange and as yet unexplained phenomenon occurred. The alloys were prepared in alumina crucibles, 22 mm inside diameter. After melting, these crucibles were affected at those places where the melt had been in direct contact with the crucible. A brownish crust, presumable due to a manganese oxide had been formed. This effect also occurred when one of the samples was remelted without adding pure Mn, indicating that Mn already dissolved in Pd was extracted from the melt. On the other hand, alumina crucibles, 14 mm inside diameter, were not affected at all after melting and chemical analysis yielded concentrations only slightly lower than the nominal ones (Pd-Mn 1.35 at. % and 2.45 at. %). On inquiry at the manufacturer's it turned out that all crucibles were made in exactly the same way and their composition should be completely identical. Thus for the moment the origin of the different behaviour of these crucibles with respect to the manganese alloys is rather obscure. A slight difference in the composition of the binding agent of alumina crucibles might be a possible explanation in all due respect to the manufacturer's assertion. On the other hand, the same brown crust was found when Pd-Mn alloys were prepared in Coors/AD 999-alumina crucibles, which have a purity of 99.98%.

## AI.2. The tables

In table AI.1 the metals used for the preparation of specimens are listed in the left column. In the other columns, the concentration of impurities are given in atomic parts per million (ppm). The left column contains an abbreviation of the manufacturer's name and a lot- or code-number; J.M. stands for Johnson-Matthey Chemicals Lim., London, Asarco for American Smelting and Refining Comp., South Plainfield, N.J. and Cominco for Consolidated Mining and Smelting Company of Canada Lim., Montreal. The analysis given for Au is a typical one, whereas for Cu the quoted figures are lower limits of the spectrographic analysis. In three cases the manufacturer only gave a qualitative spectrographic analysis.

Table A1.1.

Metal	Impurity Elements (Atomic ppm)								
	Fe	Mn	Si	Cu	Ag	Mg	Ca	Al	Other elements
Pd J.M. 38266	1		3	<1	<1	1	<1		Na 1
Pd J.M. S1499	1		5	<1	<1	<1	<1	2	
Pd J.M. W1774	4		2	<1	<1	<1	<1		
Pd J.M. W2231	4		7	1	<1	<1	1		
Pd J.M. S8750	<1		8	<1	<1	<1	<1		Na <1
Pt J.M. W1613	1		3	<1	<1	<1	<1		Pd <1, Au 5
Au Cominco 69 Grade	0.1		.	0.1	0.3	0.1			typical analysis
Cu Asarco A-58 (99.999+%)	<0.7		<0.1	-	<0.3				*)
Co J.M. 5458	<1	1	30	1		2		5	
Co J.M. 9319	5		<1	2		<1		2	
Fe J.M. 7037	-	<1	<1	<1		<1			
Mn J.M. S6759	5	-	2	<1		40			
Co J.M. 3768	*) As, Te < 2; Sb, Pb, Sn, Se, S, Ni < 1; Cr < 0.5; Bi < 0.1								
Mn J.M. 4135	Mg, Ca, Ag, Cu, Si detected spectrographically								
Mn J.M. 2944	Mg, Ca, Na " "								

In tables A1.2 and A1.3 data concerning the alloys are presented. The first four columns give, from left to right, the specimen as referred to in the text, the nominal concentration, the laboratory melt number of the specimen and, when relevant, that of the alloy from which the specimen had been prepared, respectively. In the next two columns the sources of the metals are given using the same abbreviations as in table A1.1. Times during which the alloy was kept liquid are listed in the seventh column. When two figures are given the alloy was inverted after melting the first time and remelted. In the following column data concerning the heat treatment are given; q indicates that the specimen has been quenched in water. The mass of the specimen is given next. In the last column the concentrations obtained either by neutron-activation analysis (n) or by chemical analysis (c) are listed. Samples taken from the top and bottom of the specimen are characterized by t and b, respectively. In some cases, mainly the Pd-Mn alloys, the listed values are mean values of more than one taken from top and bottom.

## References

1. M. Hansen, Constitution of Binary Alloys, McGraw-Hill Company, Inc., New York, 1958.
2. R.P. Elliott, Constitution of Binary Alloys, First Supplement, McGraw-Hill Company, Inc., New York, 1965.
3. H.J.M. Bowen and D. Gibbons, Radioactivation Analysis, Clarendon Press, Oxford, 1963.
4. D. Taylor, Neutron Irradiation and Activation Analysis, George Newnes Lim., London, 1964.
5. D.W. Osborne, H.E. Flotow and F. Schreiner, Rev.sci.Instr. 38(1967)159.

Table AI.2.

Specimen	nom. conc. (%)	Lab. number	Prepared from: lab. number	Source of base metal	Source of solute metal	Melting time(s) (min)	Heat treatment ( $^{\circ}\text{C}/\text{h}$ )	Specimen mass (g)	Concentration analyses (%)
Pd pure		6538		J.M. S1499	-	5	slowly cooled	55.000	-
Pd pure		6817		J.M. W1774	-	1	950/24	48.381	-
Pd pure		68110		J.M. W2231	-	8	slowly cooled	51.325	-
Pd-Co 0.16 %	?	6416		J.M. 38266	J.M. 3768	5	-	49.266	-
Pd-Co 0.24 %	0.25	6451		J.M. 38266	J.M. 5458	2	-	30.378	-
Pd-Co 0.24 %		6681	6451	Remelted only		5	* 1000/48, q	26.844	t 0.228 , b 0.245 n
Pd-Co 0.16 %		6682	6416		5	* 950/48, q	38.221	t 0.159 , b 0.160 n	
Pd-Co 0.017%	0.02	6790	6538		J.M. 9319	10	925/24	52.979	t 0.016 <sub>8</sub> , b 0.017 <sub>1</sub> n
Pd-Co 0.036%	0.04	67139		J.M. W1774	J.M. 9319	10	950/24	48.267	t 0.034 <sub>8</sub> , b 0.037 <sub>0</sub> n
Pd-Co 0.075%	?	6825	67108	J.M. W1774	J.M. 9319	2/10	950/24	35.419	t 0.070 , b 0.080 n
Pd-Co 0.35 %	0.35	6990		J.M. S8750	J.M. 9319	10/5	1100/48, q	42.635	t 0.41 , b 0.40 n
Pt pure		6911		J.M. W1613	-	2	slowly cooled	49.815	-
Pt-Co 0.067%	0.067	6931 6942	6911 6931		J.M. 9319	30 (short)	slowly cooled 1600/24, q	49.806 49.365	analysis failed n
Pt-Co 0.5%	0.50	6943	6942		J.M. 9319	10/12	1250/64, q	48.940	t 0.51 , b 0.45 c
Pt-Co 0.8% †	0.80	6960	6943		J.M. 9319	15/13	1225/62, q	48.630	t 0.75 , b 0.83 n

Table AI.3.

Specimen	nom. conc. (%)	Lab. number	Prepared from: lab. number	Source of base metal	Source of solute metal	Melting time(s) (min)	Heat treatment (°C/h)	Specimen mass (g)	Concentration analyses (%)
Cu (Cu I)		6668		Asarco A-58	—	30	450/3	197.452	—
Cu (Cu II)		T 3.4		Asarco A-58	—	1)	1)	259.320	1)
Au pure		6924		Cominco 247A	—	60	1000/60	96.471	—
Au-Fe 0.16%	0.16	6903		Cominco 247A	J.M. 7037	30/15	? , q	70.526	
Pd-Fe 0.16%	0.16	6944		J.M. S8750	J.M. 7037	15/10	1050/48 , q	38.240	t 0.163, b 0.165 c
Pd-Mn 0.08%	0.10	6950		J.M. S8750	J.M. 4135	15/15	900/25 , q	39.776	0.08 ± 0.01 c
Pd-Mn 0.19%	0.25	6956	6950		J.M. 4135	10/10	950/24 , q	37.165	t 0.22 , b 0.17 c
Pd-Mn 0.54%	~1.0	6971	6956		J.M. 2944	15/10	950/60 , q	27.511	t 0.55 , b 0.53 c
Pd-Mn 1.35%	1.3	6999		J.M. S8750	J.M. 2944	5/10	(1050/65 , q 1025/220, q)	(14.427 13.470)	t 1.3 <sub>3</sub> , b 1.4 <sub>1</sub> c
Pd-Mn 2.45%	2.6	69108		J.M. S8750	J.M.S6759	5/10	(1025/48 , q 1000/220, q)	(14.736 14.288)	t 2.50 , b 2.42 c

## Key to tables AI.2 and AI.3

1) see reference 4.

\* : Heat treatment carried out in a later stage of the investigation; all experiments reported refer to the homogenized state.

q : quenched in water.

t and b : analysis on samples taken from the top and bottom of the specimen, resp. Atomic percents are used throughout.

n : neutron-activation analysis.

c : chemical analysis.

† : chemical analysis : t 0.80; b 0.80.

## Appendix II

Values of the specific heat of Cu I and Cu II (see section II.6) are given at one-degree intervals in table AII.2. These values have been computed from the equation

$$C = \sum_{i=1}^6 A_i T^{2i-1} \quad (\text{AII.1})$$

using the coefficients listed in table II.1 under the captions Cu I and Cu II respectively. Relative deviations from the copper reference equation (eq.(II.7)) with coefficients listed in table II.1 under the caption  $C_{r.e.}$  are also given in %.

The specific heat of Pd, Pt and Au have been listed in table AII.3 at one-degree intervals (see section II.7). Again, the specific-heat values have been computed from eq. (AII.1) using the appropriate coefficients presented in table AII.1 with the exception of Au. In the latter case large-scale plots have been used for temperatures above 4.3 K, whereas for temperatures below 4.3 K the listed specific-heat values have been derived from the expression  $C = 0.676_3 T + 0.460_7 T^3 - 0.0011_4 T^5$   $\text{mJ}(\text{g at})^{-1} \text{K}^{-1}$ , which represents the Au data at these temperatures.

**Table AII.1.**

Specific-heat coefficients of Pd and Pt.  
C expressed in  $\text{mJ}(\text{g at})^{-1} \text{K}^{-1}$

	Pd	Pt
$A_1$	9.4473	6.5365
$A_2$	$9.7341 \times 10^{-2}$	$1.4594 \times 10^{-1}$
$A_3$	$6.6132 \times 10^{-5}$	$2.5185 \times 10^{-4}$
$A_4$	$-2.4352 \times 10^{-7}$	$-6.1378 \times 10^{-7}$
$A_5$	$3.1493 \times 10^{-10}$	$5.3681 \times 10^{-10}$
$A_6$	$-1.4663 \times 10^{-13}$	$-1.7367 \times 10^{-13}$

Table AII.2.

Specific heat of Cu I and Cu II in  $\text{mJ}(\text{g at})^{-1}\text{K}^{-1}$  at one-degree intervals, together with relative deviations from the copper reference equation, in %.  $\Delta C = C - C_{\text{r.e.}}$ .

Cu I		Cu II		Cu I		Cu II			
T	C	$\Delta C/C_{\text{r.e.}}$	C	$\Delta C/C_{\text{r.e.}}$	T	C	$\Delta C/C_{\text{r.e.}}$	C	$\Delta C/C_{\text{r.e.}}$
1	0.7412	- 0.10	0.7443	+ 0.32	16	224.9	+0.13	225.0	+0.18
2	1.770	+ 0.02	1.774	+ 0.28	17	272.6	+0.11	272.9	+0.22
3	3.373	+ 0.15	3.375	+ 0.24	18	327.6	+0.08	328.2	+0.27
4	5.838	+ 0.24	5.834	+ 0.20	19	390.5	+0.03	391.4	+0.27
5	9.456	+ 0.31	9.439	+ 0.13	20	462.1	+0.01	463.3	+0.27
6	14.52	+ 0.34	14.48	+ 0.07	21	542.7	- 0.03	544.3	+0.26
7	21.34	+ 0.34	21.27	+ 0.04	22	632.7	- 0.07	634.5	+0.21
8	30.23	+ 0.34	30.13	- 0.01	23	732.5	- 0.12	734.5	+0.16
9	41.54	+ 0.32	41.40	- 0.02	24	842.1	- 0.15	843.9	+0.06
10	55.63	+ 0.29	55.45	- 0.04	25	961.3	- 0.17	962.8	- 0.02
11	72.92	+ 0.26	72.71	- 0.03	26	1090	- 0.17	1091	- 0.09
12	93.85	+ 0.23	93.63	0.00	27	1228	- 0.08	1228	- 0.08
13	118.9	+ 0.20	118.7	+ 0.02	28	1376	+0.15	1375	+0.08
14	148.7	+ 0.18	148.6	+ 0.09	29	1534	+0.47	1533	+0.40
15	183.8	+ 0.15	183.8	+ 0.15	30	1704	+0.95	1703	+0.90

Table AII.3.

Specific heat of palladium, platinum and gold at one-degree intervals.  
 T is given in K, C is given in  $\text{mJ}(\text{g at})^{-1}\text{K}^{-1}$ .

	Pd	Pt	Au		Pd	Pt	Au
T	C	C	C	T	C	C	C
1	9.545	6.683	1.136	16	572.9	835.5	1781
2	19.68	14.25	5.001	17	665.1	991.5	2105
3	30.99	23.61	14.19	18	766.7	1164	2452
4	44.08	35.73	31.00	19	877.8	1353	2816
5	59.59	51.67	57.50	20	998.8	1558	3199
6	78.16	72.53	96.18	21	1130	1777	3591
7	100.4	99.56	150.2	22	1272	2011	3993
8	127.1	134.1	222.2	23	1426	2259	4407
9	158.9	177.4	315.2	24	1591	2519	4826
10	196.3	230.9	434.4	25	1768	2791	5250
11	240.1	296.0	582.6	26	1958	3075	5678
12	290.8	373.9	760.8	27	2159	3370	6110
13	349.1	466.0	969.8	28	2369	3678	6544
14	415.2	573.1	1211	29	2584	3996	6980
15	489.7	696.1	1482	30	2794	4322	7407

## Summary

In this thesis results of specific-heat measurements on a number of dilute magnetic alloys (Pd-Co, Pd-Fe, Pd-Mn, Pt-Co and Au-Fe) are given and discussed. It is evident from these results that the behaviour of dilute Pd-Mn alloys is, in every respect, different from that of the other dilute alloys which have been studied so far. The data on the Pd-Mn alloys will be reviewed separately in this summary. For the other alloys a number of valuable conclusions, considering the dependence of the specific heat on the concentration and on the magnetic field, could be drawn from a comparison of results on alloys with different base metals or solute atoms, as well as from a comparison of results on a series of Pd-Co alloys. Furthermore, data have been obtained on the total entropy change involved in the ordering process and on the temperature dependence of the specific heat at very low temperatures. Finally, specific-heat data on high-purity metals were obtained; on copper in the course of a series of test measurements and on palladium, platinum and gold for lack of sufficiently reliable data; specific-heat values of these metals have been tabulated in Appendix II.

In order to evaluate the magnetic contribution to the specific heat from the experimental data over a wide range of temperatures, high-accuracy measurements are required. Data obtained using the experimental procedure described in chapter II were found to be sufficiently accurate (inaccuracy 0.3-0.5%), as could be inferred from test measurements on high-purity copper specimens (section II.6) and from additional evidence concerning the calibration procedure (section II.4).

Specific-heat data on a number of dilute Pd-Co, Pd-Fe, Pt-Co and Au-Fe alloys are given in chapter IV. As has been discussed in detail in chapter III, the Pd-(Pt-)based alloys are ferromagnetic, the Co or Fe moments being coupled through the Pd (Pt)4d - (5d-) band itinerant electrons. The specific heat of one Au-Fe alloy was measured in order to have an opportunity to make a comparison with the data of Pd-based alloys; in the Au-Fe alloys the Fe moments are coupled by the Ruderman-Kittel-Kasuya-Yosida (RKKY) interaction which gives rise to a complex ferromagnetic-antiferromagnetic type of ordering (see section III.3.2). For all Co and Fe alloys broad maxima are found in the  $\Delta C$  versus T curves at  $H = 0$ , no striking differences being observed in the shape of the curves for different systems. On the other hand, an external magnetic field is found to have a large influence on the specific heat of dilute Pd- and Pt-based alloys, causing its maximum to shift rapidly towards higher temperatures upon increasing the field strength. The change of the whole specific-heat curve is much less striking for the Au-Fe alloy, see fig. IV.5 and figures IV.3,4 and 11. This differing behaviour has been suggested to arise from the difference in

the type of ordering in Au-Fe and Pd- or Pt-based alloys (section IV.3.3).

A detailed set of data has been obtained on a series of Pd-Co alloys, see sections IV.3.1 - 2. At low concentrations the temperature at which  $\Delta C$  attains its maximum is found to follow the same concentration dependence as does the transition temperature,  $T_C \propto c^2$  from resistivity data. This concentration dependence has also been found very recently (G. Chouteau and R. Tournier, preprint) from magnetization data on Pd-Fe alloys. The width of the zero-field specific-heat curve has been assumed to be a measure of the width of the distribution of internal fields. In reasonable agreement with an analysis of Mössbauer-effect data the relative width is found to decrease upon increase of the concentration, the transition thus becoming sharper. As regards its magnetic-field dependence, the specific heat is found to change as a function of concentration. Qualitatively, this change can be derived from a calculation based upon the molecular-field model given in sections V.2.3-4. The width of the distribution of effective fields is then seen to be the dominant factor which determines the shape of the  $\Delta C$  versus  $T$  curve as well as its change upon application of an external magnetic field. Quantitative agreement could not be obtained, which indicates that the molecular-field model is too simple an approximation for the Co and Fe alloys concerned (section V.2.4).

The temperature dependence of  $\Delta C$  as  $T \rightarrow 0$  turns out to be difficult to establish for the alloys investigated (section IV.6). In those cases in which the experiments have been extended to temperatures below 1 K a hyperfine-field contribution prohibits an accurate determination of this temperature dependence. Nevertheless, the data obtained at  $H = 0$  seem to indicate that  $\Delta C$  is proportional to  $T$  at the lowest temperatures. However,  $\Delta C$  is not independent of the concentration at these temperatures, in contrast to the behaviour of some dilute non-transition-metal based alloys. Specific-heat measurements on dilute Pd-Fe alloys at  $T < 1$  K might yield a more accurate estimate of the dependence of  $\Delta C$  at low temperatures on temperature and on concentration, since in this case a disturbing hyperfine-field contribution is not to be expected. The hyperfine field,  $210 \pm 20$  kOe, derived from the data on Pd-Co 0.16 at.%, is in fair agreement with a number of other determinations.

Spin values derived from entropy determinations are given in section IV.5. 'Normal' values are found for alloys which exhibit a giant moment associated with each solute atom (e.g. Pd-Co, see section III.1) as well as for alloys having a 'rather normal' moment per solute atom (e.g. Pd-Mn). Frequently, 'giant spin' values have been reported from other experiments (Mössbauer effect, magnetization). Arguments are given in section IV.5, which make it quite plausible that giant spins actually do not exist. It seems, therefore, reasonable to suppose that the discrepancy between the spin values derived from specific-heat measurements and other experiments has been disposed of in principle.

Specific-heat data on dilute Pd-Mn alloys are given in section IV.4.

They were found to be completely different from those on the other dilute ferromagnetic alloys. While the latter ones (and even any other dilute magnetic alloy studied so far) exhibit broad, almost featureless specific-heat versus temperature curves, a sharp peak is found in dilute Pd-Mn alloys, as is evident from figures IV.12-14. As can be concluded from calculations presented in chapter V, even rather small variations of  $T_C$  throughout the specimen inhibit the magnetic system to exhibit a sharp specific-heat peak. Therefore, the itinerant-electron polarization must, to a high degree, be uniform beyond nearest-neighbour distance from a Mn site. In contrast to the situation in Pd-Co and Pd-Fe alloys ( $T_C \propto c^2$ ) the temperature at which this peak occurs (which is approximately equal to  $T_C$ ) is proportional to  $c$  at low concentrations. It has been proposed in this thesis that both the rather low  $T_C$ 's and the fact that no giant moment is observed in Pd-Mn alloys can be understood, if the polarization is weaker by an order of magnitude as compared to that in Pd-Fe or Pd-Co alloys. The proper Mn moment ( $\approx 5 \mu_B$ ) is then assumed to be almost completely localized on the Mn site.

The specific heat of dilute Pd-Mn alloys in the presence of external magnetic fields is also different from that of the other alloys. Even if allowance is made for a broad distribution of internal fields, calculations based upon the Weiss molecular-field model given in sections V.2.1-5, do not lead to a satisfactory description of the specific heat of Pd-Co and Pd-Fe alloys. However, in the case of the Pd-Mn alloys, surprisingly good agreement with the data at high external fields is obtained (fig. V.4 and V.5), if a narrow distribution of internal fields is assumed; in fact, only one single value for the molecular field has been used in the calculation. This result strongly supports the idea of an almost uniform polarization in Pd-Mn alloys.

In section V.3 the specific-heat peak of Pd-Mn alloys has been analysed in terms of 'power-laws'. Careful measurements at temperatures close to the peak demonstrated this peak to be slightly rounded off. This rounding is interpretable on the assumption of a narrow Gaussian distribution of  $T_C$ 's in the specimen, using an iterative method developed by Wielinga which allows accurate determinations of the average  $T_C$  and the 'critical' exponents to be made. The width of the distribution ranges from  $0.007 T_C$  to  $0.02 T_C$ , depending, anyhow partially, upon the homogeneity of the specimens.

As is evident from fig. V.12 and V.13 the calculated curves excellently describe the specific heat across the transition region. However, considering the values of the critical exponents and the ratios of the entropy changes as well as the energy changes above and below  $T_C$ , no model calculation proposed so far accounts for the data on Pd-Mn alloys. It has been emphasized that the analysis in terms of power-laws may be considered, for the time being, as a phenomenological way to describe the specific heat near the phase transition.

Finally, it may be concluded from this investigation, (also taking into account information from other work), that 1) the shape and spatial extent of the

itinerant-electron polarization induced by the dissolved magnetic atoms and 2) the distribution of these atoms over the lattice, have a dominant influence on the properties of dilute ferromagnetic alloys. With the possible exception of Pd-Mn alloys in strong external fields, interpretation of properties of these alloys in terms of a molecular-field approach is doubtful. This is particularly so, if variations of the internal field are neglected, as many authors have done previously.

Possible extensions of this work have been suggested on many occasions. For instance, it is obvious that experiments on other properties of Pd-Mn alloys, with emphasis on critical behaviour, might be of particular importance. The conjectured uniform d-band polarization in Pd-Mn alloys might be detected by techniques probing the local polarization in these alloys. As discussed in sections V.3.3 and V.3.4, specific-heat measurements on Pd-Mn alloys with  $c > 2.5$  at. % Mn and on annealed Pd-Mn specimens will be interesting. Likewise, it is worthwhile to carry out measurements on dilute Pd-Gd (and Pt-Gd) alloys. Finally, it may be interesting to set up specific-heat measurements on ternary (Pd-Ag)-Mn, (Pd-Rh)-Mn and (Pd-Pt)-Mn alloys in order to investigate the influence of addition of Ag, Rh or Pt on the specific-heat peak of Pd-Mn alloys.

## Samenvatting

In dit proefschrift worden resultaten van metingen der soortelijke warmte van een aantal palladium- en platina-legeringen beschreven. Hoewel zuiver Pd en zuiver Pt zelf paramagnetisch gedrag vertonen, is uit metingen van anderen gebleken, dat bij voldoende lage temperaturen een ferromagnetische overgang optreedt in legeringen van deze metalen met een geringe hoeveelheid ijzer, cobalt, nikkel, mangaan of gadolinium. Speciaal in het geval van Pd-Fe - en Pd-Co - legeringen wordt nog ferromagnetisch gedrag gevonden bij zeer grote verdunningen, bijvoorbeeld bij concentraties beneden 0.05 at.% Fe of Co. Dit geldt waarschijnlijk ook voor Pd-Mn - en Pd-Gd - legeringen, terwijl voor Pd-Ni een kritische concentratie (2 at.% Ni) is gevonden, waarbeneden geen ferromagnetisme meer optreedt.

Algemeen wordt aangenomen dat de wisselwerking tussen de magnetische momenten van de opgeloste atomen plaats vindt via de geleidingselectronen van het basismetaal. Het magnetisch moment per opgelost magnetisch atoom blijkt abnormaal groot te zijn in de meeste der bovengenoemde legeringen. In Pd-Co - en Pd-Fe - legeringen is dit 10-12  $\mu_B$  per Co of Fe atoom ('giant moments'). Dit grote moment wordt toegeschreven aan exchange-wisselwerking tussen de momenten van de opgeloste magnetische atomen en de geleidingselectronen in de 4d-band van Pd. In Pd-Mn - en Pd-Gd - legeringen worden echter vrij 'normale' waarden voor het moment gevonden.

In hoofdstuk IV worden de resultaten van metingen aan een serie legeringen (Pd-Co, Pd-Fe, Pd-Mn, Pt-Co en Au-Fe) opgegeven, die zonder meer aantonen, dat er een groot verschil bestaat tussen het gedrag van enerzijds Pd-Mn - legeringen en anderzijds de overige legeringen. Met uitzondering van de Mn-legeringen blijkt de soortelijke warmte van de onderzochte legeringen als functie van de temperatuur een breed maximum te vertonen. Dit is ook gevonden voor alle verdunde magnetische legeringen, waarvan tot nu toe de soortelijke warmte is gemeten. Uit dit onderzoek is anderzijds gebleken, dat de soortelijke warmte van verdunde Pd-Mn - legeringen een scherpe piek ('cusp') vertoont bij de overgangstemperatuur, een verschijnsel dat dus uniek is in verdunde magnetische legeringen.

De soortelijke warmte van Pd- en Pt-legeringen wordt sterk beïnvloed door een uitwendig magneetveld; voor de Au-Fe - legeringen is dit in veel geringere mate het geval. Dit verschil is toegeschreven aan het verschil in de aard van de koppeling tussen de lokale momenten via de geleidingselectronen van het basismetaal. Uit berekeningen op basis van het moleculaire veldmodel (hoofdstuk V, eerste deel) van de soortelijke warmte in aanwezigheid van een uitwendig magneetveld volgt, 1) dat op een aantal details na, de soortelijke warmte van Pd-Mn op bijzonder

bevredigende wijze met dit model kan worden beschreven, indien wordt aangenomen dat slechts één inwendig veld of een zeer smalle spreiding van inwendige velden voorkomt, 2) dat de soortelijke warmte van de andere Pd-legeringen niet op basis van dit model is te beschrijven, alhoewel een brede verdeling van interne velden is aangenomen. Desalniettemin blijkt het mogelijk om kwalitatief het gedrag van de Fe- en Co-legeringen als functie van zowel de concentratie als het magneetveld te verklaren. De breedte van de verdeling der interne velden blijkt dan een overheersende rol te spelen. Deze breedte is in Pd-Co - legeringen groot bij lage concentraties en kleiner bij hogere concentraties. De verdeling der interne velden wordt toegeschreven aan de verdeling van de opgeloste atomen over het rooster (of aan concentratie-inhomogeniteiten), rekening houdend met het feit, dat de sterkte van de wisselwerking afhangt van de onderlinge afstand tussen de magnetische atomen.

Op basis van het bovenstaande is aangenomen, dat in Pd-Mn - legeringen de Mn-atomen een vrijwel uniforme polarizatie in de Pd 4d-band induceren. In het tweede deel van hoofdstuk V wordt de piek in de soortelijke warmte van deze legeringen nader geanalyseerd. De geringe afronding van deze piek kan op zeer bevredigende wijze beschreven worden door een smalle Gauss-verdeling van overgangstemperaturen aan te nemen. Dit laatste is in goede overeenstemming met de veronderstelling die men moest maken bij de berekening der soortelijke warmte van deze legeringen in uitwendige velden, omdat men de overgangstemperatuur als een maat voor de wisselwerkingssterkte moet beschouwen. Het 'critische gedrag' van Pd-Mn - legeringen wijkt volgens deze analyses sterk af van hetgeen tot nu toe in magnetische systemen is gevonden. Van voor dit systeem bruikbare modelberekeningen zal men moeten leren, wat de betekenis is van de in hoofdstuk V uit de metingen afgeleide waarden van de kritische exponent  $a$  (zie vgl. V.27a,b), de magnetische entropie en de magnetische energie.

De meest fundamentele vraag, nl. waarom de 4d-band polarizatie vrijwel uniform is in Pd-Mn - legeringen en dat niet het geval is in de andere Pd-legeringen, is voorsnog onbeantwoord gebleven.

Tenslotte blijkt uit entropieberekeningen dat de spin een vrij normale waarde heeft in alle legeringen, in tegenstelling tot de verzadigingswaarde van het moment per magnetisch atoom (giant moment). In paragraaf IV.5 worden een aantal suggesties gedaan, die hiervoor een verklaring kunnen geven.

Uit dit werk blijkt duidelijk dat naast verder experimenteel onderzoek, waarvoor een aantal mogelijkheden zijn gesuggereerd, er een grote behoefte is aan theoretisch onderzoek op dit gebied, met name wat betreft de soortelijke warmte van deze legeringen en speciaal omtrent het Pd-Mn - systeem.

Op verzoek van de Faculteit der Wiskunde en Natuurwetenschappen volgt hier een overzicht van mijn studie.

Nadat ik in 1957 het diploma HBS-B had behaald aan het Eerste Christelijk Lyceum te Haarlem, ben ik mijn studie begonnen aan de Rijksuniversiteit te Leiden. In 1961 legde ik het candidaatsexamen A' af in de Natuur- en Wiskunde met als bijvak Sterrekunde. Sinds dat jaar ben ik werkzaam geweest in de werkgroep 'F.O.M.-metalen Mt-IV', waarvan prof. dr. C.J. Gorter de leiding heeft. De dagelijkse leiding berust bij dr. G.J. van den Berg en later mede bij dr. C. van Baarle. Dr. F.J. du Chatenier en dr. J. de Nobel hebben mij op stimulerende wijze ingewijd in de problemen van het meten van de soortelijke warmte van metalen. Het doctoraal examen experimentele natuurkunde heb ik in oktober 1964 afgelegd.

Sinds 1963 ben ik verbonden geweest aan het practicum voor 2e jaarsstudenten met hoofdvak natuurkunde. In 1964 kwam ik als wetenschappelijk medewerker in dienst bij de Stichting voor Fundamenteel Onderzoek der Materie, F.O.M..

Een groot aantal medewerkers hebben gedurende enige tijd steun verleend aan mijn onderzoekingen. In het bijzonder wil ik van hen noemen drs. W.J.J. van Dissel, drs. G.J. Nieuwenhuys en de heren J.J. Zwart en J. Hansen. Hun hulp tijdens metingen tot dikwijls ver in de avonduren heb ik altijd bijzonder geapprecieerd. Discussies met vele medewerkers van de Metalengroep, met name met dr. C. van Baarle en drs. J.E. van Dam, hebben veel bijgedragen tot het tot stand komen van dit proefschrift. Veel dank ben ik verschuldigd aan dr. R.F. Wielinga voor het uitvoeren van een groot aantal berekeningen ter analyse van de soortelijke warmte van Pd-Mn-legeringen.

De hulp van vooral de heren H.R.A. Nater en J. Turenhout bij problemen van technische aard is onmisbaar geweest voor het welslagen van de experimenten. De heer C.E. Snel heeft gezorgd voor de vervaardiging van de legeringen, terwijl de concentratiebepalingen door de bereidwillige medewerking van dr. H.A. Das uitgevoerd werden in het Reactor Centrum Nederland. De samenstelling van een aantal legeringen werd onderzocht door mevr. M.A. Otten-Scholten. De heer W.F. Tegelaar heeft op vaardige wijze voor de tekeningen gezorgd.

Dr. J.K. Hoffer en dr. H. van Beelen ben ik zeer erkentelijk voor zowel het corrigeren van de Engelse tekst als voor een aantal waardevolle suggesties.

Het grootste gedeelte van het typewerk werd uitgevoerd door mevr. E.J. Boerstool-Klinkenberg.



Challenges

1. All the above issues are related to the development of high temperature materials for use in gas turbines.

2. The development of materials for use in gas turbines is a complex task. It involves the development of materials that can withstand high temperatures, high stresses, and high corrosion rates.

3. The development of materials for use in gas turbines is a complex task.

4. The development of materials for use in gas turbines is a complex task. It involves the development of materials that can withstand high temperatures, high stresses, and high corrosion rates. The development of materials for use in gas turbines is a complex task.

5. The development of materials for use in gas turbines is a complex task.

6. The development of materials for use in gas turbines is a complex task.

7. The development of materials for use in gas turbines is a complex task.

8. The development of materials for use in gas turbines is a complex task. It involves the development of materials that can withstand high temperatures, high stresses, and high corrosion rates. The development of materials for use in gas turbines is a complex task.

9. The development of materials for use in gas turbines is a complex task.

10. The development of materials for use in gas turbines is a complex task.

11. The development of materials for use in gas turbines is a complex task.

12. The development of materials for use in gas turbines is a complex task. It involves the development of materials that can withstand high temperatures, high stresses, and high corrosion rates. The development of materials for use in gas turbines is a complex task.

13. The development of materials for use in gas turbines is a complex task.

14. The development of materials for use in gas turbines is a complex task.

15. The development of materials for use in gas turbines is a complex task.

16. The development of materials for use in gas turbines is a complex task.

17. The development of materials for use in gas turbines is a complex task.



## Stellingen

1. Als standaard voor onderzoek van de soortelijke warmte bij lage temperaturen is aluminium te prefereren boven koper.
2. De nieuwe interpretatie, die door Chari wordt gegeven van het gedrag van Rh-Fe - legeringen met Fe-concentraties beneden 1 at.%, is onvoldoende gefundeerd.

M.S.R. Chari, Phys.kondens.Materie 11 (1970)317.

3. De door du Chatenier en de Nobel gegeven interpretatie der soortelijke warmte van een systeem van onderling wisselwerkende ionen (Ag-Mn) met behulp van de voor een paramagnetisch systeem berekende soortelijke warmte (Schottky-anomalie \*) is onjuist.

F.J. du Chatenier, proefschrift, 1964, p. 82, 103.

J. de Nobel en F.J. du Chatenier, Physica 25 (1959)969.

\*) W. Schottky, Phys.Z. 23 (1922)448.

4. Voor legeringen van het type Pd-Fe hangt de vorm van magnetisatie-isothermen sterk af van de spreiding der interne velden. Het is daarom twijfelachtig of het gerechtvaardigd is om tot het bestaan van hoge spinwaarden te besluiten uit aanpassingen van Brillouin-functies aan resultaten van magnetisatie- en Mössbauer-effect experimenten, indien met deze spreiding geen rekening wordt gehouden.

A.J. Manuel en M. McDougald, J. Phys. C 3 (1970) 147.

T.A. Kitchens en P.P. Craig, J. appl.Phys. 37(1966)1187.

Dit proefschrift, hoofdstuk IV.

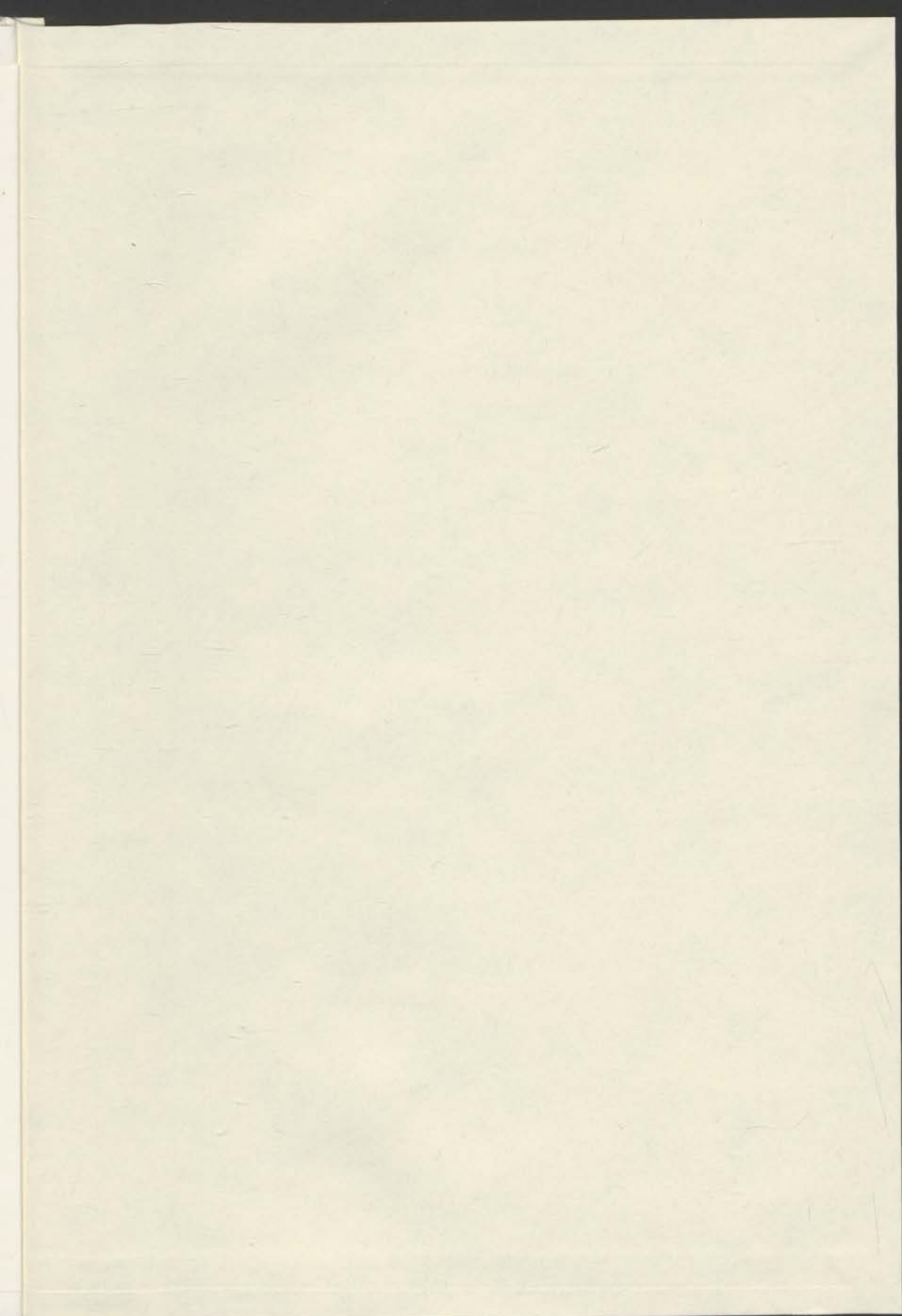
5. Het wekt verwarring om de in verscheidene leerboeken voor een gedwongen harmonisch-trillend systeem ingevoerde grootheid  $Q$ , die een functie is van de eigenfrequentie en de opgedwongen frequentie, als kwaliteitsfactor aan te duiden.

C.Kittel, W.D. Knight en M.A. Ruderman, Berkeley Physics Course, McGraw-Hill, New York, Vol. I, p. 225.

R.P. Feynman, R.B. Leighton en M. Sands, The Feynman Lectures on Physics, Addison-Wessley Publ. Comp., Reading, 1963, Vol. I, p. 23-5, 24-2.

6. De bewering van Kim en Schwartz, dat uit neutronendiffractie-experimenten van Low en Holden aan Pd-Fe - legeringen zonder meer zou volgen, dat de karakteristieke afstand van de geïnduceerde polarisatie der 4d-electronen afneemt bij toenemende Fe-concentratie, is niet gerechtvaardigd.  
D.J. Kim en B.B. Schwartz, J.appl.Phys. 40(1969)1208.  
G.G. Low en T.M. Holden, Proc.phys.Soc. 89(1966)119.
7. Voor verdunde magnetische legeringen mogen uit de concentratie-afhankelijkheid van de temperatuur van het minimum in de weerstand geen conclusies worden getrokken ten aanzien van het optreden van een onzuiverheidsbijdrage tot de weerstand die evenredig is met de logaritme van de temperatuur.  
J. Kondo, Sol.State Phys. 23(1969)183.  
E.F. Wassermann, Z. Phys. 234(1970)347.
8. De bewering, dat het 'flessenhals-effect' in de electronspin-resonantie van een verdunde magnetische legering niet optreedt, indien voor het basis-metaal de electronspin-resonantie van de geleidingselectronen niet is waargenomen, is onjuist.  
J. Dupraz, thèse, Genève, Archives des Sciences (Genève) 22(1970)755.
9. Gezien de snelle toeneming van het particuliere vervoer zal het voor een aantal steden in Nederland gewenst zijn om op korte termijn de binnenstad gedeeltelijk of geheel voor dit vervoer af te sluiten. De voordelen hiervan zullen voldoende opwegen tegen de nadelen, mits van overheidswege een juist beleid wordt gevoerd ten aanzien van het openbare vervoer, parkeervoorzieningen, e.d..
10. Het is wenselijk om girobetaalkaarten zowel voor ontvangers als voor houders daarvan betaalbaar te stellen op postkantoren.

B.M. Boerstool



The following are the names of the persons who have been appointed to the various committees of the Board of Directors of the American Telephone and Telegraph Company for the year ending December 31, 1924.

Chairman of the Board: J. Edgar Hoover  
President: J. Edgar Hoover  
Vice President: J. Edgar Hoover  
Secretary: J. Edgar Hoover  
Treasurer: J. Edgar Hoover

Committee on Finance: J. Edgar Hoover, Chairman  
Committee on Administration: J. Edgar Hoover, Chairman  
Committee on Public Relations: J. Edgar Hoover, Chairman  
Committee on Legislation: J. Edgar Hoover, Chairman

Committee on Investigation: J. Edgar Hoover, Chairman

Committee on Audit: J. Edgar Hoover, Chairman  
Committee on Internal Security: J. Edgar Hoover, Chairman  
Committee on Foreign Relations: J. Edgar Hoover, Chairman  
Committee on Labor Relations: J. Edgar Hoover, Chairman

Committee on Research and Development: J. Edgar Hoover, Chairman  
Committee on Education: J. Edgar Hoover, Chairman  
Committee on Social Welfare: J. Edgar Hoover, Chairman  
Committee on Public Safety: J. Edgar Hoover, Chairman

Committee on International Relations: J. Edgar Hoover, Chairman  
Committee on Economic Affairs: J. Edgar Hoover, Chairman  
Committee on Cultural Affairs: J. Edgar Hoover, Chairman  
Committee on Scientific Affairs: J. Edgar Hoover, Chairman

Committee on Artistic Affairs: J. Edgar Hoover, Chairman  
Committee on Literary Affairs: J. Edgar Hoover, Chairman  
Committee on Musical Affairs: J. Edgar Hoover, Chairman  
Committee on Dramatic Affairs: J. Edgar Hoover, Chairman

Committee on Cinematic Affairs: J. Edgar Hoover, Chairman  
Committee on Theatrical Affairs: J. Edgar Hoover, Chairman  
Committee on Radio Affairs: J. Edgar Hoover, Chairman  
Committee on Television Affairs: J. Edgar Hoover, Chairman

Committee on Aeronautics: J. Edgar Hoover, Chairman  
Committee on Space Affairs: J. Edgar Hoover, Chairman  
Committee on Atomic Energy: J. Edgar Hoover, Chairman  
Committee on Nuclear Power: J. Edgar Hoover, Chairman

Committee on Environmental Affairs: J. Edgar Hoover, Chairman  
Committee on Natural Resources: J. Edgar Hoover, Chairman  
Committee on Conservation: J. Edgar Hoover, Chairman  
Committee on Pollution Control: J. Edgar Hoover, Chairman

